THESIS ON NATURAL AND EXACT SCIENCES B169

Formation of Cu_2ZnSnS_4 and $Cu_2ZnSnSe_4$ by Chalcogenisation of Electrochemically Deposited Precursor Layers

JULIA LEHNER

TUT PRESS

TALLINN UNIVERSITY OF TECHNOLOGY
Faculty of Chemical and Materials Technology
Department of Materials Science
Chair of Semiconductor Materials Technology

This dissertation was accepted for the defense of the degree of Doctor of Philosophy in Natural and Exact Sciences on March 26, 2014.

Supervisors: Dr Olga Volobujeva, Senior Research Scientist Department of Materials Science, Tallinn University of Technology, Estonia

Professor Enn Mellikov, Department of Materials Science, Tallinn University of Technology, Estonia

Opponents: Professor Remigijus Juškenas, Department of Inorganic Chemistry, Vilnius University, Lithuania

Dr Jonathan J. Scragg, Department of Engineering Sciences, Uppsala University, Sweden

Defense of the thesis: May 28 at 14.00, 2014
Lecture hall: VII-226
Tallinn University of Technology,
Ehitajate tee 5, Tallinn

Declaration:
Hereby I declare that this doctoral thesis, my original investigation and achievement, submitted for the doctoral degree at Tallinn University of Technology has not been submitted for any academic degree.

Julia Lehner

ISSN 1406-4723
ISBN 978-9949-23-607-7 (publication)
ISBN 978-9949-23-608-4 (PDF)

LOODUS- JA TÄPPISTEADUSED B169

$Cu_2ZnSnSe_4$ ja Cu_2ZnSnS_4 moodustumine elektrokeemiliselt sadestatud kihtide kalkogeniseerimisel

JULIA LEHNER

TTÜ
KIRJASTUS

CONTENTS

LIST OF PUBLICATIONS

The present doctoral thesis is based on the following peer reviewed publications, referred to in the text by Roman numerals **I-V**:

I. **J. Lehner**, M. Ganchev, M. Loorits, N. Revathi, T. Raadik, J. Raudoja, M. Grossberg, E. Mellikov, O. Volobujeva. Structural and compositional properties of CZTS thin films formed by rapid thermal annealing of electrodeposited layers. *Journal of Crystal Growth*, 380 (2013) 236-240

II. **J. Iljina**, O. Volobujeva, T. Raadik, N. Revathi, J. Raudoja, M. Loorits, R. Traksmaa, E. Mellikov. Selenization of sequentially electrodeposited Cu–Zn and Sn precursor layers. *Thin Solid Films*, 535 (2013) 14–17.

III. **J. Iljina**, R. Zhang, M. Ganchev, T. Raadik, O. Volobujeva, M. Altosaar, R. Traksmaa, E. Mellikov. Formation of Cu_2ZnSnS_4 absorber layers for solar cells by electrodeposition-annealing route. *Thin Solid Films*, 537 (2013) 85–89.

IV. M. Ganchev, **J. Iljina**, L. Kaupmees, T. Raadik, O. Volobujeva, A. Mere, M. Altosaar, J. Raudoja, E. Mellikov. Phase composition of selenized $Cu_2ZnSnSe_4$ thin films determined by X-ray diffraction and Raman spectroscopy, *Thin Solid Films*, 519 (2011) 7394–7398.

V. M. Ganchev, L. Kaupmees, **J. Ilyina**, J. Raudoja, O. Volobujeva, H. Dikov, M. Altosaar, E. Mellikov, T. Varema. Formation of $Cu_2ZnSnSe_4$ thin films by selenization of electrodeposited stacked binary alloy layers. *Energy Procedia*, 2 (2010) 65–70.

Copies of these articles are included in Appendix A.

AUTHOR'S OWN CONTRIBUTION

The contribution of the author to the peer reviewed publications included in this thesis is as follows:

I. Electrodeposition of Cu-Zn and Sn layers, rapid thermal process, films' characterization (SEM and EDS), Raman spectroscopy, analysis of the results, major part of writing

II. Electrodeposition of Cu-Zn and Sn films, thermal treatment of precursor films, characterization (SEM and EDS), Raman spectroscopy, analysis of the results, major part of writing

III. Electrodeposition of Cu-Zn-Sn-S containing layers, thermal treatment of precursor films, characterization (SEM and EDS), Raman spectroscopy, analysis of the results, major part of writing

IV. Electrodeposition of Cu-Zn and Sn films, thermal treatment of precursor films, part of films' characterization (SEM and EDS), analysis of the results, minor part of writing

V. Electrodeposition of Cu-Zn and Cu-Sn alloy films, thermal treatment of precursor films, part of films' characterization (SEM and EDS), analysis of the results, minor part of writing

LIST OF ABBREVIATIONS AND SYMBOLS

AAS	Atomic absorption spectroscopy
AFM	Atomic force microscopy
CBD	Chemical bath deposition
CIG(S,Se)	$Cu(In,Ga)(S,Se)_2$
CI(S,Se)	$CuIn(S,Se)_2$
CVD	Chemical vapour deposition
CZTS	Cu_2ZnSnS_4
CZTSe	$Cu_2ZnSnSe_4$
CZTS(Se)	Cu_2ZnSnS_4 and/or $Cu_2ZnSnSe_4$
CZTSSe	$Cu_2ZnSn(S_{1-x},Se_x)_4$
DME	Dropping mercury electrode
EBSD	Electron backscatter diffraction
ED	Electrodeposition
EDTA	Ethylendiaminetetraacetic acid
EDX	Energy dispersive X-ray microscopy
EQE	External quantum efficiency
FF	Fill factor
FWHM	Full width at half maximum
FTO	Fluorine doped tin oxide
g/Ah	Gram / ampere hour
ITO	Indium tin oxide
J_{sc}	Short circuit current density
KCN	Potassium cyanide
K_s	Stability constant
Me	Metal
η	Efficiency of solar cell
N_2H	Hydrazine
PV	Photovoltaic
PVD	Physical vapor deposition
QE	Quantum efficiency
R_{rms}	Root mean square roughness
RTA	Rapid thermal annealing
SEM	Scanning electron microscopy
SEL	Sequential electrodeposition
SHE	Standard hydrogen electrode
TAA	Thioacetamide
TFSC	Thin film solar cells
TiN	Titanium nitride
T_s	Substrate temperature
USP	Ultrasonic spray technique
XPS	X-ray photoelectron spectroscopy
XRD	X-ray diffraction
ZnO:Al	Aluminium doped zinc oxide

INTRODUCTION

The global energy demand over the coming decades is expected to rise further due to population growth, improved living standards and economic growth. This will put additional pressure on energy supply and result in rising energy prices in many regions [1]. Renewable sources of energy will become essential contributors to the energy supply as they can provide the world with electricity derived from replenishable sources such as sun and wind. Renewables are considered environmentally preferable to conventional sources, and when replacing fossil fuels, have significant potential to reduce greenhouse gas emissions [1]. Among a variety of clean energy sources, solar energy is abundant in many world regions and is suitable for meeting the energy demands of modern society. In order to facilitate worldwide use of solar panels it is still necessary to develop lower-cost and highly efficient solar cells with minimal harm to the environment.

In 2012 the installed capacity of photovoltaics (PV) accounted for only 0.4% (0.1 PWh) of global electricity generation [1]; however, to provide a realistic chance to limit the global temperature increase to 2°C, IEA's 450 Scenario sees the share of PV climbing to 3.8% by 2035 [1]. Other studies concluded that even faster growth in PV deployment is required for climate change mitigation: In the second half of this century, solar cells could contribute about a third or more to the global electricity generation [2].

About 30 GWp of solar modules were installed globally in 2012 (2013 estimate: 37 GWp [3]), of which 84% belonged to crystalline silicon (c-Si) solar cells, followed by CdTe thin films at about 7% [4]. The remaining 9% are mainly shared by $CuInGa(S,Se)_2$ (CIGS(Se)) thin films and amorphous silicon thin films. Research labs have achieved conversion efficiencies of 20.4% for CdTe and 20.9% for $CuIn(S,Se)_2$/$Cu(In,Ga)n(S,Se)_2$ (CIS(Se)/CIGS(Se)) [5, 6]; however, commercially available CdTe and CIS(Se)/CIGS(Se) PV panels reach only about 13%. This is still considerably less than mono- and multicrystalline silicon, which reach up to 24% and 17% module efficiencies, respectively [4, 7]. While there is no major material limitation in c-Si technology (provided silver is avoided in front contacting), its suitability as a long term technology can be questioned due to the energy intense production process compared to thin film approaches. CdTe and CIS(Se)/CIGS(Se) thin films have the downside of using one or several expensive and potentially scarce materials (tellurium, indium, and gallium) which may hamper the strong growth of PV as outlined above. In addition, CdTe requires the use of toxic elements such as cadmium which, arguably, disqualifies it as a 'clean' technology.

The development of $Cu_2ZnSnSe_4$ and Cu_2ZnSnS_4 (CZTS(Se)) solar cells can eliminate material availability constraints and moreover all the elements in this quaternary semiconductor compound except selenium are environmentally benign. Compared to its close relative CIGS(Se), indium and gallium are substituted in CZTS(Se) by two non-toxic and earth abundant elements, zinc and tin. The current record efficiency of 12.6% for (selenium containing) mixed

$Cu_2ZnSn(S_{1-x},Se_x)_4$ (CZTSSe) absorbers was achieved by the group of Todorov and Mitzi et al. [8]. However, in this approach a highly toxic and unstable hydrazine is used as a solvent.

Reducing the complexity of industrial production processes in the thin film solar cell industry is crucial to achieve further cost reductions. In this respect, non-vacuum processes are highly desired as they can supersede expensive machinery and reduce operation and maintenance cost in production plants. Electrodeposition (ED) is a promising method for formation of compound absorber films for PV applications. In an industrial setup, this approach could potentially enable fast deposition of large areas at reasonable production costs.

Annealing of precursors at high temperatures is an essential second step of most approaches for obtaining a final well crystallized and pure phase absorber material. Annealing could be performed for different durations and in different atmospheres (e.g. argon, nitrogen, vacuum). The source of sulphur (or selenium) can be inserted in the chamber (ampoule) as a pure piece of sulphur (or selenium) or hydrogen sulphide gas can be fed through a tube into the chamber. The group of Ahmed [9] demonstrated an conversion efficiency of 7.3%, which is the record for electrodeposited Cu_2ZnSnS_4 solar devices. The performance of this device underlines the suitability of electrodeposition and annealing as a viable low-cost processes for solar cell fabrication based on earth-abundant materials.

The objective of this PhD work was to obtain CZTS(Se) absorber materials with electrochemical techniques and to find suitable annealing conditions to form homogenous, well-adherent single phase CZTS(Se) films for application in solar cells. Morphological, structural and compositional properties of precursors as well as of annealed films were investigated in this work.

This work consists of three chapters. In the first chapter an overview of the relevant literature is presented. In the second chapter details of the experimental part of the PhD research are given. In the third chapter obtained results are presented and discussed.

This doctoral thesis is based on five published articles.

1 LITERATURE REVIEW AND AIM OF THE STUDY

1.1 Thin film photovoltaic cells

Despite tremendous progress in all aspects of fabrication of Si based solar cells and the rapid decrease of production cost for PV modules, it still remains too high to compete with other sources of electricity generation [10]. Moreover, owing to its indirect band gap, silicon is not an ideal absorber material for solar cells. Semiconductor materials with indirect band gaps do not absorb light as efficiently as those with direct band gaps, and therefore a thick layer of material is needed to achieve sufficient light absorption. In comparison with a 1 μm GaAs, direct band gap semiconductor, 100 μm of crystalline silicon is needed for 90% light absorption [11]. Large thickness of silicon used in PV requires the use of very high quality material in order to allow for minority carrier lifetimes and diffusion lengths long enough so that recombination of the photo-generated charge carriers is minimized so that they can contribute to the photocurrent.

Due to these limitations of crystalline silicon, which also mean result in energy intense production processes (thick layers of high purity material), researchers had been directed to other potential materials that could be used as absorbers in solar cells.

Thin film solar cells (TFSC) are a promising approach for photovoltaics and offer a wide variety of choices in terms of the device design and fabrication. Various substrates (flexible or rigid, metal or insulator) can be used for deposition of different layers (contact, buffer, absorber, reflector and etc.) using different techniques (PVD, CVD, ED, plasma based, hybrid, etc.) [12].

The first thin/thick film Cu_2S/CdS cell was based on rather cheap and simple technology known as the 'Clevite process' [13], in which a several μm thick CdS film was vacuum deposited on to a metal or metalized plastic substrate followed by immersion of the CdS film in cuprous chloride solution to convert the CdS surface partly to Cu_2S. Cell efficiency reached 10.4% and solar cells were commercially produced by several companies in USA and France [14]. However, rapidly growing and well understood Si technology forced the Cu_2S/CdS cell out of the market. Nevertheless, basic research on the Cu_2S/CdS PV devices has proved useful for later developments in thin film solar cell technology.

Chopra *et al.* [12] defines a "thin film" as a material 'created *ab initio* by the random nucleation and growth processes of individually condensing/reacting atomic/ionic/molecular species on a substrate. The structural, chemical and physical properties of such material are strongly dependent on a large number of deposition parameters and may also be dependent on thickness.

A variety of chemical, physical, electrochemical and other methods are developed and are widely used in order to deposit thin films. However, one also

has to take into account that the high sensitivity of film properties to various deposition parameters can produce films with undesired parameters.

Promising candidates for low-cost thin film solar cells today are amorphous hydrogenated silicon (a-Si:H), CdTe (cadmium telluride), $CuInSe_2$ (copper indium diselenide) and its alloys with Ga and/or S, Cu_2ZnSnS_4, $Cu_2ZnSnSe_4$ and their mixed compound material $Cu_2ZnSn(S_{1-x},Se_x)_4$ [15, 16, 17]. The evident advantage of these polycrystalline compound semiconductor materials as compared to Si is that they are direct band gap materials and have higher absorption coefficients [18].

The photovoltaic effect is the creation of a voltage or electric current in a semiconductor under light illumination. In a solar cell, this effect occurs in the p-n junction that is formed by a p-type and n-type layer[1]. Conventional solar cells consist of different layers, each of them has its own physical and chemical properties and each affects the overall performance of the device. A conceptual schematic of a CZTS(Se) based thin film device structure is shown in *Figure 1.1*. Incident light (photons) passes through the window and buffer layer and is absorbed in the absorber layer in which excitation of electrons takes place. The n-type semiconductor film is composed of two layers: a thin buffer (here CdS) and a thicker window layer (here ZnO). The front contact can be made with different metals (In, Al, Au etc.). The back contact consists of a metal film (here Mo), which provides electrical contact to the back of the film. Antireflection coating can be deposited on the top of the film to minimize the reflection losses and to improve the efficiency of a device as less light is lost [19].

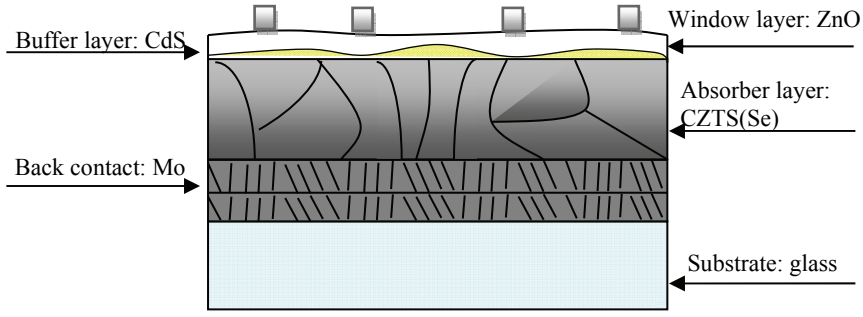

Figure 1. 1: Cross-section of polycrystalline thin film solar cell (Source: Based on [19])

1.2 Cu_2ZnSnS_4 and $Cu_2ZnSnSe_4$ as novel materials for solar cell application

Ideal absorber material for efficient solar cells is a semiconductor with a band gap between 1 and 1.5 eV and with a high optical absorption ($10^4 - 10^5$ cm^{-1}) in the wavelength region of 350 – 1000 nm, a high quantum yield for the excited

[1] Majority carriers in a n-type semiconductor are electrons (p-type: holes)

carriers, a long diffusion length and low recombination velocity [10]. If all these necessary conditions are met, the basic material is widely available, and a potentially low-cost production technique exists, then such a solar cell device should be suited for future large scale production.

The world-famed thin film absorbers CdTe and variations of $CuInSe_2$ achieved high efficiencies [5, 6] (CdTe 20.4%, CIGS 20.9%); however, the use of scarce elements like Te and In for preparation of solar cells could be considered as a limiting factor for future large scale deployment. Another issue to be solved is the recycling and use of toxic metals such as cadmium. The solution to these problems could be an alternative absorber compound that is both non-toxic and easily available. In this context, the quaternary semiconductors Cu_2ZnSnS_4 and $Cu_2ZnSnSe_4$ have emerged as the promising candidates. CZTS(Se) is a compound semiconductor material composed of copper, zinc, tin and sulphur (selenium), all of which are earth abundant and non-toxic elements (except selenium).

CZTS(Se) is a p-type semiconductor with a direct band gap of approximately 1 eV for CZTSe and 1.5 eV for CZTS. It is suitable for thin film solar cells due to its high absorption coefficient of more than 10^4 cm^{-1} [20]. CZTS(Se) is derived from the $Cu(In,Ga)(S,Se)_2$ structure by the replacement of two In (or Ga, respectively) atoms by Zn and Sn atoms. As a consequence, the properties of CZTS(Se) are similar to those of the CIG(S,Se) compound. CZTS(Se) absorber material can also be combined with CdS (buffer layer) and ZnO (window layer) for preparation of solar cells. These layers are well studied for CIG(S,Se) based solar cells, and hence researchers could build on this knowledge without having to develop entirely new buffer and window layers for solar cells based on CZTS(Se) absorbers.

Besides this, another important characteristic of CZTS(Se) is the possibility to tailor the band gap, e.g. through replacement of S by Se, similar to $CuInSe_2$, or though varying the ratio of S and Se.

Reported investigations of the phase diagram of the system showed that a single-phase CZTS(Se) material can be formed only in a very narrow region with a maximum of 1-2% (absolute) deviation in the stoichiometric composition at growth temperatures around 550ºC [21, 22, 23]. On the contrary, the phase diagram of chalcopyrite ($CuInSe_2$) allows for Cu deficiency of 4% absolute at growth temperature [24].

According to this data, during CZTS(Se) synthesis, even very small composition fluctuations could lead to formation of secondary phases. Impurities including ternary and quaternary compounds are easier to form than CZTS(Se). Therefore compared to the chalcopyrite, it is more challenging to produce pure kesterite material.

Figure 1.2 shows the phase diagram of CZTS with secondary phases that can form in dependence on composition. A fraction of 50% sulphur is assumed. In the middle (marked with an asterisk) only pure CZTS occurs. The detailed explanation of this diagram is described elsewhere [19].

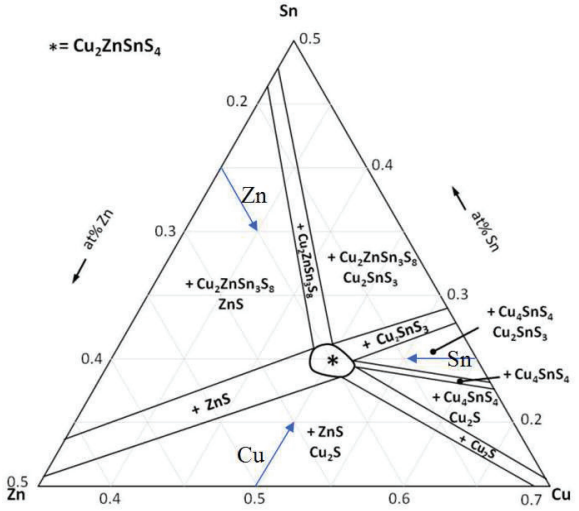

Figure 1. 2 Ternary phase diagram of CZTS with expected secondary phases at 400ºC [19]

The band gap of secondary phases can give a first indication of how detrimental different secondary phases are to the solar cell device performance [25]. Secondary phases with lower band gaps than the CZTS(Se) compound will limit the open circuit voltage of the solar cell. The presence of additional phases with a band gap lower by only 100 meV will reduce the maximum efficiency by 8% [25]. Secondary phases ZnS and ZnSe with band gaps 3.7 eV and 2.7 eV respectively are considered to be less detrimental, therefore a number of research groups aim for Zn-rich compounds during precursor film preparation. Moreover devices prepared from Zn-rich CZTS(Se) absorber layers show better efficiencies than solar cells made from Cu-rich and/or Sn-rich CZTS(Se) material.

Figure 1.3 shows reported conversion efficiencies of cell devices as a function of Zn:Sn and Cu:(Zn+Sn) content in CZTS(Se) absorbers. This composition map also indicates whether vacuum or non-vacuum processes were used. The highest efficiency was obtained in a very narrow range of the composition (Cu:(Zn+Sn) ≈ 0.85 and Zn:Sn ≈ 1.2). However, in contrast to the absorbers prepared by non-vacuum methods, CZTS(Se) made by vacuum techniques demonstrate efficiencies higher than 4% also in a wider composition range.

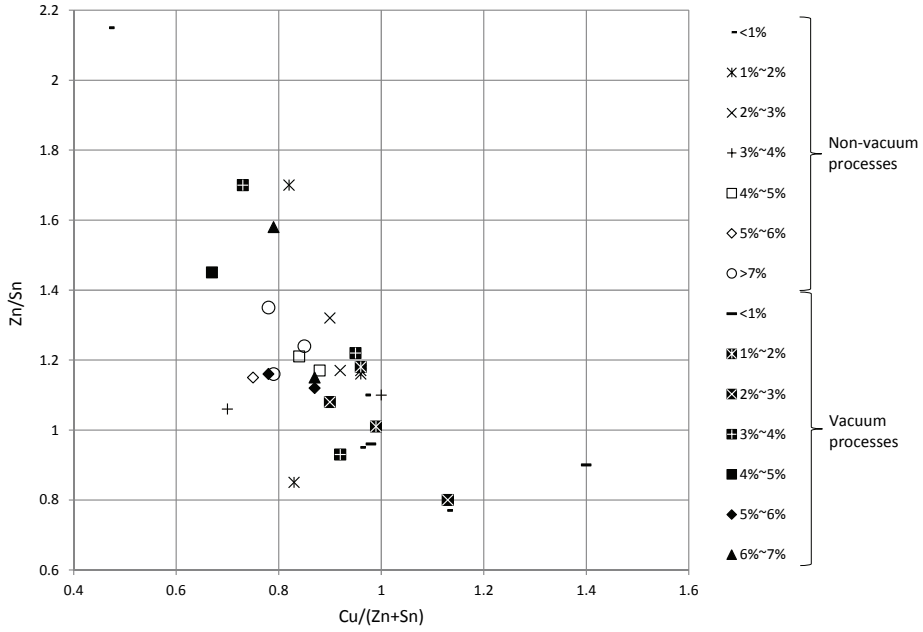

Figure 1. 3 Reported CZTS(Se) cell efficiencies versus absorber composition: Cu:(Zn+Sn) and Zn:Sn, [26-49]

Secondary phases in CZTS(Se) can be revealed using the x-ray diffraction method (XRD). One disadvantage of this method is that main diffraction peaks of $Cu_2SnS(Se)_3$, ZnS(Se) and CZTS(Se) phases are overlapping, hence making them indistinguishable by diffraction techniques [50, 51]. The presence of ZnS(Se) and $Cu_2SnS(Se)_3$ can be confirmed by Raman scattering analysis. It was also shown that secondary phases can be identified using x-ray near edge absorption spectroscopy [52]. All investigated phases showed different near edge absorption spectra at the sulphur K-edge enabling high accuracy quantification of phase mixtures using linear combination fitting [52].

CZTS phase can form either through solid-state reaction of Cu_2ZnSn_3 with ZnS or through a direct reaction of Cu_2S, ZnS and SnS_2 [53, 54, 55]. When binary sulphides are formed, formation of CZTS material is rapid. Weber et al. demonstrated that at 500ºC CZTS is formed within 10 − 70 seconds [56].

1.3 Formation of CZTS(Se) compounds by different methods

Methods for synthesis of CZTS(Se) thin films can be simply classified into two main categories: vacuum and non-vacuum based technologies. The deposition method has generally a large impact on the resulting film properties as well as on the production cost. Although a wide range of methods exist for preparation of stoichiometric CZTS(Se), only few of them led to promising solar cells efficiencies.

Vacuum based fabrication techniques involve deposition of the constitute atoms of the CZTS(Se) material on a substrate by sputtering or evaporation of the target sources under a certain pressure and temperatures [20]. These methods give control over the chemical composition in the thin films and can provide good reproducibility. However, due to the required vacuum, they can be considered as expensive techniques for producing solar cells. The best reported efficiency from using thermal evaporation of elemental sources for Cu_2ZnSnS_4 solar cell preparation so far is 8.4% [57]. Very thin (600 nm) CZTS absorber layers were deposited using a vacuum thermal evaporation process (150ºC) and subsequent short high-temperature atmospheric pressure annealing. The same group from IBM T.J. Watson Research Center reported 8.9% conversion efficiency for pure selenide CZTSe solar cells. CZTSe films were prepared by thermal evaporation followed by post-deposition treatment in Se environment [58]. Titanium nitride (TiN) was used as a diffusion barrier and results showed that the thickness of the interfacial $MoSe_2$ layer was decreased significantly, resulting in the highest obtained efficiency.

The best reported conversion efficiency for CZTS based thin film solar cell prepared via the co-sputtering technique is 5.7% [37]. Elimination of metal oxide impurities in the absorber films through using deionized water led to an improved efficiency of 6.7% [59]. A pure CZTSe device achieved the efficiency of 9.7% and was prepared via sputtering of Cu, Zn and Sn metals with subsequent annealing in H_2Se containing atmosphere [60]. The vacuum-based pulsed laser deposition technique was also employed to fabricate CZTS(Se) films. An efficiency of 5.85% was obtained with this technique [61].

Non-vacuum deposition methods were developed to reduce production cost since the deposition temperatures are generally low and equipment is rather simple. These techniques include electrodeposition, spray pyrolysis, sol-gel method, chemical bath deposition (CBD) and particulate-based processes that were used for preparation of CIGS(Se) semiconductor thin films [62]. Efficiencies of 10 – 15% were demonstrated for CIGS(Se) [63]. These rather high efficiencies of CIGS(Se) devices significantly reduced the gap between conversion efficiencies of vacuum and non-vacuum deposited CIGS(Se) [62].

The CZTS(Se) PV device with the highest conversion efficiency to date of 12.6% was produced by a non-vacuum method: a hydrazine solution-based process (particulate-based) [8]. The slurry (or ink) employed for deposition comprised a Cu–Sn chalcogenide (S or SSe) solution in hydrazine with the *in situ* formation of readily dispersible particle-based Zn-chalcogenide precursors, $ZnSe(N_2H_4)$ or $ZnS(N_2H_4)$. Multiple layers were spin coated onto Mo-coated soda-lime glass (SLG) and annealed at temperatures higher than 500ºC. The disadvantage of this method is that it employs the highly toxic and highly reactive hydrazine compound.

The spray pyrolysis deposition method was applied for CZTS(Se) fabrication as well. The group of Kamoun [64] studied the influence of substrate temperature (T_s) and the spray duration on the crystallinity of CZTS layers. The best crystallinity was obtained with $T_s = 613$ K (340ºC) which resulted in a

(112) crystal lattice orientation. Kumar et al. [65] studied the effect of T_s and the pH value of the solution on the crystallinity and the morphology of CZTS films. This group showed that good crystallinity of films can be obtained at a T_s in the range of 643 – 683 K (370 – 410ºC) with a solution of pH = 4.5. However, impurities such as ZnS were detected in the films. W. Daranfed et al. [66] used the ultrasonic spray technique (USP) to form CZTS films. Here T_s was varied between 280ºC and 360ºC. Their results exhibit the presence of zinc stannate ($ZnSnO_3$) as a secondary phase in all films. Prabhakar and Nagaraju [67] used the USP method to deposit CZTS material onto a fluorine doped tin oxide (FTO) coated soda lime glass. In their study, a Cu_2ZnSnS_4/ZnS heterojunction solar cell with a device efficiency of 1.16% was demonstrated.

Tanaka et al. [30] made a CZTS solar cell with all semiconductor layers being coated by non-vacuum deposition techniques. The CdS buffer layer was coated using the CBD method. The CZTS absorber layer and the ZnO:Al window layer were deposited using a sol-gel approach. The solution for preparation of CZTS layer contained ions of copper, zinc and tin. After deposition sulphurisation was employed at 500ºC under H_2S/N_2 gases. Authors of the same group in another publication [34] varied the H_2S concentration from 3% to 20%. CZTS thin films prepared with a H_2S concentration of 3% contained grains in size of 1 μm and resulted in the best conversion efficiency in this study of 2.23%. This is so far the highest efficiency for CZTS solar cells prepared by the sol-gel method.

CBD is a solution-based deposition technique used for growth of thin films on a variety of substrates. The method is widely used for many different materials, including oxides and sulphides. In the case of CZTS the method involves the growth of films from a solution comprising metal salts, sulphur-containing chemicals (thiourea) and various complexing agents. A three-layer stack design of separated Cu_2S, ZnS and SnS layers is one route towards Cu_2ZnSnS_4 deposition [68]. A single layer of ZnS is deposited by CBD and subsequent exposure to concentrated solutions containing Sn^{2+} and Cu^{2+} ions, both of which have more positive standard reduction potentials than Zn^{2+}, yields incorporation of these ions into the semiconducting film via ion exchange reaction. After deposition of the precursor layers, annealing at 400 – 600°C is performed in a hydrogen sulphur environment to convert the layers into polycrystalline CZTS films. The XPS depth profile measurement clearly shows a uniform profile of the copper, zinc, tin and sulphur elements. The atomic concentrations show excess Zn above the expected stoichiometry for pure CZTS. [68]. M. Cao also reported about growth of CZTS using only the CBD technique together with sulphurisation treatment [69]. Except metal salts, the solution also contained C_2H_5NS, Na_2EDTA and H_2NCONH_2 and was kept at 85ºC. The pH value was varied and it was found that primarily CZTS phase is presented in the film deposited from the solution at pH 3.5 – 4 with a $ZnCl_2$ concentration of 1.6 – 2mM. The disadvantage of this approach is the time consuming deposition from 4 up to 16 hours. The reported conversion efficiency reached 0.3%.

The electrodeposition technique will be discussed in the next chapter in more detail as it is the main method used in this work for CZTS(Se) precursor preparation.

1.4 Electrochemical deposition approach

Electrodeposition refers to the deposition of different material or alloy in the thin film form from solution (electrolyte). The method is based on redox reactions that occur on the electrodes in an electrochemical cell when electric current is passing through the cell. Besides the power supply, at least two electrodes are required, between which the current can flow in the electrolyte. Negative electrode-cathode can be used as a working electrode on which the film growths and reduction occurs:

R 1. 1

$$Me^{+n} + ne^{-} \rightarrow Me$$

The anode can be used as a counter electrode, where oxidation takes place:

R 1. 2

$$Me \rightarrow Me^{+n} + ne^{-}$$

The mass of the depositing Me (metal) can be calculated with Faraday's first law of electrolysis which states that the mass of a deposited element at the cathode during electrolysis is directly proportional to the quantity of electricity transferred at the electrode:

Eq 1. 1

$$m = \left(\frac{Q}{F}\right)\left(\frac{M}{n}\right)$$

where:
m is mass of the substance liberated at an electrode in grams
Q is the quantity of electric charges passed through the substance in C (Coulombs)
F = 96485 C mol^{-1} which is the Faraday constant
M is the molar mass of the substance
n is the valence number of ions of the substance (electrons transferred per ion)

The morphology, structure and other properties of a deposit are determined by numerous factors including the concentrations of constituents in the electrolyte, the pH value of the electrolyte, the temperature and agitation, the potential difference and the current density. The obtained films can be crystalline or amorphous, metallic or non-metallic. Deposition at very low overpotential leads to the growth of large, solitary crystals, while deposition under high overpotential results in formation of a large amount of small crystals. However, these small crystals grow randomly and form a dendrite-like structure. The formation of rough layers is expected for deposition at too high overpotential.

Electrolytes are usually prepared from aqueous solutions, although many materials have been deposited also from non-aqueous solutions [70].

Conventionally a three-electrode setup is used for the thin film deposition, where the third electrode (besides working and counter electrode) is a reference electrode with respect to which the electrochemical potential of the working electrode is measured. Deposition can be carried out at a constant potential or at a constant current.

One of the most important concepts in electrochemistry is the electrochemical potential, which relates to the formation of an electrical double layer on the metal-solution interface [71] . If to take a metallic wafer and use it as an electrode which is immersed in water, then under the influence of polar molecules of water the ions of the metal surface layer become hydrated and move into the electrolyte. The electrolyte charges positively and the excess of electrons in the metal create a negative charge. Negative charge on the electrode prevents the exit of cations into the solution. However, the cations from the solution interact with the electrons of the metal crystal lattice and move into the lattice site they left before. When the rate of leaving the metal cations and the rate of cations that are moving into the lattice is equal, a dynamic equilibrium is formed:

R 1. 3

$$Me + aq \leftrightarrow Me^{n+} \cdot aq + n\,e^{-}$$

where Me is metal atom, Me^{n+} is metal ion, n is ion charge, e^{-} is electron, aq is molecules of water. The equilibrium results in formation of an electrical double layer (*Figure 1. 4*).

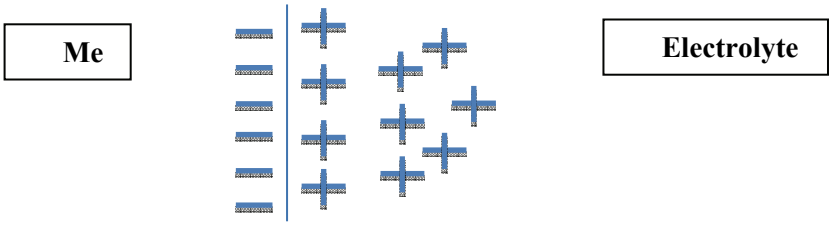

Figure 1. 4 Formation of a double layer on the metal-solution interface

A potential difference forms on the phase border between solution and metal, which can be called either potential drop or electrode potential. An analogue process occurs also by immersion of metal into the solution of the same metal salt.

The formation of a double electrical layer and consequently formation of the electrode potential depends on the material of the electrode, on the concentration of the metal salt in the electrolyte and on the temperature of the electrolyte. Therefore the potential between the metal and the electrolyte cannot be measured through cathode and anode, hence the concept of the reference electrode (namely standard hydrogen electrode) has been introduced. A standard hydrogen electrode (SHE) relates to the electrode that is used as a reference for

all half-cell potential reactions. The value of the potential of the SHE is zero, and on the basis of this, cell potentials using different electrodes or different concentrations can be calculated. Moreover other reference electrodes exist that have a stable electrochemical potential and can be widely used in electrochemical experiments. The most common laboratory reference electrodes are the saturated calomel electrode (SCE) and the silver/silver chloride (Ag/AgCl) electrode. With respect to the standard hydrogen electrode the potential of the saturated calomel electrode is E = +0.241V and for the silver chloride electrode E = +0.197V (saturated). These values have to be taken into consideration when calculating the potential.

The relation of electrode potential to the concentration of ions in the solution ($E_{Me^{n+}/Me}$) can be described by the Nernst equation:

Eq 1. 2

$$E_{Me^{n+}/Me} = E_0 + \frac{RT}{nF} \ln \frac{a(ox)}{a(red)}$$

where R is the universal gas constant (R = 8.314 J K^{-1} mol^{-1}), T is the absolute temperature (K), n is the valence number of ions of the substance, F is the Faraday constant, a(ox) and a(red) are activities of oxidized and reduced species, respectively. E_0 is the standard electrode potential.

Equation 1.2 provides the electrode potential at conditions that differ from standard conditions. In this equation standard electrode potential (E_0) is defined as the potential which is created by immersion of the metallic electrode in the solution of the same metallic salt at standard conditions (T = 298K, concentration of cations of the metal = 1M) and measured against the hydrogen electrode [71].

In case of an alloy deposition, coatings can be obtained by simultaneous reduction of two or more metallic cations present in an electrolyte. Simultaneous deposition is generally obtained by using complexing agents to decrease the activity of the nobler ion in solution. The complexing agent has the tendency to form more stable complexes with nobler ions and less stable complexes with less noble ions. Stability constants are usually used to characterize complexes that are present in the solution. For example for any metal complexation:

R 1. 4

$$Me^{n+} + qX^{p-} \leftrightarrow (Me\,X_q)^{n-pq}$$

Eq 1. 3

$$K_s = \frac{[MeXq]^{n-pq}}{Me^{n+} + qX^{p-}}$$

where K_s is the stability constant, Me^{n+} is metal ion, X^{p-} is ligand (complexing agent). The larger the stability constant, the higher the proportion of formed metal complexes, that exist in the solution.

When an electrolyte contains complexing agents, the Nernst equation transforms as follows:

Eq 1. 4

$$E_{Me^{n+}/Me} = E^0 - \frac{RT}{nF} \ln K_s + \frac{RT}{nF} \ln \frac{a_{M_q}^{n-pq}}{a_{X_{p-}}^{q}}$$

Since K_s will be large for very stable complexes, the potential can shift substantially to the negative [72].

1.4.1 Calculation of layer thickness

The thickness of each layer (Cu-Zn, Cu-Sn, Sn) can be calculated using the following equation:

Eq 1. 5

$$T = \frac{10^3 \, m}{\rho \, S}$$

Where T is the thickness of the layer in μm, m is the mass of the deposited material in grams, ρ is the density in grams per cubic centimetre, S is the surface area of the plated part in square centimetres, 10^3 multiplicative constant to convert cm to μm [19].

The first Faraday law states that the amount of material deposited at the electrode is proportional to the quantity of electricity transferred at the electrode; keeping this in mind, Eq 1. 5 is transformed as follows:

Eq 1. 6

$$T = \frac{I \, t \, M \, 10^3}{n \, F \, \rho \, S}$$

where I is the electric current in amperes, t is the time in seconds, n is the charge of the metal ion, F is the Faraday constant (C mol^{-1}) and M is the molar mass of the substance.

The amount of deposited material by a given quantity of electric current is proportional to its equivalent weight. This allows converting Eq 1. 6 to:

Eq 1. 7

$$T = \frac{I \, t \, E_w \, 10^3}{F \, \rho \, S}$$

where E_w is the equivalent weight of the metal. To simplify the equation the term electrochemical equivalent Z (g/Ah) can be used, which can be defined as the amount of material which is deposited on the electrode when one coulomb of electric charge has passed through the solution. The rearranged equation is:

Eq 1. 8

$$T = \frac{I\,t\,Z\,10^3}{\rho\,S}$$

Eq 1. 8 allows calculating the thickness of each deposited layer. To calculate the thickness of deposited compound material like Cu_2ZnSnS_4, it is reasonable to use Eq 1. 5. The mass of deposited material can be calculated using Faraday's first law and current efficiency of the process has to be taken into consideration. Reported CZTS density is equal to ≈ 4.6 g/cm^3 [21].

In the experimental part of this work, the following electrochemical equivalents are used: Z_{Cu} = 1.186 g/Ah; Z_{Zn} = 1.22 g/Ah; Z_{Sn} = 1.107 g/Ah [73].

1.4.2 Determination of current efficiency

To calculate the mass of the deposited material it is necessary to determine the current efficiency, which is defined as the amount of substance produced on the electrode divided by the amount of substance that theoretically (according to Faraday's law) could have been produced based on direct current applied through the electrolytic cell. In practice, a current efficiency of 100% cannot be attained due to side reactions [74]. Alongside with the convenient weight method, the current efficiency can be determined by several techniques based on measuring the concentration of dissolved elements in acidic media. Some methods that can determine elements dissolved in acidic solution are atomic absorption spectroscopy (AAS), titration, mass spectrometry and polarography. Another way to calculate the efficiency is to perform electrochemical measurements by re-oxidising the deposited layer at a more positive reduction potential of the substance. The consumed charge for stripping of the deposited layer can be compared with the charge consumed for the reduction of the targeted layer. Hence the efficiency of the deposition process can be calculated.

1.4.3 Electrodeposition approaches for CZTS(Se) precursor preparation

Electrochemical techniques for the fabrication of CZTS(Se)-based films include co-deposition of metals, sequential deposition of elemental layers/binary compounds and one-step deposition followed by annealing in inert or reactive atmosphere.

1.4.3.1 Co-deposition of metals

The co-deposition method can be described as simultaneous deposition of all metals at the same potential from one electrolyte. Deposition of films with desired properties can be obtained by adjusting the concentration in the electrolyte, finding the suitable redox potential as well as regulating pH of the solution. The disadvantage of this method in case of Cu-Zn-Sn deposition is the large region between standard redox potentials of the constituent elements (Cu +0.34 V, Sn -0.13 V, Zn -0.76 V). This problem can be solved by shifting

reduction potentials closer to each other through the use of a suitable complexing agent that strongly bonds nobler ions (copper) and forms weak complexes with less noble ions (zinc).

The most common complexing agent for Cu-Zn-Sn co-deposition is citric acid or salt of this acid (trisodium citrate) that can act as pH buffer [44, 46, 47].

H. Araki electrodeposited Cu-Zn-Sn precursors onto Mo-coated borosilicate glass [46]. The electrolyte contained 20mM copper(II) sulphate pentahydrate, 0.2M zinc sulphate heptahydrate, 10mM tin(II) chloride dehydrate and 0.5M trisodium citrate dehydrate. Deposition was carried out potentiostatically (-1.1 V vs. Ag/AgCl) in solution for 20 minutes. The XRD of precursor Cu-Zn-Sn showed the presence of peaks which can be attributed to CuZn, Cu_5Zn_8, Cu and Sn phases. These results are in agreement with findings of another group [75]. Both groups were using Cu-poor precursors.

R. Schurr investigated the formation of CZTS from Cu-poor and Cu-rich precursors. In Cu-poor precursors the Cu_6Sn_5 phase was detected (additionally to CuZn and Cu_3Sn) [76]. The presence of Cu_6Sn_5 leads to a preferred formation of Cu_2SnS_3 via the reaction of $Cu_{2-x}S$ and SnS_2 in the presence of a SnS_2 melt, which is the result of the decay of the Cu_4SnS_6 phase. In the Cu-rich sample, the formation of the binary sulphides takes place at higher temperatures prior to consuming the precursor phases Cu_3Sn and CuZn [76]. In both cases the formation reaction of CZTS was completed by the solid state reaction of Cu_2SnS_3 and ZnS. R. Juškenas et al. [77] revealed $CuZn_5$, Sn and $Cu_{6.25}Sn_5$ phases both in Cu-poor and Cu-rich precursors. The amount of $CuZn_5$ increased with an increase of the Zn quantity in the alloy. In contrast to R. Schurr's results the appearance of the $Cu_{6.25}Sn_5$ phase in Cu-rich films can be explained by the composition difference shown in Table 1. 1.

Precursor	Cu:(Zn+Sn)	Zn:Sn
Cu-rich [76]	1.5 – 1.6	0.95 – 0.98
Cu-rich [77]	1.09	0.87

Table 1. 1 Comparison of precursor composition in [76] and [77]

The larger amount of Cu in the alloy in the experiments by R. Schurr compared to those of R. Juškenas' group probably suppressed the formation of the Cu_6Sn_5 phase in the precursor alloy. Additionally, some groups detected pure Sn, Zn or Cu in formed precursor films [47, 44, 78].

In order to study cathodic potential shifts caused by adding complexing agents in the electrolyte, a series of cyclic voltammetry experiments were carried out [47]. Well-defined cathodic peaks were observed for each element using $C_6H_8O_7/Na_3C_6H_5O_7$ as a complexing agent. The potential for co-deposition of elements was chosen at -1.3 V. Differing from the other reported results [46, 79], low concentrations of metal sulphates were adopted in this study (4mM $CuSO_4$, 2mM $ZnSO_4$ and 3mM $SnSO_4$) which could be beneficial for obtaining dense precursors films with good adhesion to the substrate. The highest conversion efficiency achieved was 4.5%.

Ennaoui et al. [54] co-deposited Cu-Zn-Sn films from electrolyte with concentrations of Cu (II) and Zn(II) salts in a range of 3mM, whereas the concentration of Sn(IV) was about 10 times higher (~30mM). Solution with this content provided stoichiometric precursor composition. The precursor exhibited a pillar shaped structure with a grain size of 0.5 – 1μm. The formation of the absorber layer was finished by a solid-state reaction in H_2S atmosphere. The device that was fabricated using CZTS as an absorber with Cu-poor composition (Cu:(Zn+Sn) = 0.969, Zn:Sn = 1.08) showed a conversion efficiency of 3.4%. SEM and EDX analysis indicate the presence of secondary ZnS phase.

Potassium sodium tartrate was used for preparation of electrolyte for Cu-Zn-Sn (CZT) deposition in [80]. Linear sweep scans were conducted to find a potential where all dissolved ions can be reduced and the CZT alloy was deposited at -1.6 V vs. Hg/Hg_2Cl_2. Two substrates, Mo-coated SLG and FTO, were used and results showed that the doping density of both films is $10^{15}/cm^3$. The photoelectrochemical response exhibited by the films grown on molybdenum substrate is greater than that obtained for films synthesized on FTO substrate.

1.4.3.2 SEL deposition approach

The approach of sequential electrodeposition of stacked precursor metallic layers was first time studied by J.J. Scragg et al. [81]. Cu, Sn and Zn layers were deposited sequentially on a Mo/SLG substrate using a conventional three-electrode configuration with Ag/AgCl as the reference electrode. Cu and Sn thin films were deposited at -1.14 V and -1.21 V, respectively, using a NaOH solution. Zn was deposited at -1.20 V in an acidic environment (pH = 3). Fine-grained Cu deposit was fabricated, followed by an island-like Sn layer with incomplete surface coverage; the following Zn layer covered the surface completely. Poor morphology of the deposited Sn layer was improved by changing the alkaline sorbitol electrolyte with a methanesulphonic acid electrolyte and addition of Empigen BB [45].

M. Kurihara et al. reported about deviations in photoresponse, thickness and composition over a scale of a few millimetres in annealed CZTS films [82]. The lateral inhomogeneity was caused by differences in the flux of ions to the working electrode at different points of the surface during the electrodeposition process. J.J. Scragg et al. also reported about thickness variations in precursor films [83]. The use of a rotating disc electrode helped to improve homogeneity of films and precursors of uniform thickness and with uniform composition were deposited. Modified stacking order of precursors (Cu/Zn/Cu/Sn) led, after sulphurisation, to a device with 3.2% conversion efficiency. H. Araki et al. reported that a precursor stack, where Cu and Zn are neighbours, gave the best performing devices after annealing [26].

H. Araki and G. Ma et al. [36, 84] used a $PdCl_2$ solution for coating glass/Mo substrate with Pd in order to improve adhesion of the Cu precursor. Araki also investigated the influence of Zn-rich and Sn-rich precursors on

formation of Cu_2ZnSnS_4. Both series of stacked metal films were sulphurised at 600ºC and had a single phase CZTS XRD pattern after sulphurisation; no extra phases were detected. The composition of the films was slightly Zn-rich and S-poor in case of a Zn-rich precursor and slightly Sn-rich in case of a Sn-rich precursor [36]. The effect of the Zn:Sn ratio was studied in [83]. In contrast to findings for evaporated films [85], Zn-rich precursors did not give improved conversion efficiencies: The optimal Zn:Sn ratio for best device performance was 1.0.

The record efficiency for electroplated Cu_2ZnSnS_4 device, was obtained by S. Ahmed using the SEL approach, and obtained a conversion efficiency of 7.3% [9]. Electroplated photovoltaic devices were fabricated by this group in a three-step method:

1) electroplating of metal stacks of either Cu/Zn/Sn or Cu/Sn/Zn
2) low temperature annealing (soft annealing) of these stacks at 210 – 350°C in N_2 environment in order to produce homogeneous (Cu, Zn) and (Cu, Sn) alloys
3) annealing of these well-mixed CuZn and CuSn alloys at 585°C in a sulphur atmosphere for 12 minutes yielded into a single highly crystalline Cu_2ZnSnS_4 phase.

The device had Cu-poor (Cu:Sn = 1.83, Zn:Sn = 1.35, Cu:(Zn+Sn) = 0.78) composition and was only 670 nm thick. The sulphurised film had a bimodal grain distribution. The grains next to the molybdenum back contact electrode were about 0.5 – 1.0 μm in size. The grains on top were as large as 2 μm.

1.4.3.3 Single-step electrodeposition

The single-step electrodeposition technique was employed by a number of researchers in order to form $CuInSe_2$ [86, 87, 88]. The popular complexing agent was also citric acid and mildly acidic solutions were used to facilitate the reduction of $HSeO_3^-$.

W. Septina et al. used Na_2SeO_3 as a Se source and lactic acid as a complexing agent for simultaneous deposition of $Cu_2ZnSnSe_4$ [89]. Films obtained using this electrolyte were Cu-rich and Se-poor and consisted of micron-sized granular particles homogeneously distributed on the surface. However, annealing at 550ºC resulted in further grain growth and formation of voids and cracks. S.M. Pawar et al. [90] used both sodium citrate and tartaric acid to prepare electrolytes for Cu_2ZnSnS_4 deposition. Sodium thiosulphate was added as a source of sulphur. The as-deposited films were amorphous in nature with nearly stoichiometric composition. The crystalline nature of CZTS (grain size, surface flatness) started to improve when the annealing temperature was increased from 350 to 550°C. The study of B.S Pawar showed that the crystallinity of CZTS films after thermal treatment was improved only when 0.2M $Na_3C_6H_5O_7$ was added to the precursor solution. 0.4 and 0.6M addition of sodium citrate led to a decreased intensity of diffraction peaks after annealing [91].

Table 1.2 summarises preparation conditions and results of some selected publications about CZTS(Se) films formed by the electrodeposition and annealing route. Devices with the highest conversion efficiencies (5.6 and 7.3%) were achieved by sequential electrodeposition (SEL) and in both cases preheating (soft annealing) of precursors was performed. This indicates that formation of CuSn and CuZn alloys is preferable before treating samples in Se/S atmosphere at high temperatures. Preheating at 250ºC was also done for CZT co-deposited precursors. However, a device made from this absorber resulted in an efficiency of only 1.7% [44]. CZT precursors co-deposited at 65ºC showed the presence of elemental Sn and Cu (together with CuZn and CuSn phases), and after rapid thermal annealing for 12 minutes a solar cell device with a conversion efficiency of 4.5% was built [47].

Electro-deposition approach	Electrolyte composition	Precursor composition		Phases detected	Annealing parameters	Phases detected	Composition of annealed sample			Voc, mV	Jsc, mA /cm²	FF,%	Eff, %	Remarks	Ref.
		Cu: (Zn+Sn)	Zn:Sn				Cu: (Zn+Sn)	Zn:Sn	S(Se): Me						
Co-deposition	Cu^{2+},Zn^{2+},Sn^{2+}, $Na_3C_6H_5O_7$	0.72	0.71	Zn, Sn, Cu_6Sn_5, $CuZn_2$	Two-temperature annealing, sample at 550ºC	CZTSe, ZnSe	0.83	0.85	1.27	171	28.4	35.1	1.7	Soft annealing at 250ºC	[44]
Sequential electro-deposition	Cu^{2+}, NaOH, $C_6H_{14}O_6$,SAA; Sn^{2+}, CH_3SO_3H, SAA; Zn^{2+}, hydrion buffer, K_2SO_4	0.8	1.37	Cu, Cu_5Sn_4 and Cu_4Zn	575ºC for 2 h, in graphite container with 100 mg of sulphur	CZTS	0.7	1.06	-	480	15.3	45	3.2	Stack order – Cu/Sn/Cu/Zn	[45]
Co-deposition	Cu^{2+},Zn^{2+}, Sn^{2+}, $Na_3C_6H_5O_7$	0.97	1.4	Cu, Sn, CuZn, Cu_5Zn_8	Glass container with sulphur, 600°C for 2 h	CZTS	1.0	1.1	0.89	540	12.6	46.4	3.16	Heating rate 10°C/min	[46]
Co-deposition	Cu^{2+},Zn^{2+}, Sn^{2+}, Na_3PO_4, Na_2HPO_4, $Na_2C_2O_4$, Na_2SO_3, Na_2SnO_3, KSAC	0.97	1.08	-	In H_2S at 550ºC for 2 h, heating until 200ºC 10°C/min, until 550°C 2°C/min	-	-	-	-	562.9	14.8	40.6	3.4	Sulphurisation process time ≥8 h	[54]
Sequential electro-deposition	Cu^{2+}, H_2SO_4; Sn^{2+}, H_2SO_4, additive; zinc sulphate solution	0.64	0.83	-	Glass plate with piece of S, at 600ºC	CZTS	0.96	0.95	0.9	262	9.85	37.9	0.98	$PdCl_2$ layer before electro-deposition	[36]
Co-deposition	Cu^{2+},Zn^{2+}, Sn^{2+}, $C_6H_8O_7$/$Na_3C_6H_5O_7$	0.81	1.15	Cu, Sn, CuZn, CuSn, Cu_5Sn_8	RTA At 500ºC, in quartz tube with piece of Se	CZTSe	0.84	1.21	1.13	307	38.8	37.4	4.5	ED at 65ºC	[47]
Sequential electro-deposition	Cu^{2+}, $C_6H_8O_7$/$Na_3C_6H_5O_7$, Sn^{2+}, CH_3SO_3H, SAA; Zn^{2+}, K_2SO_4	-	-	Cu_6Sn, Cu_5Zn, Cu_3Sn	In evacuated ampoule with piece of S, 580ºC for 10 min	CZTS, MoS_2	Cu = 23%	1.2	-	640	19.8	45	5.6	Preheating of precursors at 350ºC for 20 min	[171]
Sequential electro-deposition	Cu from commercially available bath with organic additives, Sn from Technistan 89 RTU, Zn^{2+} and CH_3SO_3H	0.78	1.35	-	At 585ºC for 12 min in quartz tube with piece of S	CZTS	0.78	1.35	0.92	567	22	58.1	7.3	Soft annealing at 350ºC for 30 min, bimodal grain distribution	[9]

Table 1. 2 Conditions of preparation and results of electrodeposited and annealed CZTS(Se) films

1.4.4 Non-aqueous deposition methods

The solutions obtained by dissolving any substance in a solvent other than water are called non-aqueous solutions. $Cu_2ZnSnSe_4$ and Cu_2ZnSnS_4 were prepared using choline chloride and ethylene glycol [92], pyridine [93], mixture of ethanol and 1,2-propanediol [94] and dimethyl sulphoxide [27] as non-aqueous solvents. Choline chloride and ethylene glycol at a molar ratio of 1:2 were used for dissolving anhydrous chloride salts of copper(II), zinc(II) and tin(II) [92]. The reduction potential for depositing Cu-Zn-Sn alloy was -1.15 V vs Ag/AgCl. After annealing at 450ºC for 1.5 hours no secondary phases were observed and formed CZTS films had a composition near to stoichiometry. C.M. Fella et al. used ethanol and 1,2-propanediol for preparing the solution. Moreover, the second solution with ethyl cellulose dissolved in 1-penthanol was made and added to the first one. After selenisation at 470ºC, crack free crystalline Cu-poor and Zn-rich absorber films were obtained. The conversion efficiency of the device reached 4.28%. However, a 2.5 µm thick carbon-rich layer between Mo and CZTSe was revealed [94]. In another report from the same group, monoethanolamine was added instead of ethylcellulose, and through this the thickness of the carbon layer was significantly reduced, though it was still present [95].

Preparation of kesterite thin films from metal salts using either thioacetamide (TAA) or thiourea as sulphur source was employed in [27, 93]. Pyridine was used as a solvent. Two series of solutions containing 3.5-fold and 5-fold of a stoichiometric amount of TAA were prepared. After low-temperature of sulphurisation, it was found that the average grain size is larger in case of 5-fold containing TAA solution. However at higher temperatures crystallite diameters in both cases were in the range 100 – 160 nm [93]. Powders exhibited Cu-poor and Zn-rich nature, despite of stoichiometric precursor solution. In both cases single–phase CZTS films were fabricated. The disadvantage of this method was the application of the toxic compounds pyridine and thioacetamide, where the latter one belongs to class 2B carcinogen group[2].

Sulphoselenides were fabricated by selenisation of doctor-blade coated CZTS precursors at 540ºC (for 6 minutes) [27]. Metal salts and thiourea were dissolved in dimethyl sulphoxide followed by magnetic stirring for several hours at room temperature. According to the Raman results, except for the CZTSSe phase, $MoSe_2$ and ZnSe phases were detected. The absorber layer was Se-rich and S-poor and had carbon residues of below 3%. The conversion efficiency of the device was 7.5%.

[2] Group 2B: the agent (mixture) is possibly carcinogenic to humans. The exposure circumstance entails exposures that are possibly carcinogenic to humans [170].

1.5 Thermal treatment of precursors

Annealing of precursors in different reactive (S, Se, SnS, SnSe, Ar, H_2S) and/or in inert (vacuum, N_2, Ar) atmospheres improves morphology and composition of absorber materials substantially. This is why thermal treatment is commonly used as the second step in fabrication of high-quality materials for photovoltaic devices. The heating step provides the required energy needed for atoms to diffuse to their corresponding equilibrium positions, which might mean re-crystallization of starting materials and changes of defect structures.

Factors that influence the process include:

- Temperature and annealing time
- Composition of initial precursor films
- Heating up and cooling down rates
- Composition of a vapour phase

1.5.1 Conventional furnace annealing

Although traditional sulphurisation and selenisation are not providing the possibility of adjusting heating up and cooling down rates, these two methods are widely used, and many studies demonstrated the formation of crack-free, continuous single-phase CZTS(Se) absorber layers after traditional sulphurisation/selenisation. Sulphurisation/selenisation can be done using sulphur/selenium powder or pellet which is inserted into a graphite crucible, glass container or quartz tube together with the precursors [45, 46, 82, 92, 96]. Another possible way is to anneal films using hydrogen sulphide/selenide flow [17, 69]. In order to eliminate oxygen residuals, the heating system is usually filled either with Ar or N_2+H_2 (or pure N_2) gases prior the annealing.

There are only a few studies that were conducted to follow the kesterite phase formation during heat treatment [76, 97, 98]. R. Schurr demonstrated results from in-situ XRD measurements of the annealing process of Cu-rich and Cu-poor precursors. It was shown that the crystallization of kesterite is determined by the precursor's composition. Temperature of formation of binary and ternary sulphides differs, which leads to two different pathways of CZTS synthesis. However in both cases formation is completed by a solid state reaction between Cu_2ZnSn_3 and ZnS. A. Weber et al. [97] used the same process of in-situ XRD during annealing of co-electroplated Cu-Zn-Sn precursors. They found that above 400ºC a broad peak, which can be related to Cu_2ZnSnS_4, appeared. Further heating to 550ºC led to a reduction of the Cu_2ZnSn_3 phase peak intensity and to the complete formation of CZTS. In case of selenisation of Sn/Cu/Zn stacked precursors, the formation of $CuSe_2$ as the first step took place (at 250ºC). These results are in agreement with other publications, where the presence of copper binaries was detected at the lower temperatures of selenisation [99, 100]. Ternary Cu_2SnSe_3 and quaternary

$Cu_2ZnSnSe_4$ phases were revealed after annealing at 300ºC. Selenised films at 470ºC consisted of the dominating CZTSe phase and phases of ZnSe and $MoSe_2$ in smaller quantities [99]. The formation of CZTSe absorber material at temperatures in the range of 350 – 400ºC was described in [101]. The dependence of the CZTS band gap on the selenisation temperature was studied by S. M. Pawar et al. [90]. The decrement in band gap energies from 2.70 eV to 1.50 eV with the increase in annealing temperature has been observed, which is in agreement with reported E_g values for CZTS thin films [83, 92].

Besides the reports on formation pathway of CZTS, other aspects of annealing and its influence on absorber parameters were studied as well, including comparison of annealing in sulphur and/or H_2S vapour, two-temperature zone selenisation, growth of interfacial $MoSe_2/MoS_2$ layer, order of layers in stacked precursors, soft annealing method. The most important results will be briefly mentioned below.

Annealing in sulphur or H_2S containing ambient is a widely used way to convert metallic precursors to compound semiconductors. Sulphur containing vapour is preferable compared to highly toxic H_2S. However, results indicate that annealing in H_2S produces more uniform films which contain much larger grains when compared to annealing in sulphur atmosphere. Despite reduction in film integrity, the EQE spectrum showed that CZTS of better crystalline quality was formed through annealing in H_2S [102]. The group of Katagiri produced a CZTS device with a conversion efficiency of 6.77% using sulphurisation in H_2S containing N_2 atmosphere [59].

Annealing in SnS(Se) and S(Se) atmosphere prevent the decomposition reaction of the CZTS(Se) at high temperatures and fill up missing tin into the CZTS film. This annealing process is gaining more attention in the scientific community as it facilitates composition control and allows to deposit only two elements in precursor films [55], hence simplifying the preparation of precursors. The effect of the composition on CZTS(Se) devices prepared by annealing in SnS and S_2 gas atmosphere of co-sputtered precursors was investigated by V. Chawla and B. Clemens [103]. Cu_2S appeared to be an exceptionally detrimental phase for achieving a highly efficient device. Although the Se:S ratio had almost no effect on extraneous phases or on the efficiency of devices, it had a significant impact on the carrier concentration observed in the device. The carrier density increases with decreasing selenium content.

K. V. Gurav et al. investigated the effect of soft annealing treatment on sulphurised films. Prior to main sulphurisation at 580ºC in H_2S, metal CZT precursors were soft-annealed in Ar atmosphere for 1 hour at 250, 300 and 350ºC [104] . Results indicate a strong dependence of CZTS formation on the soft annealing temperature. A temperature of 300ºC was shown to be favourable in order to form single CZTS layers with improved crystallinity.

Some research groups prefer two-temperature zone sulphurisation (selenisation) to conventional isothermal annealing. Samples are heated up in a furnace where the temperature of the Se source and the reaction zone can be

independently controlled [105]. Substrates are conventionally heated in the higher temperature zone compared to the Se containing zone. C. M. Fella et al. [29] studied the conversion process of metal precursors into the kesterite compound in the two-temperature zone annealing process. A rapid increase in the $MoSe_2$ content was observed for Se zone temperatures of 370ºC [29, 106]. It was also found that the decomposition reaction of kesterite takes place at substrate temperatures higher than 600ºC due to Sn loss via formation of volatile SnSe phase. Densely packed and crack free crystalline Zn-rich films were formed using a substrate temperature of 470ºC.

Co-electrodeposited CZT precursors were selenised in a two-temperature zone closed quartz reactor where the Se source temperature reached 380ºC and the substrate varied from 300 to 550ºC. Before the selenisation, precursors were soft-annealed at 250ºC in vacuum. Elemental metals were converted to Cu_6Sn_5, CuSn and CuZn alloys after soft annealing [44]. Although the annealing in Se atmosphere at 550ºC produced almost stoichiometric films, the additional phase on the Mo/CZTS interface still remained which could cause an increase in series resistance.

The formation of $Mo_xS(Se)_y$ at the Mo/CZTS(Se) interface has a substantial impact on the efficiency of solar cells. Many research groups observed that the $MoSe_2$ interfacial layer has a positive effect on $Cu(InGa)Se_2$ device performance [107, 108, 109]. Discussions appeared in case of CZTS solar cells, as some reports contain information that $Mo(S)Se_2$ layer is detrimental for obtaining a highly efficient solar cell, whereas other groups consider it necessary because it provides an ohmic contact to CZTS(Se). B. Shin studied the formation of $MoSe_2$ at different temperatures and partial Se pressures. It was shown that the $MoSe_2$ thickness reduces with decreasing annealing temperature and improved efficiency is seen for less thick $MoSe_2$ layers. When the Se pressure is varied, the best efficiency of 6.36% was obtained for a device with a less than 10nm thick $MoSe_2$ layer and at decreased partial pressure (~0.8 torr). TiN used as diffusion barrier on top of the Mo back contact allows stopping rapid growth of the $MoSe_2$ layer. However, the best device with a conversion efficiency of 8.9% was produced with a ≈ 220 nm thick $MoSe_2$ layer [58].

Another phase which has recently started to gain interest is ZnSe(S). As described earlier, the preferred precursor composition is Zn-rich because this results in better conversion efficiencies of devices due to probable suppression of formation of highly conductive $CuS(Se)_x$ phases. In the majority of studies Zn-rich precursors led to segregation of the ZnSe(S) phase after thermal treatment. Only some investigations were conducted in order to study the influence of this phase on the parameters CZTS(Se) solar cells. In studies of co-evaporated CZTSe by NREL, it was demonstrated that a thin Zn-rich cap on the surface of the absorber layer enhances the open-circuit voltage, the short-circuit current and the fill factor [110]. W. C. Hsu in cooperation with the group from NREL reported later that not every absorber that is very rich in ZnSe is able to yield good efficiency. It is necessary that ZnSe grains are at the back of the absorber [111, 112]. Large amount of ZnSe grains on the front of the CZTSe

layer are detrimental to device performance and lead to a conversion efficiency decrease from 8.3 to 6.5% [113].

1.5.2 Rapid thermal annealing

Rapid thermal annealing is generally used as a manufacturing process during which silicon wafers are heated to high temperatures (up to 1200°C or greater) on a timescale of several seconds or less [114]. For quaternary and ternary compounds this process is used to convert metal precursors to chalcogenide semiconductors and/or to densify deposited films. One of the advantages of this method is rapid heating and cooling of samples, which is energy and time saving. High-power infrared lamps that are built in the furnace provide an energy density 10 to 15 times higher than from conventional heating elements [115]. Rapid cooling is available with water cooling of the furnace body and additional gas cooling mechanism [115].

The temperature of the sample can be controlled by combining furnace and temperature controller. To keep the annealing process running as close as possible to a desired set point, a proportional integral derivative (PID) controller can be used. A PID controller calculates an "error" value from the difference between the measured process variable and the desired set point. The controller attempts to minimize the error by adjusting the process control outputs. Detailed information on PID controllers can be found elsewhere [116].

After adjusting the PID parameters, heating and cooling rates have to be determined. For CZTS(Se) formation very fast heating and cooling rates are preferable as it is assumed that after rapid cooling, phases detected in the film are representative of the phases that were present at the time of the quench [19].

Cheng et al. suggests that during the conventional annealing process the Cu_2SnS_3 phase forms before the quaternary phase and converts into CZTSe at temperatures above 500ºC [117]. Sn losses through desorption of SnSe from CZTSe and formation of Cu_2SnSe_3 phases at high temperatures were reported in many articles. These losses can hinder the formation of a dense CZTSe layer with good homogeneity and desired composition. Heating time of conventional furnace annealing is longer compared to the RTA process, therefore the ternary compound Cu_2SnSe_3 would form first as a stable phase and more Sn loss occurs during annealing. Cu_2SnSe_3 did not convert to CZTSe completely at 500ºC and remained as the secondary phase in the film. However, from room temperature up to 500ºC, RTA can only take a few seconds and pass the intermediate temperature ranges rapidly, hence facilitating the formation of the desired phase. RTA assists the rapid diffusion of each element and leads to homogenous films [47].

R. Juškenas compared to annealing approaches [77]: electrodeposited precursor layers were annealed 1) with a slow temperature increase up to 200ºC for 20 minutes and afterwards with an increase of 10ºC/minute to 500ºC and 2) fast 20ºC/minute increase up to 500ºC followed by keeping samples for 120 minutes at that temperature. Slow annealing led to the formation of a rough CZTSe layer containing a large number of voids and other phases (Cu_2Se and

SnSe and possibly $Cu_{6.25}Sn$ and Cu_5Zn_8). A lesser amount of phases and no evidence of Cu_2Se and SnSe was found in the CZTSe films formed according to the fast annealing approach.

S. M. Pawar et al. [28] performed sulphurisation of sputtered metallic precursors (750 nm thick) at temperatures ranging from 500 to 580ºC for 5 minutes. It was shown that annealing at 500ºC leads to incomplete sulphurisation of the film as the S:Me ratio is 0.85. A ratio of S:Me equal to 0.99 was achieved at an annealing temperature of 580ºC. On the contrary, electrodeposited metallic precursors with a thickness of 1500 nm were sulphurised by RTA for 10 minutes at 500ºC and it was demonstrated that fully sulphurised films can be obtained already at this temperature [78]. The explanation can be found by looking at the way of precursor preparation: One approach was SEL by sputtering and the other was co-electrodeposition of metals, where the precursor density is significantly lower than the density of each layer separately thus allowing for faster incorporation of sulphur in the precursor film.

Reactively sputtered Cu-Zn-Sn-S precursors were annealed for 3 minutes at 550ºC [118]. The sample temperature rose to 550ºC within 3 minutes. Cooling down to below 200ºC was done within 2.5 minutes. According to Raman measurements, sputtered precursors already contained a CZTS-like phase with a high defect density and a functioning device with 0.31% efficiency could subsequently be built. Drastic increase in grain growth, QE results, V_{OC} and J_{SC} was observed after a short annealing procedure. The ZnS phase was detected in the annealed film using 325 nm excitation wavelengths for Raman measurements. A device with 4.6% conversion efficiency was fabricated.

1.6 Summary of the literature overview and aim of the study

Polycrystalline chalcopyrite-type Cu_2ZnSnS_4 and $Cu_2ZnSnSe_4$ thin films are promising candidates for production of low-cost solar cells. Since these compounds are composed from abundant elements they can be considered as a suitable alternative to highly-efficient $Cu(In,Ga)(Se,S)_2$ absorbers, that are potentially limited by the indium price and/or availability. However, investigations of the phase diagrams of quaternary systems have shown that CZTS(Se) as a single phase exists only within a rather narrow range of compositions. According to theory even a 1 – 2% compositional variation could lead to the formation of secondary (binary or ternary) phases in the films. Therefore it is challenging to fabricate single phase $Cu_2ZnSnSe_4$ and Cu_2ZnSnS_4.

Non-vacuum methods for absorber layer deposition appear to be beneficial with regard to capital expenditure and materials costs. Electrodeposition is a promising technique for low-cost solution preparation of semiconductors.
Metallic and non-metallic precursors were obtained using preferentially citrate ions as ligands in ED solution.

The results showed that electrodeposited non-metallic films are amorphous and poorly adherent, whereas metallic precursors are polycrystalline and have a dense and well-defined structure. The as deposited precursor layers typically have different multiphase compositions dependent on either co-deposition of metals and/or stacked metal layers was used or simultaneous deposition of Cu-Zn-Sn-S was used. In both cases the annealing step was essential for final CZTS formation with improving the crystallinity, and correcting the phase composition in the CZTS film.

Several studies were conducted where different heat treatment procedures were used: annealing in two-temperature-zone reactor, rapid thermal annealing, isothermal annealing with additional S(Se) source or in H_2S gas flow; however, only few results demonstrated the formation of well-adherent, homogenous and smooth CZTS(Se) layer.

Cu_2ZnSnS_4 single phase material was obtained at 550°C using conventional annealing in an electric furnace. $Cu_2ZnSnSe_4$ films were formed at 470ºC and consisted of the dominating CZTSe phase and additional phases of ZnSe and $MoSe_2$ in smaller quantities. Both CZTS and CZTSe films were homogenous and could contain copper binaries on the surface which were subsequently removed by etching in KCN.

The loss of Sn during annealing impedes the thorough control of film composition and film homogeneity. At elevated temperatures (≥300°C) Sn forms SnS(Se) phases which are highly volatile. To avoid Sn loss by decomposition of quaternary compounds during annealing, it is crucial to keep the sulphur (selenium) pressure high using tin dichalcogenides or elemental sulphur or selenium containing atmospheres. Annealing in H_2S flow can also provide a sufficiently high partial pressure of S and move the CZTS decomposition reaction in the direction of CZTS formation.

Films with Zn excess and Cu deficiency (Cu:(Zn+Sn) ≈ 0.85; Zn:Sn ≈ 1.1 – 1.2) gave so far the best results.

The objectives of the present doctoral thesis were:

Development of a technology with the aim to get homogenous and uniform CZTS(Se) absorber films for solar cells using electrodeposited layers; by

- development of electrolytes for deposition of metal alloys (Cu-Zn, Cu-Sn) and co-deposition of all elements (Cu, Zn, Sn) together with a chalcogenide source (sulphur) in order to obtain Cu-Zn-Sn or/and Cu_2ZnSnS_4 precursor films.
- finding the optimized annealing conditions for converting the electrodeposited precursor layers finally into high quality single phase Cu_2ZnSnS_4 and/or $Cu_2ZnSnSe_4$ semiconductor thin films.

2 EXPERIMENTAL

This chapter gives an overview of the main experimental processes used during this PhD study. In the first section (2.1) the techniques and reagents used for electrolyte preparation as well as the conditions for electrodeposition are described. The second section (2.2) describes the post-deposition treatment techniques, whereas the third section (2.3) provides an overview of the characterization methods used in this study. Further detail on the experimental aspects can also be found in the publications [I-V].

2.1 Electrodeposition of precursor films

Electrodeposition of precursor layers was performed potentiostatically, i.e. at constant potential. In the work published in articles [III-V], precursors were prepared using a Wenking Bank PGstat 3440 potentiostat. Gamry 3000 potentiostat was employed for experiments which were described in articles [I,II]. A conventional three-electrode electrochemical cell was built for films deposition and a silver chloride electrode (Ag/AgCl, 3M KCl, 0.210 vs SHE) was used as reference electrode in articles [I,II,V] , in articles [III,IV] Mercury/Mercurous Sulphate Reference Electrode (Hg/Hg_2SO_4, saturated K_2SO_4 0.651 vs SHE) was employed. The counter electrode (anode) consisted of platinum gauze with a larger active surface area than the cathode. In some experiments, a brass plate was used as an anode in order to prevent fast loss of Cu and Zn contents in the solution during deposition [IV,V]. Working electrodes (cathode) were molybdenum (~1 μm) covered soda-lime glass substrates with a sheet resistance of 0.2 – 0.3 Ω/sq. Commercially available ITO/glass substrates were used in this work as well [III].

All the experiments were carried out at room temperature (20 – 22°C) using Milli-Q water. Aqueous solutions comprising copper sulphate, zinc sulphate and tin chloride (sulphate) reagents were mixed. The metallic precursors were prepared in two different routes of sequential electrodeposition:

1) Sequential electrodeposition of Cu-Zn (brass) and Cu-Sn (bronze) alloys [V]
2) Sequential electrodeposition of Cu-Zn (brass) alloy and Sn [I, II,IV]

whereas the approach of co-deposition of all metals and sulphur was employed in publication [III].

Potassium (or sodium) pyrophosphate as well as sodium citrate acting as sources of ligand ions was used in concentrations varying from 0.1M to 0.6M for electrodeposition of metals or metal alloys. Potassium thiocyanate was tested for simultaneous Cu-Zn-Sn-S deposition. The pH of electrolytes was in a range of 6 to 10 dependent on the composition of the solution. Details of electrolyte compositions used in different studies are shown in Table 2. 1.

First solution for precursor preparation –containing *pyrophosphate ions* [V]

⇩

Electro-lyte	$K_4P_2O_7$	$Na_4P_2O_7$	$CuSO_4$	$ZnSO_4$	$SnSO_4$	Hydro-quinone	E_i,V vs Ag/AgCl
Cu-Zn layer	0.6M	-	2mM	20mM	-	-	-1.4 to -1.44
Cu-Sn layer	0.6M	-	2mM	-	10mM	0.1M	-1.3

Second solution for precursor preparation –containing *pyrophosphate ions* [IV]

⇩

Electro-lyte	$K_4P_2O_7$	$Na_4P_2O_7$	$CuSO_4$	$ZnSO_4$	$SnSO_4$	Hydro-quinone	E_i,V vs Hg/Hg_2SO_4
Cu-Zn layer	0.4M	0.3M	20mM	20mM	-	-	-1.84 to -1.88
Sn layer	0.4M	0.3M	-	-	10mM	-	-1.75

Solutions with *pyrophosphate* and *citrate ions* [I, II]

⇩

	$Na_3C_6H_5O_7$	$Na_4P_2O_7$	$CuSO_4$	$ZnSO_4$	$SnCl_2$	Hydro-quinone	E_i,V vs Ag/AgCl
Cu-Zn layer	0.1M	-	2mM	15 – 20mM	-	-	-1.2 to -1.25
Sn layer	-	Saturated sol-on	-	-	20mM	-	-0.9 to -1.3

Solution with *thiocyanate ions* [III]

⇩

	KSCN	$NaC_2H_3O_2$	CuCl	$ZnCl_2$	$SnCl_2$	$Na_2S_2O_3$	E_i,V vs Hg/Hg_2SO_4
Cu-Zn-Sn-S	4M	0.4M	3.6mM	3.2mM	1.2mM	1mM	-1.86

Table 2. 1 Composition of electrolytes for electrodeposition of metallic films and Cu-Zn-Sn-S films used in different parts of studies

Cyclic voltammograms were made to define the behaviour of metals deposition and to find suitable redox potentials for all metals in different media. The scan rate was kept constant and equal to 20 mV/s.

Rotating disc electrode (RDE) with a CTV 101 controller from Radiometer Analytical was used as a working electrode in article [I] and [II].

2.2 Post-deposition treatment

This section is divided into two subsections; one on heat treatment of precursor layers in conventional tubular furnace and the other subsection on treatments in infrared furnace (RTA).

2.2.1 Annealing in electric tubular furnace

After electrodeposition, the metallic precursors were annealed in an electric tubular furnace (*Figure 2. 1 a*). The heat treatment was carried out in sealed quartz ampoules at isothermal conditions. Annealing was done in small (Ø 1 cm), around 5 cm long, ampoules with an added Se piece. The temperature along the whole ampoule length was kept constant. Elemental Se (30 mg) as selenium source was placed into one end of the ampoules and electrodeposited precursors in the opposite end. Temperature determines the Se vapour pressure in the ampoule if the amount of Se is sufficient to saturate the empty volume of the ampoule. After annealing, the ampoules were taken out of the furnace and left to cool down to room temperature. A description of the thermal treatment procedure is given in articles [II,IV,V]. Annealing in Se vapour atmosphere was performed at temperatures varied from 450 to 560°C. The duration of post treatment varied from 20 to 60 minutes. Se vapour pressure dependent on temperature is shown in *Figure 2. 1 b*.

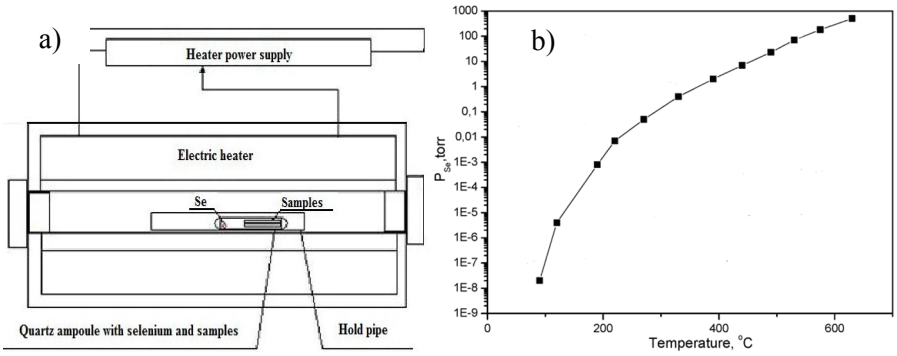

Figure 2. 1 a) Furnace for selenisation experiments, b) dependence of Se vapour pressure on temperature (constructed on the base of data Я. И. Герасимов, А. Н. Крестовников, А. С Шахов , Химическая термодинамика в цветной металлургии. Металлургия, p.23, 1966)

2.2.2 Rapid thermal annealing (RTA)

A tubular type infrared furnace with elliptical reflectors and four infrared lamps as heating sources (Figure 2. 2) was used for rapid thermal annealing (RTA). Thermal treatment was carried out in H_2S atmosphere. The powerful infrared lamps for sample heating allowed fast heating and fast cooling in a precise temperature range.

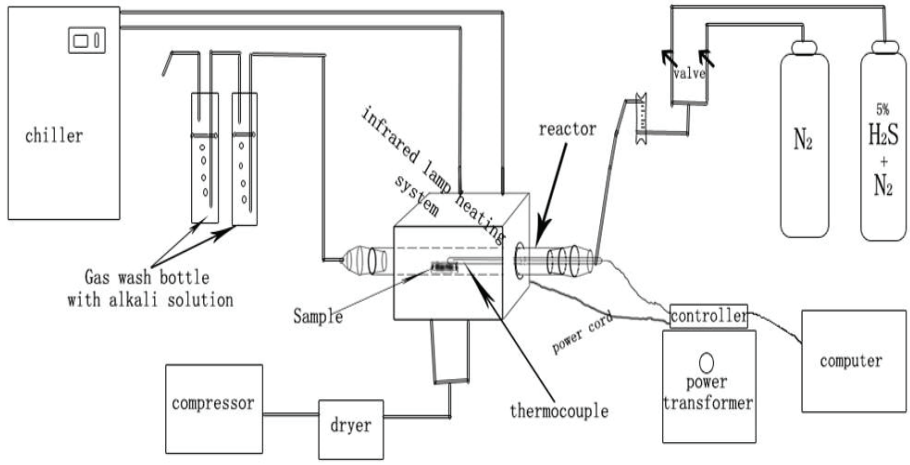

Figure 2. 2 Schematic system for RTA

The sulphurisation process of metallic precursors included three steps. First, a 15 minutes purging cycle with N_2; second, heating up and cooling down the furnace with a defined programme; and third, purging again with N_2. Sulphurisation was carried out at 470°C, 500°C and 550°C in a tubular furnace in $H_2S + N_2$ atmosphere with a H_2S concentration of 5%. The heating rate was varied between 2°C/s and 3.3°C/s. During rapid annealing at 500°C the samples reached temporarily a temperature of up to 520°C. After annealing, samples were cooled down to 25°C for 5, 8 or 15 minutes. Short time overheating was noticed in all RTA experiments and the samples reached temporarily a maximum temperature of 490°C and 570°C [I,III].

The PID control of the furnace system was set to proportional Band (P), Integral Time (I), and Derivative Time (D) parameters of 15, 30 and 10 respectively. For adjusting the temperature and PID parameters, a Temperature Controller TPC5000 was used.

2.3 Characterization of Cu_2ZnSnS_4 and $Cu_2ZnSnSe_4$ thin films

For characterizing the obtained precursors and formed Cu_2ZnSnS_4 and $Cu_2ZnSnSe_4$ thin films, the analytical techniques listed in Table 2. 2 were used. More detailed information regarding the equipment and measurements can be found in the experimental sections in the publications [I – V].

Properties	Analytical method	Apparatus	Ref.
Elemental Composition	Energy dispersive x-ray Spectroscopy (EDX)	Röntec EDX XFlash 3001 detector	[I-V]
		Hitachi 1000	
Morphology	High resolution scanning electron microscope (SEM)	ZEISS HR SEM ULTRA 55	[I-V]
		Hitachi 1000	
Phase composition	Room temperature (RT) Micro Raman spectroscopy (Raman)	Horiba's LabRam HR spectrometer	[I-V]
Phase composition	X-Ray Diffraction (XRD)	Rigaku ULTIMA IV diffractometer	[IV,V]
		Bruker D5005 diffractometer	[I-III]
Surface roughness	Atomic force microscope (AFM)	Bruker Nanoscope V	[I]
Redox potentials of Me, electrochemical window	Cyclic voltammetry (CV)	Wenking Bank 3440 potentiostat	PhD thesis
		Gamry 3000, Potentiostat	
Determination of current efficiency	Polarography	Metrohm 746 VA Trace Analyzer	PhD thesis

Table 2. 2 Overview of analytical techniques and apparatus used in this work

3 RESULTS AND DISCUSSION

3.1 Peculiarities of the electrodeposition approach of stacked alloys and metals

As described in the experimental section of this work, for this investigation two different routes for metallic precursor preparation were applied. In the earlier work [V] the approach of stacked Cu-Sn on Cu-Zn layer deposition followed by selenisation was used. In the following publications [I,II,IV] a simplified method was adopted: deposition of a pure Sn layer on a Cu-Zn layer followed by annealing.

In both cases the interaction between the stacked layers had to be taken into account. Compared to the SEL deposition in which three layers were deposited separately (development of three electrolytes), or to the simultaneous co-deposition of all metals with chalcogenide (development of a complex electrolyte), the new route is in principle much simpler, but certain drawbacks became obvious: the main disadvantage of both approaches was a loss of zinc and as a consequence the variation in Cu:Zn ratio after Sn (Cu-Sn) deposition. One possible explanation of loss of Zn can be attributed to the dissolution of Zn in the tin (or/and copper) containing electrolytes. Zn as a more active metal than Sn or Cu reacts with the $SnCl_2$ (or/and $CuSO_4$) electrolyte and a displacement reaction consequently occurs. Before applying this method preliminary experiments were done in order to control the Zn loss. Cu-Zn layers with different Zn concentrations were deposited and the composition was measured by EDX. After electrodeposition of Sn the composition was determined again. The diagram (*Figure 3. 1*) presents the results of the precursor compositions before and after Sn deposition.

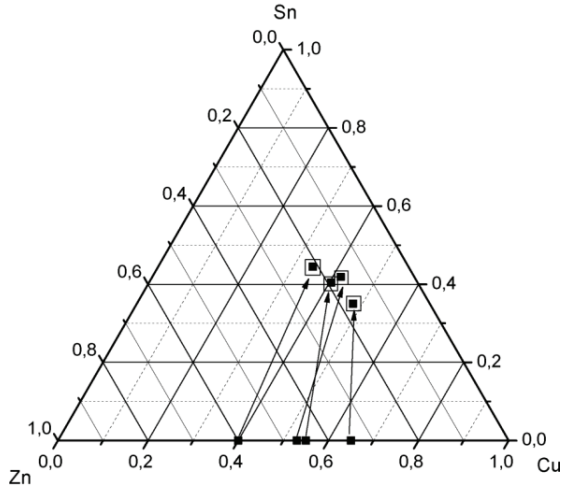

Figure 3. 1 Variations in precursor compositions before and after tin electrodeposition. Solid dots on Zn-Cu line are the initial composition of Cu-Zn layers. The arrows show the composition change of the same layers after tin deposition.

As it can be seen from the diagram, initially the Zn-richest sample (60 at%) contains the highest amount of Sn. In contrast, the sample with the lowest Zn amount after Sn electrodeposition contains the least amount of Sn. It can be concluded that the more Zn is present in the initial film the more active the Sn deposition occurs.

Cu concentration is decreasing (after Sn deposition) in accordance to the initial Cu-Zn layer composition, while the Zn concentration is parallel to the line around 20 at% and stays around this for almost all precursors and only precursor with the highest amount of Zn in initial layer results in a higher concentration of Zn after Sn deposition. Following above given it can be concluded that in order to get Cu-poor precursor a very Zn-rich (40 – 50 at% of Zn) initial Cu-Zn layer has to be deposited.

3.2 Current efficiency of the electrodeposition process

For determination of the current efficiency of electrodeposited layers two methods have been employed. At first a convenient weight method was used: substrate was measured before and after electroplating using an accurate balance with an accuracy of 0.1 mg. This method was used in the articles [III-V] and the current efficiency for Cu-Zn deposition was measured to 79% and for Cu-Sn to 85%.

The polarography method was also applied for qualitative and quantitative analysis of metal ions (here specifically for Cu^{2+} and Zn^{2+}) [I,II]. Electrodeposited films were dissolved in acid, afterwards the background electrolyte was added and measurements occurred in a given potential range at the indicator electrode, a dropping mercury electrode (DME). The polarographic curve demonstrated, where the reduction of the presented substance in solution occurred, by reflecting the position of the wave with respect to the potential. Under a set of defined experimental condition, each ion has its own characteristic half wave potential which is the basis of qualitative polarographic analysis [119].

Quantitative polarographic analysis was based on the linear linkage between the diffusion current and bulk concentration of the electroactive species. In general, the most precise measurements of concentration are carried out by constructing a calibration curve with a set of standard solutions. Standard addition and internal standard methods are also used in concentration measurements. They are implemented in obvious ways and reach a typical precision of a few percent [120]. In this work the second way of addition of two standard solutions of each metal ion (Cu^{2+} and Zn^{2+}) has been employed. The disadvantage of this method was that Mo also dissolves in acid and renders to perform Sn analyses since peaks of these elements overlap. The efficiency of Sn deposition was also calculated using the traditional weight method. According to the polarography results the current efficiency of the Cu-Zn layer deposited from the electrolyte containing citrate ions as ligands is 89%.

3.3 Electrochemical deposition of Cu-Zn (brass) and Cu-Sn (bronze) stacked films

This section describes the first approach of precursor preparation (Cu-Sn layer on Cu-Zn), used in publication [V]. The process steps were organized with the aim to ensure reliable conditions for electrodeposition of metallic thin layers. Preliminary investigations were directed to electrolyte compositions for deposition of Cu-Zn and Cu-Sn alloys with suitable element composition and morphological properties.

Electrodeposition of multicomponent layers requires the preparation of complex electrolytes. The complications in choice of electrolyte usually come from the difference of electrochemical properties of deposited components in electrolyte and in this instance they are rather distinct. A large variety of solutions (citrate, rhodanide, cyanide etc.) was proposed in literature for electrodeposition of brass (Cu-Zn) and bronze (Cu-Sn) alloy layers. Cyanide is most appropriate but its high toxicity raises occupational safety and environmental concerns. A reasonable solution without any exploitation risks and with acceptable properties is the pyrophosphate electrolyte. The special feature here is its strong negative deposition potential causing a considerable hydrogen evolution that could seriously affect current efficiency and the quality of deposits. All these features were preliminary aspects of the research and had to be taken into the account before preparation of the electrolytes.

3.3.1 Cyclic voltammetry of electrodeposited films

The process for deposition of alloys Cu-Zn and Cu-Sn in pyrophosphate electrolyte was developed and used in commercial industry [121]. The complication of these solutions lies in the fact that different brighteners and a variety of other additives are used that counteract the aim to create simple water based electrolytes for facile and high purity metal alloy deposition. Therefore a simplified composition of the electrolyte was examined: alloys were deposited from alkaline solutions containing metal salts of Cu^{2+}, Zn^{2+} for Cu-Zn deposition and Cu^{2+}, Sn^{2+} ions for Cu-Sn deposition respectively. The 0.6M $K_4P_2O_7$ served as a source of $P_2O_7^{4-}$ ligand ions. The pH value was adjusted to 9.5 – 9.7.

Initial analysis of electrodeposition of metals was performed, where the reduction potentials of elements were calculated using the Nernst equation. Standard deposition potentials were found from Pourbaix diagrams [122], and binding constants of presented complexes and concentrations of elements and ligands were also taken into account.

Stability (binding) constants usually used to characterize complexes that are present in the solution. An example for deriving the stability constant (K_s) in case of copper complexation is shown below:

R 3. 1

$$Cu^{2+} + 2P_2O_7^{4-} \rightarrow Cu(P_2O_7)_2^{6-}$$

Eq 3. 1

$$K_s = \frac{[Cu(P_2O_7)_2{}^{6-}]}{[Cu^{2+}] + [2\,P_2O_7{}^{4-}]}$$

where K_s is a stability constant. The larger the stability constant, the higher the proportion of complexed metal complexes, that exist in the solution.

The stability constants for pyrophosphate ligands complexed with Cu and Zn are shown in Table 3. 1. As can be seen from the table, Cu(II) can be complexed in as $CuP_2O_7^{2-}$ and $Cu(P_2O_7)_2^{6-}$. It was reported in literature that in concentrated solutions $Cu(P_2O_7)_2^{6-}$ is the predominant phase. The ratio $[CuP_2O_7^{2-}]$:$[Cu(P_2O_7)_2^{6-}]$ increases with dilution and $CuP_2O_7^{2-}$ predominates in extremely diluted solutions [123, 124, 125]. In the experiments of this PhD work, the copper concentration was 0.005M for pure Cu layer deposition and 0.002M for Cu-Zn alloy deposition. The concentration of pyrophosphate was 0.6M.

According to literature the predominant species in this solution types is $CuP_2O_7^{2-}$ [123]. Stability constants for this Cu and for Zn species are almost equal. Therefore, for Cu-Zn alloy deposition a higher concentration of Zn^{2+} ions is needed in the electrolyte in order to ensure the desired Zn composition in the film. In this work the concentration of Zn^{2+} ions was tenfold higher than that of Cu^{2+} ions.

	Stability constant, K_S	**log K_S**	**Ref.**
$CuP_2O_7^{2-}$	5×10^6	6.7	[126]
$Cu(P_2O_7)_2^{6-}$	1×10^9	9	[126]
$Zn(P_2O_7)_2^{6-}$	2.9×10^6	6.46	[126]

Table 3. 1 Stability constants for pyrophosphate ion and Cu(II) and Zn(II) species

Using the above given data and substituting this together with standard potentials and concentrations of constituents in equation Eq 1. 4, the reduction potential for metals deposited in the actual conditions can be calculated. In Table 3. 2 the calculated values of reduction potentials are given.

Type of ions	**Ligand**	**E vsAg/AgCl, V**
Copper (II) ions	$P_2O_7^{4-}$	-0.57
Zinc (II) ions	$P_2O_7^{4-}$	-1.40

Table 3. 2 Calculated reduction potentials for Cu(II) ions and Zn(II) ions in alkaline media

Cyclic voltammetry was performed to find out experimentally the reduction potentials of Cu(II), Zn(II) and containing both Cu(II) and Zn(II) ions from electrolytes used in this work. The results are shown in *Figure 3. 2*.

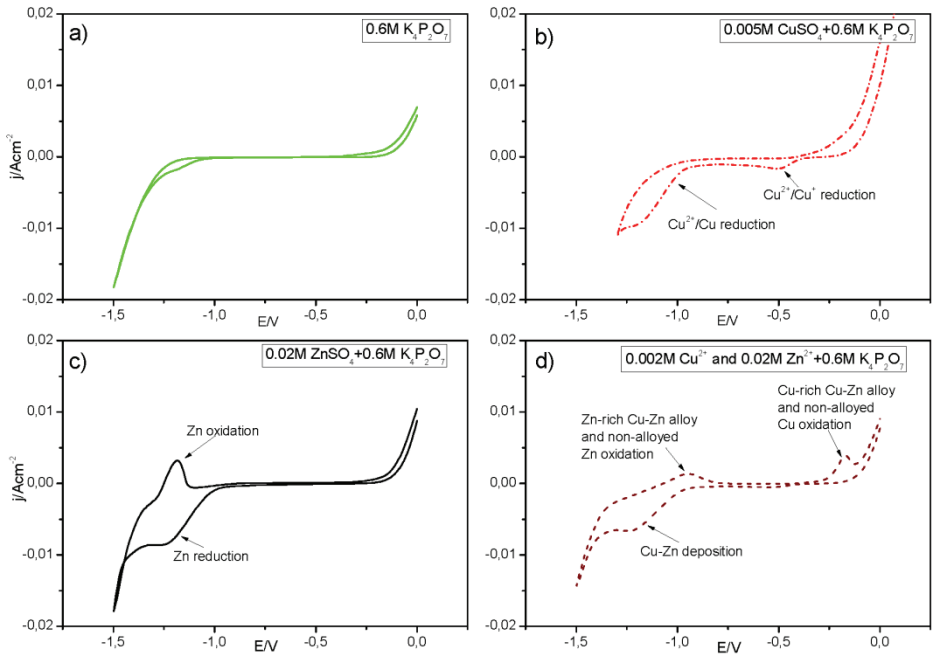

Figure 3. 2 Cyclic voltammetry curves on Mo electrode for a) 0.6M $K_4P_2O_7$; b) 0.005M Cu^{2+} and 0.6M $K_4P_2O_7$; c) 0.02M Zn^{2+} and 0.6M $K_4P_2O_7$; d) containing both 0.002M Cu^{2+} and 0.02M Zn^{2+} ions in 0.6M $K_4P_2O_7$ solution, vs. Ag/AgCl, scan rate 20 mV s^{-1}

SLG/Mo was immersed in solution containing 0.6M potassium pyrophosphate to determine the electrochemical window of deposition. The pH value reached 9.7. Hydrogen starts to evolve already at -1.08 V; however, drastic hydrogen evolution begins only at -1.25 V. Formation of small bubbles on the electrode surface was observed. In positive scan direction the electrochemical window is limited by oxidation of Mo which starts at -0.32 V.

The cyclic voltammetry curve for copper(II) ions solution in pyrophosphate shows two reduction peaks after which follows the hydrogen evolution region (see *Figure 3. 2 b*). In anodic direction an oxidation peak is not well seen, most likely due to the oxidation of Cu that occurs at around the same potential as for Mo oxidation. The presence of the first cathode peak can be explained by the reduction of Cu^{2+} into Cu^{1+} ions [125]. The second peak represents a reduction peak that can be attributed to the transfer of Cu^{2+} to metal copper. The visual appearance of the electrode, after keeping the substrate at -1.0 V for several minutes, changed into red, indicating Cu deposition at this potential. In contrast to the calculated value of the reduction potential for Cu (see Table 3. 2), the cyclic voltammogram is displaced moved in more negative direction. A possible explanation for this is the formation of copper hydroxycomplexes. At increased pH, there is an increasing tendency for the formation of $Cu(OH)_x^y$ compounds which can reduce the free Cu ions concentration as well.

The calculated value for the reduction potential of Zn is -1.4 V. The approximate onset of the reduction peak for Zn(II) ions in pyrophosphate solution is shifted to positive direction from the calculated value. However, it is difficult to evaluate the starting point of the Zn reduction as it can coincide with the hydrogen evolution which can strongly disturb it. The hydrogen begins to evolve earlier and after equilibrium potential of Zn^{2+}/Zn they go competitively together but because of H_2 high overpotential on Zn, reduction of Zn^{2+} appears to be favourable. At high cathode potentials hydrogen evolution is the dominating reaction.

The last graph shows the electrodeposition of the Cu-Zn alloy. Reduction of copper starts at around -1.0 V and it is followed by reduction of zinc and by forming a large plateau from -1.2 to -1.4 V. The oxidation wave for zinc is missing in graph (d) suggesting that part of Zn is alloyed with Cu and that the new oxidation peak at around -0.95 V is due to stripping of the Zn-rich Cu-Zn alloy and non-alloyed Zn together. The oxidation peak of Cu is more pronounced and forms a clear peak, indicating anodic stripping of the Cu-rich Cu-Zn alloys and non-alloyed Cu.

Pyrophosphate was used as a complexing agent for Cu-Sn deposition as well, since the same agent was also used for Cu-Zn deposition.

Electroplating of elemental tin or its alloy with copper (bronze) was typically performed using cyanide complexes [127]. Later some reports were published, where it was demonstrated that tin plating can be carried out from solutions containing pyrophosphate. Vaid and Rama Char used the solution obtained from stannous pyrophosphate and sodium pyrophosphate and reported that the pyrophosphate ligand forms complexes with tin. [128]. However, a large amount of other reports on divalent metals in pyrophosphate media published in 1936 did not contain any tin(II) examples [129]. Polarographic and potentiometric studies [130] [131] demonstrated later that $[SnP_2O_7]^{2-}$ and $[Sn(P_2O_7)_2]^{6-}$ complexes can be formed, additionally a mixed hydroxycomplex $[Sn(OH)(P_2O_7)]^{3-}$ was considered. For higher pH (8.3 − 11.1), the anions $[Sn(OH)_2(P_2O_7)]^{4-}$ and $[Sn(OH)(P_2O_7)_2]^{7-}$ were revealed. In fact, it was shown that the chemistry of tin(II) pyrophosphates in aqueous solution is still not well understood.

The stability constant used in this study ($1 \cdot 10^{14}$) was found for $[SnP_2O_7]^{2-}$complex from literature [132]. The presence of this complex in the pyrophosphate electrolyte is most likely as there are many reports that confirm the formation of the $[SnP_2O_7]^{2-}$complex [128, 129, 131].

According to this data it can be concluded that Sn forms complexes with pyrophosphate ligands. However, no study could be identified that examined the distribution of species depending on pH. There is no exact agreement among researchers which definite complexes can form in this media.

The stability constant for Sn is very high compared to those of Zn and Cu. However, in this case the difference between standard potentials of Sn and Cu is not as large as for Cu and Zn. Therefore the most suitable concentration for the work presented here was found to be 0.01M for $SnSO_4$ and 0.002M for $CuSO_4$.

Figure 3. 3 shows the electrodeposition of Sn on Mo substrate (a) and deposition of Cu-Sn on Cu-Zn substrate (b). The reduction of Sn(II) on Mo substrate starts around -1.1 V which differs from the calculated reduction potential which is -1.35 V. The explanation can be found in the different values for the stability constants which were used in the Nernst equation, hence shifting the potential in negative direction. In this calculations K_s equals to $1 \cdot 10^{14}$ respondent to $[SnP_2O_7]^{2-}$ complex was used. However, the formation of other complexes with Sn in the basic alkaline electrolyte, which can cause Sn reduction at lower potentials, cannot be excluded. The deposition of the Cu-Sn layer on Cu-Zn substrate is shown in *Figure 3. 3 b*. It is seen that like in case of Cu-Zn the simultaneous deposition of Cu-Sn starts at around -1.0 V. Interesting here is the formation of second oxidation peak next to the peak for Cu-Sn oxidation, which probably can arise from zinc stripping from the initial Cu-Zn layer.

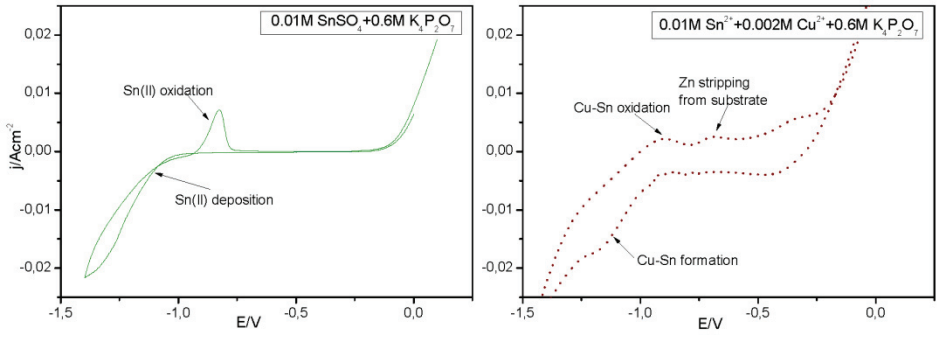

Figure 3. 3 Cyclic voltammetry curves for a) 0.01M Sn^{2+} and 0.6M $K_4P_2O_7$ electrolyte on Mo substrate and b) 0.002M Cu^{2+}, 0.01M Sn^{2+} and 0.6M $K_4P_2O_7$ electrolyte on Cu-Zn layer, vs Ag/AgCl, scan rate 20mV s^{-1}

The above data (CV curves, values of stability constants) were used to determine the electrochemical window and to follow the behaviour of separate ions in the pyrophosphate electrolyte. Based on these results potassium pyrophosphate was used for deposition of stacked alloy layers of Cu-Zn and Cu-Sn.

3.3.2 Morphology, elemental and phase composition of deposited metallic alloys

The approach of stacked alloys used as precursors for formation of $Cu_2ZnSnSe_4$ compounds was investigated and summarised in the publication [V]. The standard electrochemical cell with saturated Ag/AgCl as a reference electrode was used. The first step was the deposition of brass. Cu-Zn films were deposited for 50 – 60 minutes at a potential between -1.4 and -1.44 V on Mo/glass substrates. The elemental composition of the deposited Cu-Zn films is shown in Table 3. 3.

Sample	Cu [at%]	Zn [at%]	E_i,V vs. Ag/AgCl	Dep. time [min]
Sol 1	49.0	51.1	-1.40	60
Sol 2	44.1	55.9	-1.44	50
Sol 4	48.1	51.9	-1.40	60

Table 3. 3 Composition of electrodeposited Cu-Zn films

The details of the electrolyte preparation are presented in chapter 2.1. The thickness of brass layers varied from 0.3 up to 0.5 µm. All deposited films were Zn-rich. However it is possible to deposit Cu-Zn films with different composition by changing potential and ion concentration in the electrolyte. After electrodeposition of the first layer, films were washed and dried. Therefore the bronze layer was deposited on the Cu-Zn layer for 3 – 4 minutes at -1.3 V. The thickness of the deposited Cu-Sn layer was around 0.1 – 0.2 µm. The total composition of the electrodeposited films is presented in Table 3. 4.

Sample	Cu [at%]	Zn [at%]	Sn [at%]	Dep.time [min]
Sol 1	43.7	8.4	47.9	3.15
Sol 2	43.6	16.2	40.2	3.00
Sol 4	35.6	17.2	46.2	3.30

Table 3. 4 Compositions of electrodeposited precursor films (Cu-Zn→Cu-Sn)

The final precursor composition is Sn-rich, which was determined especially to compensate the tin loss at higher temperatures in the subsequent selenisation process. The prepared stacked films (*Cu-Zn → Cu-Sn*) were used as precursors for CZTSe films in the annealing experiments in selenium vapour. The SEM surface images of these layers are depicted in *Figure 3. 4*.

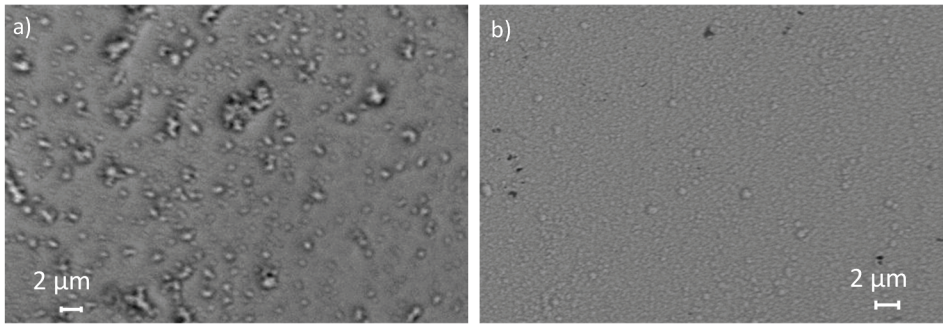

Figure 3. 4 SEM images of a) Cu-Zn layer and b) Cu-Sn on Cu-Zn layer

The Cu-Zn layers show some inclusions on the surface that are probably a result of hydrogen evolution that occurred together with Zn deposition. The Cu-Sn

layer shown in *Figure 3. 4 b)* exhibits a smooth morphology of the film; however, the formation of bigger agglomerates is also seen on the surface.

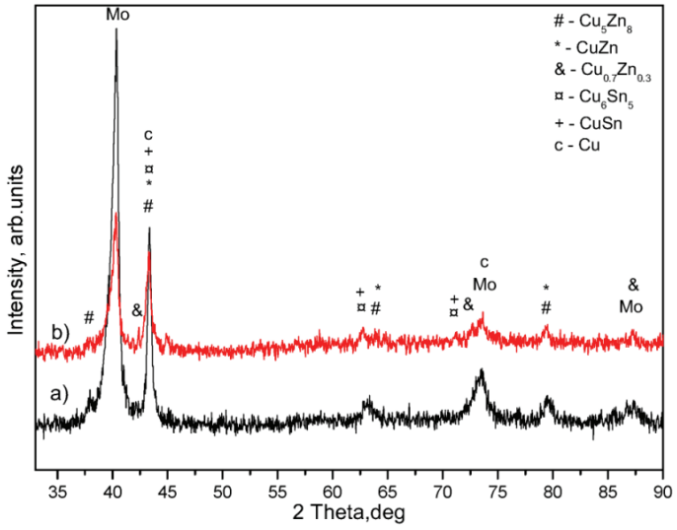

Figure 3. 5 XRD pattern of as-deposited a) Cu-Zn alloy, b) stacked layers of Cu-Sn on Cu-Zn

The XRD pattern of deposited Cu-Zn film containing from 50 to 55 at% of Zn is shown in *Figure 3. 5*. Three main peaks at 40.30, 73.6 and 87.35° can be attributed to the Mo substrate. Other reflexes can be assigned whether to the Cu_5Zn_8 or to the CuZn phase as the strongest XRD peaks of these phases coincide. However, the presence of a small peak at the left shoulder of the first Mo peak indicates evidence of existence of the γ-Cu_5Zn_8 phase in this film. These results are consistent with the equilibrium phase diagram of Cu-Zn from which can be expected that a mixture of disordered β-CuZn and γ-Cu_5Zn_8 phases is formed in this region of the Zn concentration [133]. No evidence of elemental Cu or Zn was revealed.

The XRD pattern of complete Cu-Sn and Cu-Zn precursor indicates the presence of Cu_5Sn_6 and/or CuSn phases. These phases were also found in Cu-Zn-Sn co-electroplated precursors in [44, 76, 77, 104]. Additionally, precursors could contain elemental Zn [44, 104] or Sn [44, 77, 104]. A small peak at around 45° indicates traces of Sn in the film. Cu_5Sn_6 was also found to be formed in precursors during evaporation and sputtering [40, 99]. Interestingly, a small amount of the Cu-rich brass phase ($Cu_{0.7}Zn_{0.3}$) can be observed in *Figure 3. 5 b)*, which may have arisen because of Zn dissolution in the electrolyte containing Cu and Sn.

A list of XRD pattern standards for this thesis can be found in Appendix B.

3.3.3 Selenisation of Cu-Zn and Cu-Sn stacked layers

Several groups [17, 92] are using long time annealing procedures to form a final Cu_2ZnSnS_4 layer. In this work precursors were selenised in an electric tubular furnace and two different annealing procedures were performed. The first procedure involved preliminary homogenization through annealing in vacuum for 1 hour at 400°C and that was followed by reactive isothermal annealing in selenium vapour for 1 hour at 560°C. The other procedure consisted of a short (15, 10 minutes) treatment at 530°C followed by cooling down with slow rate. To compare these two procedures an XRD analysis was conducted for the obtained films, which is shown in *Figure 3. 6.*

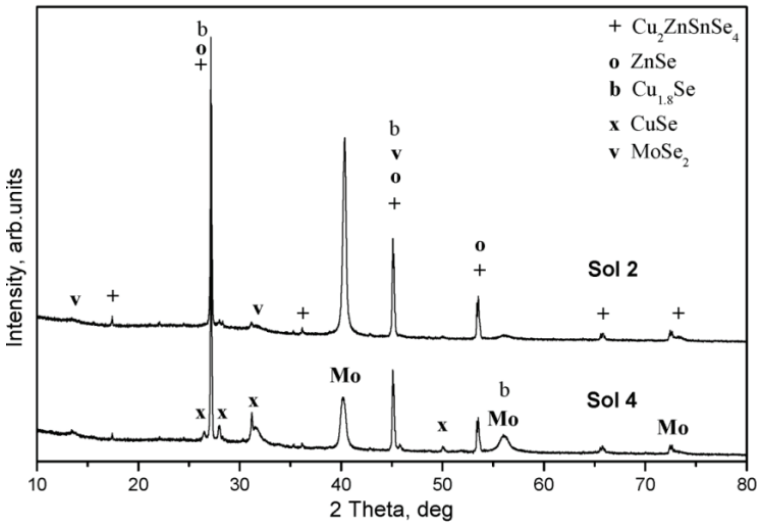

Figure 3. 6 X-ray diffraction patterns of thin $Cu_2ZnSnSe_4$ layers annealed in different regimes: Sample Sol 2 – selenisation for 15 minutes at 530°C and slow cooling down; sample Sol 4 –1 hour selenisation at 560°C.

For both patterns typical main reflexes corresponding to the $Cu_2ZnSnSe_4$ phase at 27.16, 45.1 and 53.52^o in 2θ scale are dominating. Minor peaks of the $Cu_2ZnSnSe_4$ phase are seen at 17.44, 36.25, 65.98 and 72.65°. Signals are strong and sharp indicating the formation of a well-crystallized structure. Well-defined reflexes from the molybdenum substrate layer at 40.3, 56.03 and 73.45° in 2θ scale are also detected. Assuming the strongest peak at 45.1° is not caused only by the CZTSe phase, there could be evidence of $MoSe_2$ – a product of selenisation of the Mo substrate. Detailed structural analysis in both cases indicated non-monophase thin film materials. Additionally there are minor but well distinguished reflexes at 26.58, 28, 31.2 and 50.02° related to a separate CuSe phase. Thin film material could contain an additional cubic ZnSe phase as ZnSe peaks coincide with the CZTSe peaks at 27.16, 45.1 and 53.52° in 2θ scale. In addition to this, the analysis suggests the existence of the Cu_2Se phase with reflexes at 27.16, 45.1 and 56.03°.

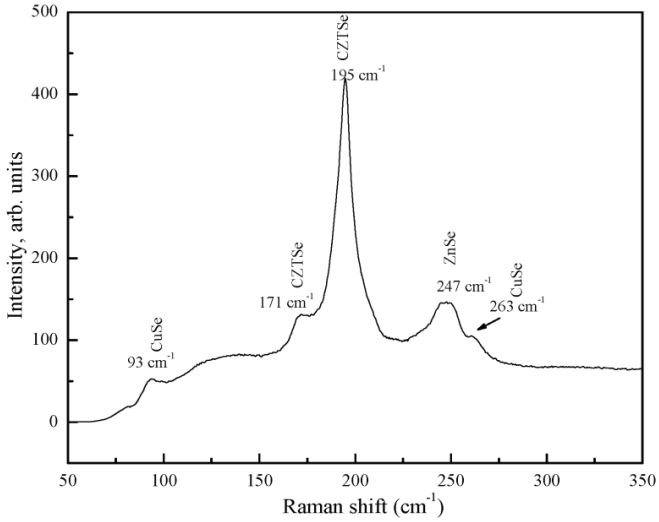

Figure 3. 7 Room temperature Raman spectrum of Sol 1 precursor annealed at 530ºC for 10 minutes

The room temperature Raman spectrum shows a well-formed CZTSe by vibrations at 171 cm^{-1} and 195 cm^{-1} respectively. There are two additional peaks that could be attributed to CuSe (at 93 cm^{-1} and at 263 cm^{-1}). A signal at 247 cm^{-1} could indicate the existence of the cubic ZnSe phase in sample. Sources for Raman shifts used in this work are listed in Appendix B.

Figure 3. 8 shows the dependence of the $(\alpha h\nu)^2$ curves on energy ($h\nu$) axis for CZTSe layers.

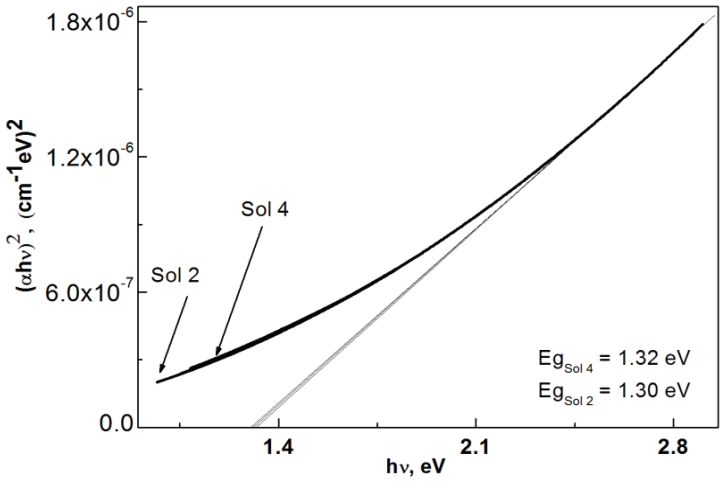

Figure 3. 8 Plot for determining the band gap of $Cu_2ZnSnSe_4$ films selenised in different conditions: Sol 4- hour at 400ºC in vacuum +1 hour at 560ºC and Sol 2 for 15 minutes at 530ºC. The analysis is based on the assumption that CZTSe is a direct band gap material.

The direct optical band gap was calculated by plotting $(\alpha h\nu)^2$ versus the energy in eV and extrapolating the linear part of the spectrum $(\alpha h\nu)^2 = f(h\nu)$ to zero. Thus, the band gap of the CZTSe thin films was estimated to be 1.31 eV ± 0.01 eV.

Drawback of Cu-Sn and Cu-Zn stacked alloys approach

The disadvantage of this method was the unstable electrolyte performance for Cu-Sn layer deposition. After exposing to the air during first depositions, divalent tin started to oxidize at the anode to tetravalent tin [134]. The resulting stannate (IV) was more stable and accumulated in the electrolyte. This method was not pursued further due to difficulties in controlling the precise Cu:Sn ratio for deposited in a row Cu-Zn layers . Although there are several substances ("stabilizers") described as antioxidants that avoid or slow down the oxidation process [134] (pyrocatecol, hydroquinone, resorcinol, phloroglucinol, pyrogallol, 3-amino phenol, hydroquinone sulphuric acid ester, cresolsulphonic acid and others) the use of these leads to undesired reactions that could occur on the surface and will contaminate the layers. Initially, in this work, in order to stabilize Sn, hydroquinone was used as an antioxidant. However, because of the toxicity of this element and because of fast degradation of its stability properties in solution, this reagent was not used in further experiments.

3.4 Sequential electrodeposition of Sn layer on Cu-Zn layers

To avoid the premature degradation of bronze electrolytes a novel method of depositing Sn on Cu-Zn layer was employed. The new electrolyte for Sn was an aqueous solution containing sodium pyrophosphate and $SnCl_2$. This electrolyte demonstrated stable behaviour and enabled multiple depositions of Sn layers. As the copper ions are absent in new solution there is no competition between Sn^{2+} and Cu^{2+} ions in deposition on the substrate. Copper as the ion with more positive redox potential does not interfere with the reduction of tin ions (with more negative redox potential) allowing it to be deposited in a natural way.

3.4.1 Cyclic voltammetry of electrodeposited Cu-Zn layers

It was shown before that the morphology of the Cu-Zn layer is imperfect, which is probably due to intensive hydrogen evolution which occurs at high potentials. At the locations of the electrode where hydrogen bubbles form, the electrode surface is insulated and therefore deposition cannot take place. On the border of the bubbles the electrolyte penetration is constrained resulting in non-uniform deposited material of large grain size. Therefore it was required to search for different complexing agents, which allow simultaneous Cu-Zn deposition and lead to uniform and homogenous films.

Trisodium citrate was used as a source of $C_6H_5O_7^{3-}$ ions used as ligands for electrodeposition of copper [135], zinc [136] and their alloys [137]. Pawar et. al [90] suggested to use trisodium citrate for co-electrodeposition of Cu-Zn-Sn. The ability of this ligand to from stable complexes with several metals, particularly with copper allowed to move the potentials of Cu^{2+}, Zn^{2+} and Sn^{2+} closer and to find suitable conditions for co-deposition of metallic films with a desired composition.

Conversion efficiency of 3.16% was obtained for a device prepared by annealing of electrodeposited Cu-Zn-Sn alloy using trisodium citrate for electrolyte preparation [36].

In this PhD work, $C_6H_5O_7^{3-}$ ions were used as ligands. The deposition of Cu-Zn layers was obtained using these ligands. The disappearance of tin salt in the electrolyte composition considerably eases the task of multi-metal electrodeposition since it bypasses the necessity to take into account the easily alternating oxidation levels of Sn in different conditions.

Table 3. 5 presents the stability constants for copper(II) and zinc(II) citrate complexes. According to literature 14 copper-citrate complexes of Cu(II) can be formed [138]. The table represents stability constants only of two copper-citrate species which are found at pH ≥ 6 in accordance with the distribution of species in the graph reported by S. Rode et al. [138]. When the citrate is in excess, the dimmers $Cu_2Cit_2H_{-1}^{3-}$ and $Cu_2Cit_2H_{-2}^{4-}$ are the dominant species. In the presence of cupric ions, coordination effects render the hydrogen of the hydroxyl group labile, and the citrate ion may become quadruply ionized, thereby resulting in a negative value for the subscript with minus [138].

The predominant species in distribution of zinc-citrate complexes is reported to be $Zn(Cit)_2^{4-}$ at pH ≥ 6 [136], which has the highest value among all zinc species, still the stability constant for the copper complex $Cu_2Cit_2H_{-1}^{3-}$ is higher. These investigations are the good basis for elaborating an electrolyte for Cu-Zn alloy electrodeposition. In this PhD work equal concentration of Cu(II) and Zn(II) ions were added to the electrolyte and uniform films with good adhesion to the substrate were obtained. The Cu:Zn ratio varied around one dependent on the deposition potential.

	Stability constant, Ks	**log Ks**	**Ref.**
$Cu_2Cit_2H_{-1}^{3-}$	$7.1 \cdot 10^{10}$	10.85	[138]
$Cu_2Cit_2H_{-2}^{4-}$	$7.4 \cdot 10^{5}$	5.87	[138]
ZnH_2Cit^{+}	$1.8 \cdot 10^{1}$	1.25	[136]
ZnHCit	$9.5 \cdot 10^{2}$	2.98	[136]
$ZnCit^{-}$	$9.5 \cdot 10^{4}$	4.98	[136]
$Zn(Cit)_2^{4-}$	$7.9 \cdot 10^{5}$	5.90	[136]

Table 3. 5 Stability constants for citrate ion and Cu(II) and Zn(II) species

The calculated values for reduction potentials of metals in electrolyte with citrate ions as ligands are shown in Table 3. 6. These were calculated analogous

to the calculation conducted for pyrophosphate media (see 3.3.1). Standard reduction potentials for Cu (0.337 V) and Zn (-0.76 V) were taken.

Type of ions	Ligand	E vsAg/AgCl
Copper(II) ions	$C_6H_5O_7^{3-}$	-0.36
Zinc(II) ions	$C_6H_5O_7^{3-}$	-1.16

Table 3. 6 Calculated reduction potentials for copper(II) and zinc(II) in acidic media, at pH 6

The electrochemical window for 0.1M $Na_3C_6H_5O_7$ is narrower than for $K_4P_2O_7$. The current starts to flow already at around -0.6 V. This phenomenon can be explained by dissociation of trisodium citrate and adsorption of citrate anions on Mo substrate. Hydrogen evolution begins at -1.15 V and limits the window. The oxidation of Mo substrate, however, moved in more positive direction and starts around -0.22 V.

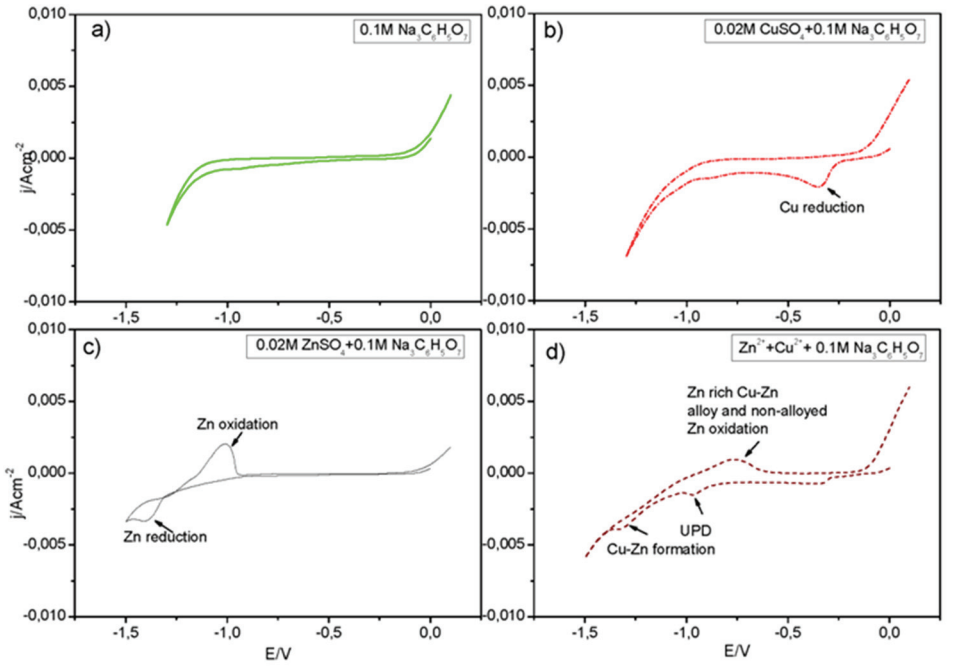

Figure 3. 9 Cyclic voltammetry curves on Mo electrode for a) 0.1M $Na_3C_6H_5O_7$; b) 0.02M Cu^{2+} and 0.1M $Na_3C_6H_5O_7$; c) 0.02M Zn^{2+} and 0.1M $Na_3C_6H_5O_7$; d) containing both 0.02M Cu^{2+} and 0.02M Zn^{2+} ions in 0.1M $Na_3C_6H_5O_7$ solution, vs. Ag/AgCl, scan rate 20 mV s^{-1}

As it was mentioned before, citrate ions bind copper(II) ions relatively strong and can move copper potential in more negative direction. In graph b) the reduction peak for Cu is seen at -0.34 V and since oxidation of Cu occurs at a

potential similar to that of Mo, the peak is not extractable from the Mo electrode oxidation one.

Reduction peak for zinc(II) is shown at -1.39 V followed by the oxidation peak at -1.0 V in reverse scan (*Figure 3. 9 c*). The calculated values for Cu and Zn are in good agreement with the onsets of starting points of the reduction potentials for Zn(II) and Cu(II) ions deposition respectively.

Graph d) presents the cyclic voltammetry curve for electrodeposition of the Cu-Zn alloy. The first reduction peak is assigned to reduction of Cu(II) ions. The second peak situated at -0.96 V could be attributed to underpotential deposition of Zn (UPD). It is worth noting that the substrate, during electrodeposition, never has the same original substrate composition as in the beginning, as it gets covered with Cu deposit with time. Therefore the way of interaction behaviour between Zn and substrate is changed. The phenomenon of UPD refers to the deposition of metals on foreign metal substrates at potentials that are more positive than that predicted by the Nernst equation for bulk deposition [139]. When the solution contains both Cu(II) and Zn(II) ions, the underpotential deposition of Zn occurs simultaneously with deposition of Cu, as a result of which an alloy is formed. In this case the higher rate of Zn deposition in Cu can be favoured by kinetic factors, such as non-equilibrium trapping of Zn adatoms, by growing deposits of Cu, by the presence of steps and kinks on the surface, and also by an enhanced concentration of vacancies in the lattice of the solvent metal and high amount of grain boundaries in the film [140]. The oxidation peak in reversed scan respectively corresponds to stripping of Cu-Zn alloy and non-alloyed zinc.

3.4.2 Morphology and phase composition of precursors

SEM images of a) electrodeposited Cu-Zn layer, b) Sn on Cu-Zn layer and c) the cross-section of the whole stacked precursor is depicted in *Figure 3. 10.* The initial Cu-Zn alloy film consists of small densely packed crystals and appeared mirror bright showing a gold-like colour. The Sn layer deposited onto the Cu–Zn alloy layer consisted of crystals sized 0.2 – 0.3 μm with prolonged equally distributed holes between the crystals. According to the cross-sectional image the thickness of the Sn layer reached 200 nm and the total precursor thickness was around 600 nm.

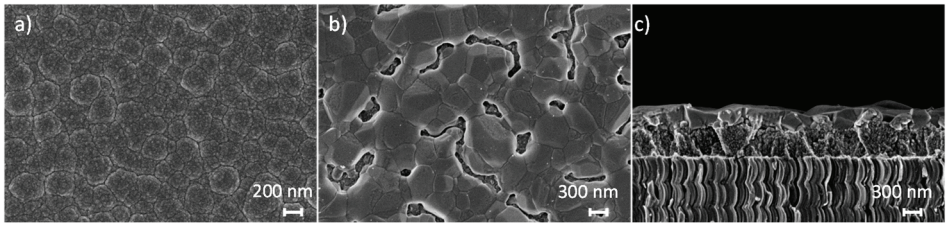

Figure 3. 10 a) SEM image of electrodeposited Cu-Zn layer b) Cu-Zn-Sn layer and c) cross-section of the precursor

The XRD pattern of deposited Sn on Cu-Zn precursor is shown in *Figure 3. 11*. Reflexes of elemental Sn are seen in the figure; however, peaks assigned to Cu_5Sn_6/CuSn phases are also present, indicating the alloy formation of Sn with Cu. According to literature Cu and Sn can form the alloy Cu_6Sn_5 already at room temperature [141]. M. Date et al. [142] demonstrated the formation of the Cu_6Sn_5 phase between Sn and the Cu_5Zn_8 phase, and proposed that Sn may have started the process by penetrating into the grain boundaries of Cu_5Zn_8. The interdiffusion of Sn increased with aging time, and slowly it led to the formation of Cu-Sn intermetallic compounds within the Cu_5Zn_8. Complete interdiffusion of one metal into another to form bronze or brass phases occurs only after low temperature annealing [19, 77].

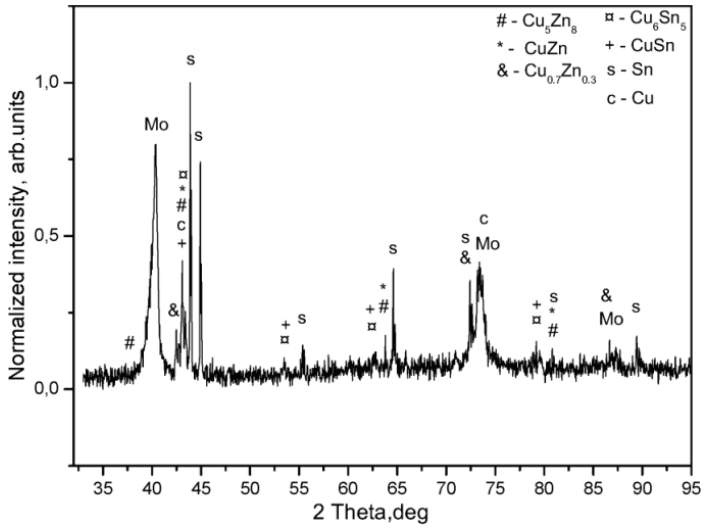

Figure 3. 11 XRD pattern of as-deposited Sn on Cu-Zn alloy

The Cu-rich phase - $Cu_{0.7}Zn_{0.3}$ is also present in the XRD pattern and the reason for formation of this phase is possibly the same as was explained before.

3.4.3 Electrodeposition of films using rotating disc electrode

The growth of electrodeposited films occurs through convection currents. At a usual vertical working electrode films grow unevenly as convention currents produce non-uniform electrolyte transport. This results in thickness variations over the deposited area and could lead to compositional gradients [82]. The control of the mass transport during electrodeposition is therefore of utmost importance.

The simplest way to achieve uniform convection, i.e. supplying the same electrolyte flow over the entire electrode area, is to use a rotating disc electrode (RDE). When the electrode is rotated, it pumps fresh solution from the bulk of the electrolyte onto the disc, hence providing the same flow across the whole

area. The relationship between the limiting current and the rotation rate of the electrode is given by the Levich equation:

Eq 3. 2

$$J = 0.62\ z\ F\ D^{2/3}\ \omega^{1/2}\ v^{-1/6}\ c_0$$

Where z is the number of electrons transferred per ion, F is the Faraday constant (96485 C/mol), D is the diffusion coefficient of the transferred ion, c_0 is the initial concentration of the ion in the electrolyte, ω is the angular velocity of the RDE (rad/sec) and v is the kinematic viscosity of the electrolyte (0.01 cm^2/s for water).

An electrochemical cell with a rotating disc electrode as the working electrode was used in the work presented in the publications [I] and [II].

EDS line scanning profiles for Cu-Zn layer are presented in Figure 3. 12 and *Figure 3. 13*. Figure 3. 12 represents the employment of a vertical working electrode and Figure 3. 13 employment of a rotating disc electrode. The EDS analysis was made in two locations (at the top and at the bottom of the deposited layer, shown in images of *Figure 3. 12* and *Figure 3. 13*).

The first sample (prepared with the vertical working electrode) showed compositional changes all over the substrate of deposited film: Cu fluctuations were in range of 40 at% to 50 at%. The cross-section images and concentrational line scans were taken from the top and the bottom of the same film and are given in *Figure 3. 12*.

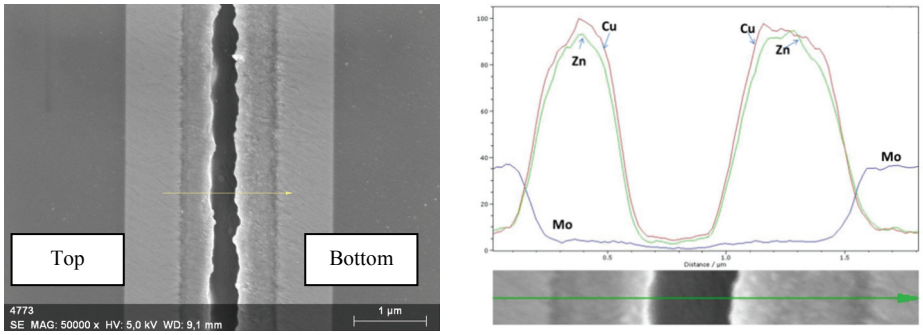

Figure 3. 12 EDS line scans applied on the cross-sections of the top and the bottom part of the Cu-Zn deposited film using a vertical electrode

The difference in width between two peaks at the line scans can be noticed and indicates that the bottom part of the film is thicker than the upper part. Thickness variations of the electrodeposited films using different working electrodes were also discussed in [19]. The line scans of the top and the bottom part of film show that zinc is more amassed in the middle part of the film, whereas copper on the bottom of the films is confined to the surface of the precursor. This indicates that the growth of the bottom part of the film is caused preferentially by copper deposition. On the other hand, natural convection in the electrolyte causes decelerated mass transport at the top slowing down the

deposition of ions in the upper part of the film. Therefore Cu diffuses deeper in the bulk and forms an alloy.

Scan line of the film prepared using RDE is shown in *Figure 3. 13*. Here Cu and Zn are distributed relatively homogeneously in the film and no thickness variations were observed. Only slight elemental segregation with higher Cu concentration near the Mo substrate was noticed. EDS analysis indicates small compositional fluctuations over the substrate of films (Cu: 55 – 57 at%; Zn: 43 – 45 at%).

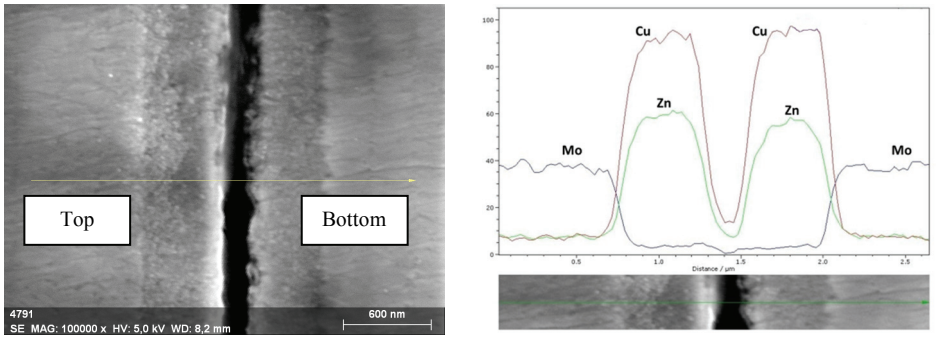

Figure 3. 13 EDS line scans applied on the cross-sections of the top and the bottom parts of the Cu-Zn deposited film using RDE.

3.4.4 Cu-poor and Cu-rich precursors

Based on the formula $Cu_2ZnSnSe_4$, the ratio of metals in the electrodeposited Cu-Zn alloy must be approximately two in order to obtain a stoichiometric atomic ratio of metals in the final $Cu_2ZnSnSe_4$ film. However, it was reported that Cu-poor precursors tend to show better conversion efficiency [40, 47].

In this work two series of precursor layers, named Sol A and Sol B, were prepared. In both series, the Cu:Zn ratio was varied: in Sol A, the Cu:Zn ratio was equal to 1.7, whereas in Sol B, the Cu:Zn ratio was equal to 1.1. After electrodeposition of Sn, there was a loss of Zn (dissolution of Zn in Sn containing electrolyte) from the precursors and the ratio of Cu:Zn changed from the initial 1.7 to 2.3 and 1.1. to 1.8, respectively. The results are presented in Table 3. 7.

Type	**Cu (at%)**	**Zn (at%)**	**Sn (at%)**	**Se (at%)**	**Cu:Zn**
Metallic precursors					
Sol A-1	62.6	37.4	-	-	1.7
Sol B-1	53.1	46.9	-	-	1.1
Sol A-2	51.4	21.9	27.2	-	2.3
Sol B-2	43.1	23.9	33.0	-	1.8

Table 3. 7 Compositions of the precursors of Sol A and Sol B.

All deposited stacked precursors were in excess of Sn to compensate the possible loss of Sn after annealing. In this experiment the possibility of losing Sn is very high, as the Sn layer was the upper one, thus exposed to the atmosphere.

The 2D and 3D AFM results exhibit structures of deposited Cu-Zn layers with different Cu:Zn ratio. The Sol A-1 type of precursor is shown in part a) and b) of *Figure 3. 14*. Sol B-1 precursors are presented in part c) and d). The surface of films was scanned over an area of 1 µm x 1 µm. It is clearly seen that the Sol A precursor consists of smaller crystallites and has a more dense structure. The Sol B Cu-Zn layer has bigger crystallites that have strong orientation. According to AFM the average crystallite size was 30 nm for Sol A and 42 nm for Sol B precursors. A possible explanation may be found in comparison of ionic radiuses for copper and zinc ions. The ionic radius of Zn^{2+} is larger (0.82 Å) than the ionic radius of Cu^{2+} (0.72 Å). Therefore higher Zn^{2+} concentration leads to larger expansion of the lattice, thus the lattice parameter increases more in comparison to the Cu^{2+} substitution in deposited crystallites [143]. Consequently a bigger amount of Cu in the alloy leads to a more dense structure of the layer that consists of smaller crystallites. The surface roughness R_{ms} of both precursors were almost equal and had a value of 10 nm, indicating that formed alloys had a smooth structure.

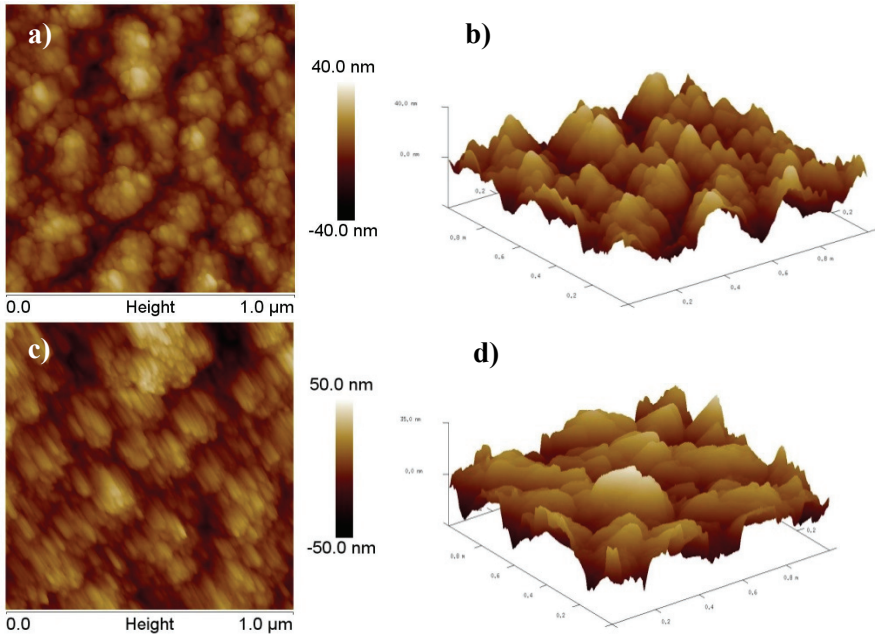

Figure 3. 14 AFM 2D and 3D micrographs of electrodeposited Cu-Zn alloys: a) and b) Sol A type, c) and d) Sol B type (see Table 3. 7)

3.4.5 Characterization of annealed $Cu_2ZnSnSe_4$ thin films with different Cu:Zn ratio

The stacks of Sol A and Sol B precursors were selenised at 470°C for 40 minutes in sealed quartz ampoules in selenium atmosphere. The compositions of the resulting CZTSe films are presented in Table 3. 8.

Type	Cu (at%)	Zn (at%)	Sn (at%)	Se (at%)	Cu:Zn
Sol A	24.7	10.7	13.3	51.4	2.3
Sol B	21.3	12.3	14.9	51.4	1.7

Table 3. 8 Elemental composition of selenised films of Sol A and Sol B annealed at 470ºC for 40 min

Films from both series were surprisingly Sn-rich; however, in the Sol B-type CZTSe films the concentration of Zn is higher and closer to that required by stoichiometry. A decrease in the Cu concentration is also observed (see Table 3. 8). SEM images of the surfaces of the selenised films (*Figure 3. 15*) indicate that the Sol B-type precursors results in a uniform and smooth CZTSe layer with small-sized crystals, which have different shapes with round edges. However, the use of the Sol A-type precursors resulted in non-homogenous and non-uniform CZTSe films. Large formations with a hexagonal shape of approximately 4 μm were detected on the surfaces of these films.

The EDS analyses allowed to determine that these formations are separate CuSe crystals ([Cu] = 49 at%, [Se] = 51 at%). The formed CZTSe layer exhibits a "wrinkled" structure, which indicates the loss of contact with the Mo substrate. As a result the formed films easily peeled off of the Mo substrate.

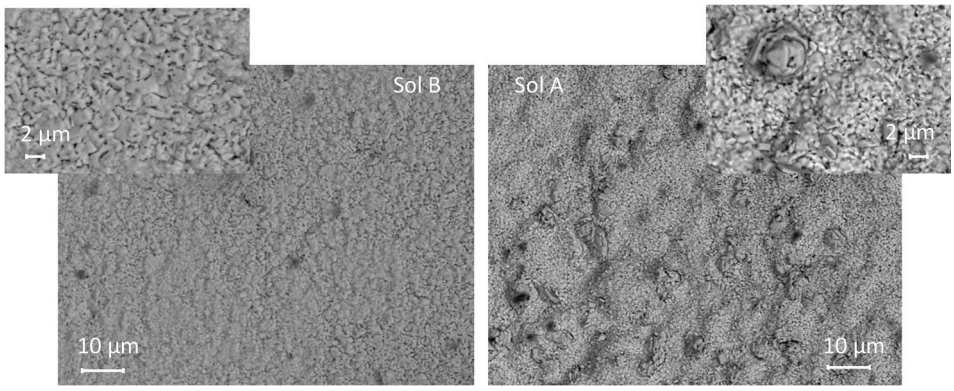

Figure 3. 15 SEM surface images of the films selenised at 470°C for 40 minutes

The Raman scattering spectra from the surface of the CZTSe thin films from both series of precursors are depicted in *Figure 3. 16* and provide evidence of the presence of foreign phases in the selenised films. The peaks at 171 cm^{-1}, 195 cm^{-1}, and 233 cm^{-1}, which correspond to CZTSe, are dominant in both

graphs. However, it is clearly seen that in the Raman spectrum of the surface of Sol A-type films, there is an additional peak at 260 cm^{-1} that is related to the separate CuSe phase.

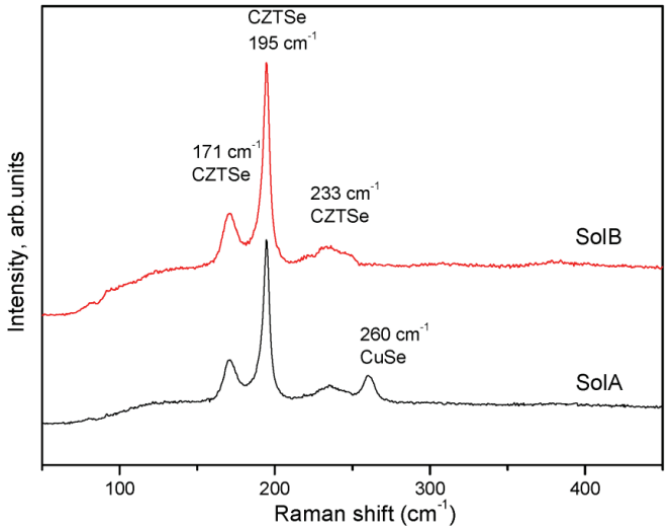

Figure 3. 16 Raman spectra of $Cu_2ZnSnSe_4$ thin layers selenised at 470°C for 40 minutes. For precursor composition of Sol A and Sol B see Table 3. 8

These Raman results are in a good agreement with the findings from the EDS analysis. The presence of the CuSe phase as well as the wrinkled morphology of the film does not lead to a high performance of solar cells. Following the above-given data, Cu-poor precursors were used for the next experiments.

3.4.6 Phase composition of selenised $Cu_2ZnSnSe_4$ in dependency on temperature

The selenisation at different temperatures starting from 450 to 560°C was performed in sealed ampoules. The results are published in [IV].

Precursors were annealed in selenium vapour and the composition of formed CZTSe layers is shown in Table 3. 9. As it was discussed in 3.4.3, the use of a vertical working electrode in precursor layer preparation could lead to thickness variations of the deposited films. As a consequence differences of composition in the different places of the annealed layers were found. Table 3. 9 presents the mean values of measured composition in three different micro-places.

T, ºC	Cu, at%	Zn,at%	Sn	Se	Cu:(Zn+Sn)	Zn:Sn
450	26.4	12.9	11.8	48.9	1.1	1.1
490	15.4	25.0	10.8	48.8	0.4	2.3
530	19.9	17.5	13.4	49.2	0.5	1.2
560	13.5	20.7	9.1	56.7	0.5	2.2

Table 3. 9 The average values of composition in three different micro-places of the films

The influence of the selenisation temperature is presented in *Figure 3. 17*. It shows the XRD patterns of absorber films grown at 450, 490, 530 and 560°C for 30 minutes.

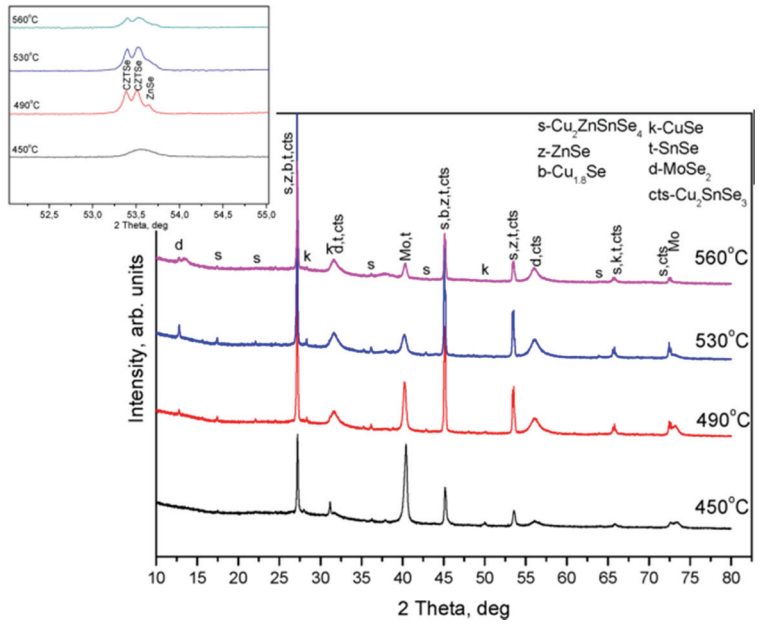

Figure 3. 17 XRD patterns of absorber films grown at 450°C, 490°C, 530°C and 560°C for 30 minutes. Inset presents the pattern in interval 52 – 55° for distinct CZTSe and ZnSe.

The existence of the $Cu_2ZnSnSe_4$ phase is recognisable in all patterns by its main reflections at 27.1, 45.1 and 53.5° and other minor peaks which are marked with 's'. In addition there are reflections of Mo at 40.2° and 73.5° and three other peaks at 11.5, 31.6 and 56.0° which correspond to $MoSe_2$. Detailed analysis confirmed the existence of $Cu_{1.8}Se$ (marked as 'b') with reflections at 27.2, 45.1 and 56.1°. A possible phase is also ZnSe (marked as 'z'), the main peaks of which coincide or lie very close to those of CZTSe at 27.16, 45.1 and 53.5°. One could expect the formation of the ZnSe phase as according to the compositions of annealed films Zn is in excess. Minor presence of CuSe was registered also but their intensity decreases sharply with the temperature increasing. When the temperature rises, the signal of the substrate fades and reflection from the CZTSe layer becomes dominant. CZTSe and ZnSe phases can be distinguished in the vicinity of peaks at 53 – 54°. Here the CZTSe phase presents twin peaks at 53.39 and 53.45°, whereas cubic ZnSe is indicated by a peak at 53.56° [101]. As it can be seen in the inset to the *Figure 3. 17*, at lower and higher temperatures ZnSe exists as a minor phase and its crystallinity improves at 490°C. A similar trend can be seen in the crystallization of the phase $Cu_2ZnSnSe_4$.

SEM surface and cross-sectional images (*Figure 3. 18 a, b*) of the film annealed at 490°C show crystallized CZTSe absorber material consisting of large crystals in size of 1.5 – 2 µm. These big grains are mixed with small crystallites sized 0.5 – 0.7 µm which are in different shapes starting from roundly formed particles and ending up in cubic or triangle shaped crystals. The cross-section of the film shows a bi-layer of annealed films. According to the EDS results the bottom layer corresponds to the ZnSe phase.

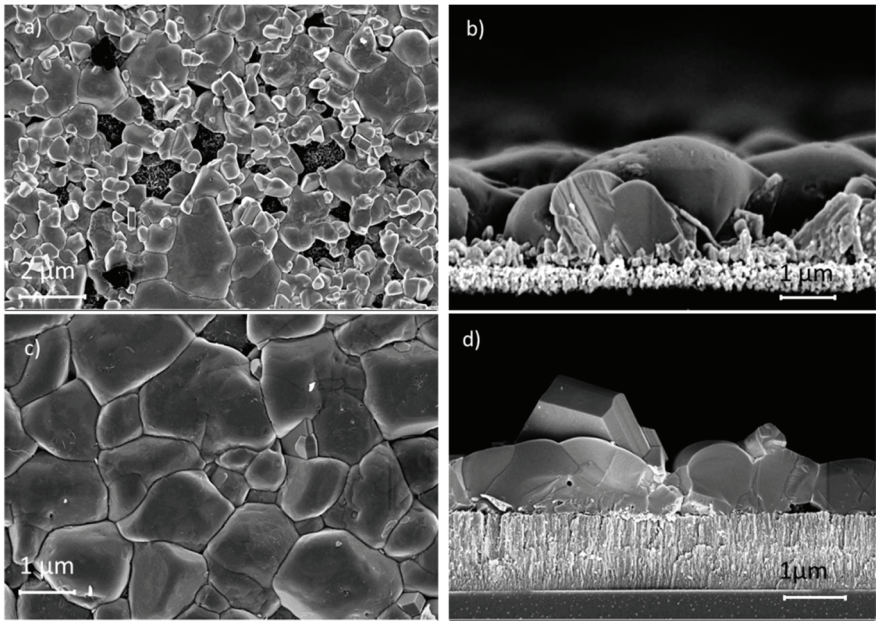

Figure 3. 18 High resolution SEM surface and cross-section of CZTSe films selenised (a), (b) at 490°C; (c), (d) selenised at 530ºC for 30 minutes in closed isothermal conditions

Film annealed at 530ºC is shown in *Figure 3. 18 c*, it consists mainly of big crystals in size of 1 – 2 µm. The existence of a separate CuSe phase in the film was well identified by XRD and EDS analysis. The CuSe phase is clearly seen additionally as plate-like hexagonal shape crystals on the CZTSe layer (*Figure 3. 18 d*).

3.4.7 Influence of selenisation duration on the crystal growth in CZTSe films

Only precursor stacks of composition Sol B (see subsection 3.4.4) were used for this investigation. Precursors were placed in evacuated quartz ampoules (1.3 Pa) and subsequently heated isothermally at 470ºC for 20, 40 and 60 minutes. A piece of selenium was inserted into the ampoule before sealing. SEM results showed that the surface of films selenised for 20 minutes at 470°C consist of mixture of small triangle crystals with a size less than 0.7 µm and middle-sized

rectangular crystals (*Figure 3. 19*). Formed crystals are densely packed and have sharp angles.

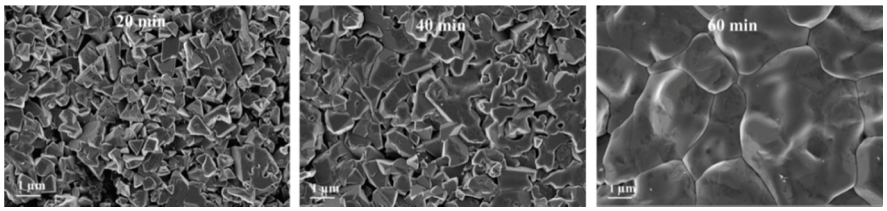

Figure 3. 19 SEM surface images of CZTSe films annealed for 20, 40 and 60 minutes at 470°C.

The presence of separate phases and elements in films was investigated by Raman measurements. The main peak of CZTSe at 195 cm^{-1} is seen already in Raman spectra of films that had the shortest selenisation duration. Raman peaks at 237 cm^{-1} and 250 cm^{-1} can be attributed to pure Se and ZnSe phase, respectively (see *Figure 3. 20*).

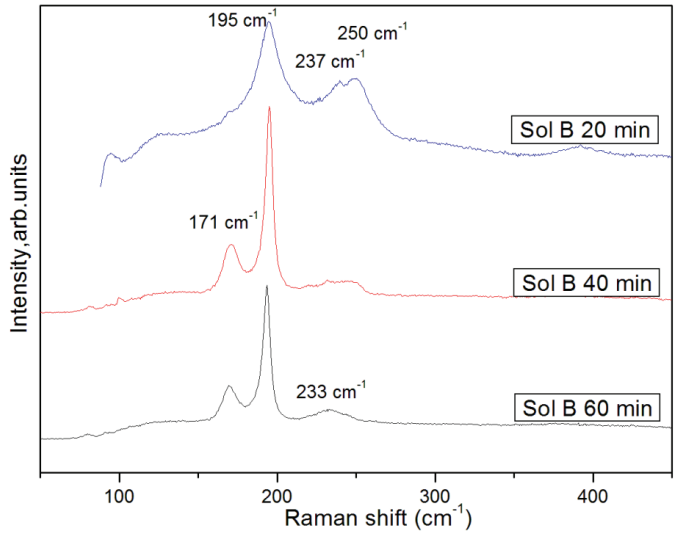

Figure 3. 20 Raman spectra of CZTSe films selenised at 470°C for different durations

With an increase of selenisation duration up to 40 minutes the size of crystals increases (*Figure 3. 19*). Grain growth continues, implying that small crystallites of different phases grow together to larger agglomerates. Raman spectra show a broad peak in the region starting from 231 to 252 cm^{-1}. The intensity of peaks at 250 and 237 cm^{-1} is decreasing, thus pointing out at contribution of ZnSe and Se to the CZTSe layer.

Large crystals in size of 1.5 to 4 μm are dominant in the films annealed for 60 minutes in *Figure 3. 19*. The Raman spectrum does not reveal presence of other phases; all peaks belong to the CZTSe compound. Full width at half

maximum (FWHM) of the main CZTSe peaks at 171 and 196 cm^{-1} becomes more narrow, indicating improved crystallinity of films selenised for 60 minutes. An additional peak at 233 cm^{-1} appears in the Raman spectrum which could be referred to the third CZTS peak.

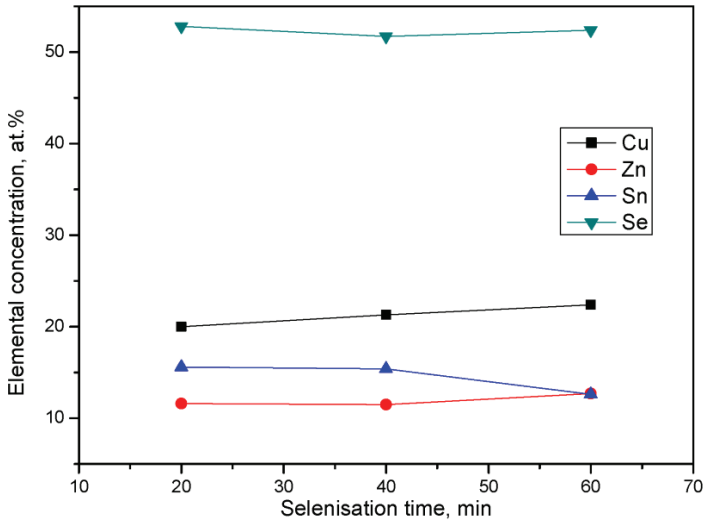

Figure 3. 21 Elemental composition of selenised films at 470ºC for different time

The composition of CZTSe films is changing to Zn-rich with increasing the duration of annealing. This probably happens due to Sn loss during longer times of selenisation. However, it is worth to note that no Sn deficiency films were observed even after 60 minutes annealing (Sn = 12.8 at%).

The XRD pattern of a film selenised at 470ºC for 60 minutes (*Figure 3. 22*) has almost all peaks attributed to the CZTSe phase. Additionally observed small and broad peaks at 13, 31 and 56° indicate the selenisation of Mo substrate and result in the presence of the $MoSe_2$ phase (drysdallite).

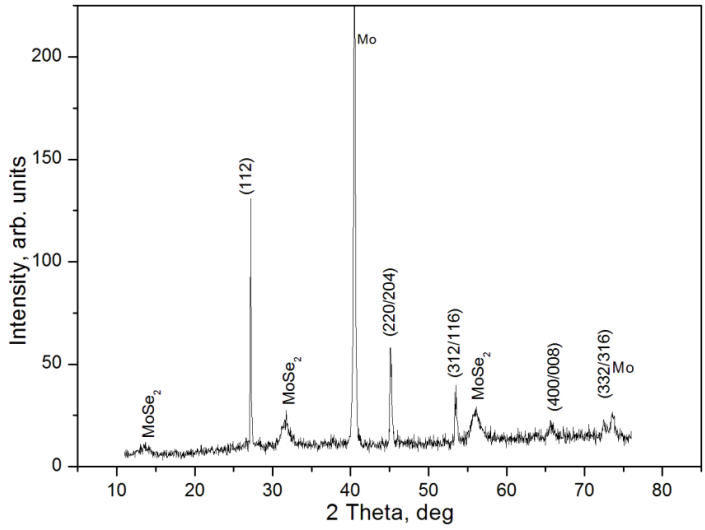

Figure 3. 22 XRD pattern of film selenised at 470ºC for 60 minutes

As there is a difference in band gaps between the absorber and the $MoSe_2$ layers, the $MoSe_2$ layer could be used as a mirror for the electrons and can reduce back surface recombination [105].

3.4.8 Rapid thermal annealing of Cu-Zn and Sn stacked films

Rapid thermal annealing (RTA) is an alternative to conventional furnace annealing. Its advantages include short annealing times and precise control of the annealing profile. PID control allows to regulate overshooting and to keep the process running as close as possible to the desired set point

Precursor compositions are given in Table 3. 10. Time of Sn deposition on the Cu-Zn layer varied and led to increased amount of the Sn in the layer. Preliminary experiments were carried out with a heating rate of 10°C/s; however, this very fast heating led to cracking of the substrate. In order to find suitable conditions for rapid thermal annealing of electrodeposited precursors, six different thermal treatment regimens were applied.

Duration of tin deposition	Cu,at%	Zn, at%	Sn, at%	Cu:(Zn+S)	Zn:Sn
200 sec	42.18	19.51	38.31	0.73	0.51
170 sec	45.97	22.32	32.14	0.84	0.70

Table 3. 10 Composition of stacked precursor layers determined by EDS as a function of Sn electrodeposition time

At first the speed of raising the temperature up to 470°C was varied between 3.3 and 2°C/s (*Figure 3. 23 a*) and samples were cooled down to room temperature (25°C) within 15 minutes. Precursor films that were annealed under the fastest temperature rise (3.3°C/s, fast ramp) contained a large number of

cracks in the film and in some cases, the glass substrate was found split up after annealing. This made these films not suitable for further investigations. The films sulphurised under a temperature ramp up of 2.4°C/s showed a diminished amount of cracks. The quality of the films obtained under "slow" temperature ramping (2°C/s) was significantly better and these films were used for further analysis.

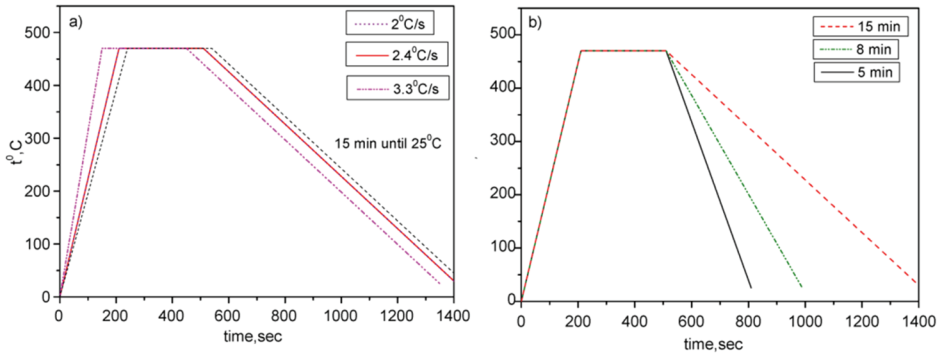

Figure 3. 23 Thermal profiles with three distinct heating (a) and cooling (b) rates

The thermal profile (*Figure 3. 23 b*) was used in experiments with variable cooling durations (from 5 to 15 minutes). The speed of temperature rise was kept constant and was equal to 2°C/s. The films with the fast and medium cooling rate (cooling down to 25°C during 5 or 8 minutes) tend to peel off from the substrate. This is probably due to the strain in films resulting from the difference of thermal coefficients of substrates and film. Only cooling for 15 minutes resulted in CZTS layers with good adhesion to the substrate. Therefore, the optimised heating and cooling parameters were found to be a ramp up of 2°C/s and cooling down to 25°C during 15 minutes.

The XRD patterns (*Figure 3. 24*) for the films annealed at 470 or 500°C for 8 minutes exhibited several peaks corresponding to diffraction lines of the kesterite structure of CZTS. The dominant peak of the XRD pattern of these polycrystalline films corresponds to the (112) diffraction line of the kesterite structure of CZTS. Additional small peaks in XRD pattern were attributed to the appearance of a separate Sn_3S_4 phase (Sn_2S_3 + SnS) [144]. The presence of a Sn containing secondary phase in CZTS films explains the excess of Sn determined by EDS in precursor films (see Table 3. 10).

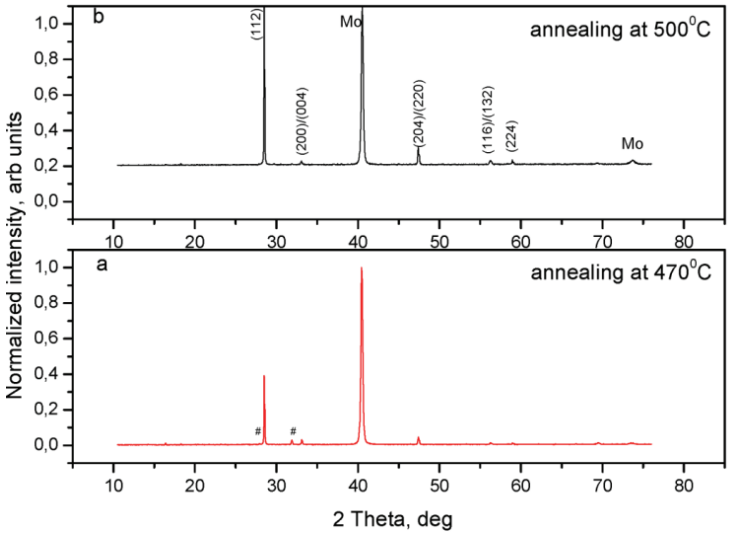

Figure 3. 24 XRD patterns of annealed CZTS films at 500°C and 470°C

The crystallite size of the CZTS films was calculated with the Debye Scherrer formula [145] using full width at half maximum of the (112) peak. The evaluated crystallite size of the films annealed at 470°C was equal to 71 nm, whereas the crystallite size increased to 84 nm at 500°C, which might be due to the higher thermal energy of the atoms at 500°C [146]. The analogous results for annealed CZTS thin films were demonstrated by Yamaguchi et al. [147]. Several groups have reported about crystal growth dependent on temperature [148, 149]. The CZTS films annealed with moderate heating rate (2.4°C/s) showed smaller crystallite size of 61 nm than those (71 nm) which are produced with the slowest heating rate (see Table 3. 11).

t, °C	Crystallite size, nm	Heating, °C/s	Strain
500	84	2.0	-0.4019
470	71	2.0	-0.3067
470	61	2.4	0.0345

Table 3. 11 Calculated crystallite size and strain values for films annealed at 470°C and 500°C with different heating rates.

The strain in films was calculated using the relation from [150],

Eq 3. 3

$$\varepsilon = \frac{c - c_0}{c_0} \cdot 100\%$$

Where c is the lattice constant evaluated from the XRD data and c_0 is the bulk lattice constant. The strain in the films was found to be compressive and found to be lower for slow heating rates when compared to faster heating rates. This infers that a decrease of strain could enhance the crystallinity of the films.

The SEM surface morphological and cross-sectional images of the films annealed at 470°C for 8 and 15 minutes are shown in *Figure 3. 25*. Surfaces of the films are similar to each other; however, SEM cross sectional image for a film annealed for 15 minutes (*Figure 3. 25 d*) allows discerning a very thin layer of MoS_2 (around 70 nm) on the interface between the substrate and CZTS film. The thickness of the sulphurised films was measured by SEM in randomly chosen places and there is no big difference between the thicknesses of CZTS layers annealed for 8 or 15 minutes.

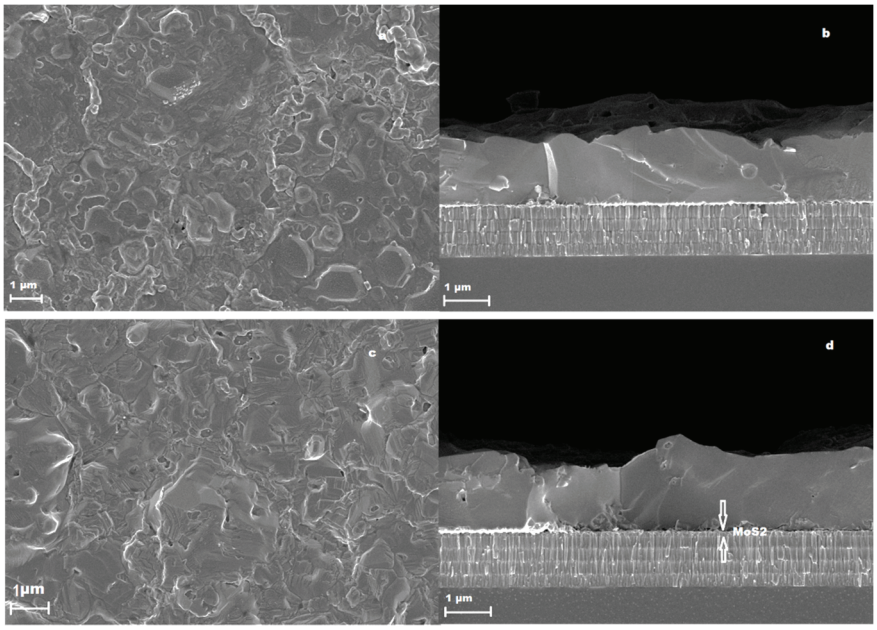

Figure 3. 25 SEM surface and cross-sectional images of the film annealed at 470°C for 8 minutes (a),(b) and (c),(d) for 15 minutes

Films annealed for shorter and longer periods are in average 1.33 µm and 1.42 µm thick, respectively. EDS analysis showed a composition close to stoichiometry for both layers (see Table 3. 12); however, the signal at 2.308 keV (sulphur) in the EDS spectra was higher than stoichiometrically desired. This probably occurs due to overlapping energy peaks for sulphur and Mo in the EDS spectra, namely Mo Lα and S Kα.

Time of Sn deposition	**Sulphurisation**	**Cu**	**Zn**	**Sn**	**S**	**Cu: (Zn+Sn)**	**Zn:Sn**
200 sec	470ºC,15 min	22.94	10.25	12.37	54.43	1.00	0.83
170 sec	470ºC, 8 min	22.35	11.10	12.05	54.50	0.96	0.92
170 sec	500ºC, 8 min	21.54	10.97	11.02	56.47	0.98	0.99

Table 3. 12. Composition of CZTS layer after RTA

The reaction pathway of sulphurisation and formation of MoS_2 seems to be similar to the pathway reported by Kim et al. [151] for formation of $CuInSe_2$ in the selenisation process. The detailed observation of XRD data by Kim shows that the formation of $MoSe_2$ begins at above 450°C, after the completion of CISe formation. Taking into account thicknesses and EDS results of the films, for this PhD work, the assumption was made, that 8 minutes of sulphurisation at 470°C leads to complete formation of CZTS layer and subsequently Mo begins to sulphurise forming MoS_2. In case of $CuInSe_2$, it is reported by several groups [107, 152] that formation of a thin $MoSe_2$ layer is beneficial for cell performance. On the contrary the latest report for CZTS compounds by B. Shin [58] suggests that a reverse correlation between device performance and $MoSe_2$ thickness exists, showing the best efficiency for solar cells with almost no $MoSe_2$ layer. Therefore it is crucial to control MoS_2 formation through optimising sulphurisation parameters.

To identify the chemical nature of separate binary or ternary phases which could also be present in the formed CZTS, films were analysed by Raman spectroscopy. The Raman spectra in *Figure 3. 26* show the results for films annealed at 470°C for 5, 8 and 15 minutes and film annealed at 500°C for 8 min.

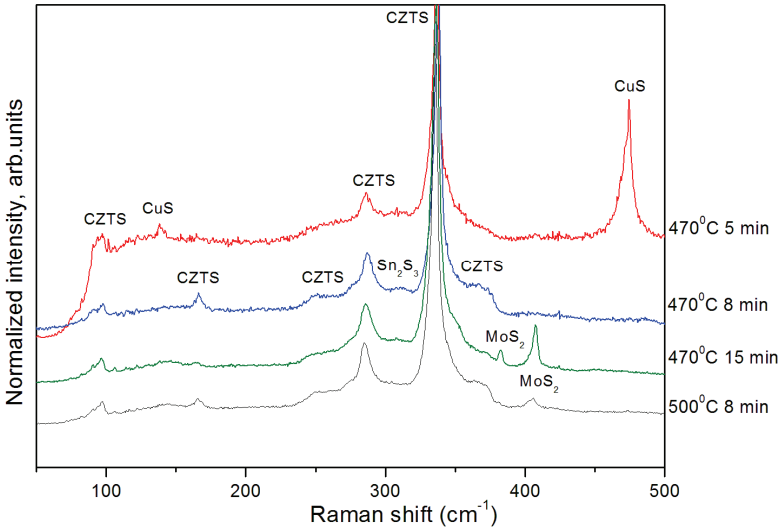

Figure 3. 26 Raman spectra for films sulphurised with different temperatures and durations

All spectra are characterised by the presence of two strong peaks at about 286 and 337 cm^{-1}, that are identified by the main vibrational A1 symmetry modes from CZTS. The spectra also have weaker peaks at about 96 and 166 cm^{-1} which could be identified as E and/or B symmetry modes of CZTS. Peaks at 474 and 142 cm^{-1}, in the spectrum of the sample annealed for 5 minutes, could be assigned to a separate CuS phase, suggesting the partial incompleteness of CZTS formation reaction within 5 minutes of sulphurisation. The spectrum for

the film annealed for 15 minutes shows additional dominant peaks at 380 and 408 cm^{-1} that are connected with the formation of an interfacial MoS_2 phase. This result is consistent with the results obtained from cross-sectional SEM images. Almost all peaks in the Raman spectrum of the precursor film sulphurised at 500°C for 8 minutes could be attributed to the CZTS phase except small peaks at 380 and 408 cm^{-1} that are assigned to MoS_2. This indicates that the sulphurisation reaction of precursors goes faster at 500°C and as a result the CZTS layer could be obtained already in less than 8 minutes of sulphurisation. The only additional small peak at 308 cm^{-1} in the Raman spectrum of the film sulphurised during 8 minutes at 470°C could be attributed to the main characteristic mode of the Sn_2S_3 phase.

3.5 One-step electrochemical deposition of Cu-Zn-Sn-S from one solution

As it was discussed earlier the key question in the one-step electrodeposition technique is finding the appropriate electrolyte composition. Electrodeposition of chalcogenide thin films from one electrolyte is based on Kroger's findings [153]. A simple example of chalcogenide deposition for PV applications is the binary compound CdTe, for which an epitaxial effect through electrodeposition was achieved. When depositing multicomponent compounds, the order and relative disposition of standard electrode potentials for each metal constituent have to be considered [154]. For example, for $CuInSe_2$ the equilibrium potentials of metals could be manipulated by introducing an appropriate ligand [155] whereas the equilibrium potential of the non-metal element depends on the concomitant water splitting reaction and as such depends on the acidity of the solution [156]. When all these considerations are taken into account, the electrodeposition of ternary $CuInSe_2$ compounds could be performed by two different regimes: (a) by induced co-deposition mechanism [157], and (b) under the conditions of diffusion limitations [158, 159]. In case (a), the deposition reaction takes place close to the equilibrium and therefore allows more appropriate arrangement of the complete structure. In this case the speed of deposition is slow and the composition of the deposit remains constant over a large interval of deposition potentials, although being distant from the desired components ratio. In case (b), the obtained structure is again imperfect but the growth speed is higher compared to case (a) and the composition and the components ratio can be controlled by simple process parameters such as applied potential, concentration of elements in the electrolyte, temperature, agitation, etc. [160]. Since deposits are amorphous in both cases and additional annealing treatments are compulsory, the variant (b) appears to be favourable, since it also results in efficient PV devices and can be time efficient [158, 159].

In this section the simultaneous deposition of all four elements will be discussed. According to discussions above, the possibility of fast and controlled co-deposition is possible under the conditions of diffusion limitations. Since deposits are amorphous, additional annealing treatments are compulsory.

3.5.1 Electrolyte elaboration

M. Ganchev et al. [155, 156] investigated the ability of thiocyanate ions as appropriate ligands for simultaneous electrodeposition of Cu, In and Se. Following these results, experiment focused on verifying the thiocyanate ions as suitable ligand for electrodeposition of Cu-Zn-Sn-S precursor, was performed.

The criteria determining the suitability of a ligand for simultaneous electrodeposition of a few elements is again the interrelation of stability constants of their respective compounds. As it was mentioned above on the one hand, ligands should fix stronger to the elements with most positive standard electrode potentials and at the same time form weak complexes with the elements with more negative standard electrode potentials.

Table 3. 13 shows the logarithms of the stability constant values for thiocyanate complexes with Cu^{+}, Zn^{2+} and Sn^{2+} [161]. Stability constant for the element with most positive standard electrode potential (Cu) has a high value (around 10) whereas Sn and Zn ions are under weak influence of the thiocyanate and their complexes are much lower in magnitude. This means that the deposition potential of copper is moved in negative direction, whereas Sn and Zn are not bound as strong to the ligand. Therefore deposition potential of copper shifts closer to the potentials of metals with more negative standard electrode potentials.

	log K_s [1]	**log K_s [2]**	**log K_s [3]**	**log K_s [4]**
Cu^{+}	-	-	-	10.1
Sn^{2+}	1.2	1.8	-	1.7
Zn^{2+}	1.46	2.16	2.33	2.01

Table 3. 13 Thiocyanate complex stability constants by critical survey of stability constants of complexes of thiocyanate ion [161]

As far as sulphur deposition is concerned thiocyanate is indifferent. In the present work, the sulphur supply is provided by a cathodic reduction of the thiosulphate ion ($S_2O_3^{2-}$). Reduction of thiosulphate is elucidated in details in [162], and following conclusions reported in there the thiosulphate undergoes reduction via two ways. The first one is the direct reduction with two electrons near the potential of the zero charge of the surface:

R 3. 2

$$S_2O_3^{2-} + 2e^{-} = S^{2-} + SO_3^{2-}$$

At more negative potentials reduction goes through nascent hydrogen evolved on cathode:

R 3. 3

$$S_2O_3^{2-} + H + OH^{-} + e^{-} = S^{2-} + SO_3^{2-} + H_2O$$

Following the reported data, the general equation for electrodeposition of kesterite could be described as:

R 3. 4

$$2Cu^{+} + Zn^{2+} + Sn^{2+} + 4S_2O_3^{2-} + 6e^{-} \rightarrow Cu_2ZnSnS_4 + 4SO_3^{2-}$$

3.5.2 Composition of electrolyte and of metallic precursor films

The electrolyte was stable long enough to enable the deposition of Cu-Sn-Zn-S thin films with different component ratios. Films that contained high sulphur concentrations were rough and powdery, whereas films with low sulphur content were more compact and stable, allowing further processing.

Figure 3. 27 shows the current and charge density in dependent on the cathode potential (curves 1 and 2). Both curves give information about the current related efficiency of the electrodeposition process dependent on the cathode potential. Curves for a partial charge of individual components Cu, Sn, Zn and S are depicted in *Figure 3. 27* as well. The current density was calculated using the established value of the current after 15 minutes plating time related to the active surface of the electrode. Charge density and respective partial charge densities for the elements are derived by weight measurements of the electrodeposited layers and data for the composition by EDX, following the Faraday's law.

Total charge density is the sum of partials densities, while the hydrogen evolved is not taken into account. In order to increase the reliability of the calculations, these are performed by triple independent EDX measurements at different points on the electrode.

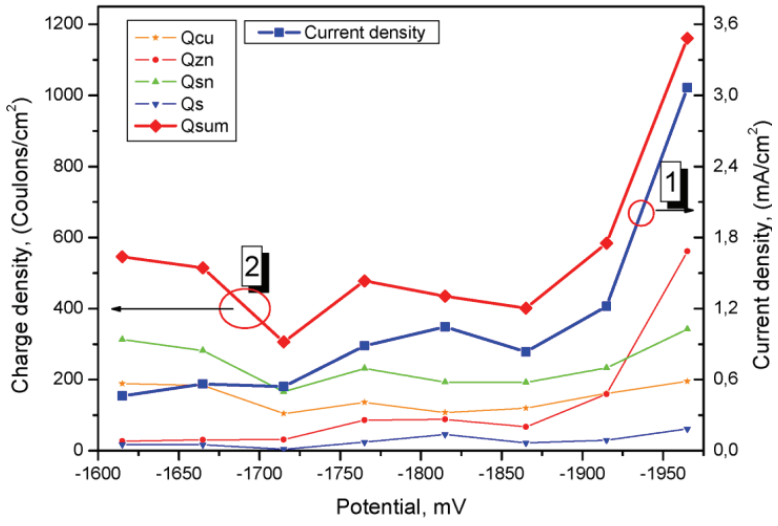

Figure 3. 27 Cathodic current density, charge density and partial charge densities for electrodeposition of Cu–Zn–Sn–S thin films from thiocyanate electrolyte 4M KSCN in 0.4 M acetic buffer (pH 5.0); $[Cu^{+}]:[Zn^{2+}]:[Sn^{2+}]:[S_2O_3^{2-}]$ = 3.6:3.2:1.2:1 mM.

At initial deposition potentials the shapes of curves 1 and 2 (*Figure 3. 27*) as the partial curves of the components show the same tendency without drastic changes. The sharp rise of curves 1 and 2 begins from -1.865 V, and could be explained by beginning hydrogen evolution. This is a typical process observed at cathodes. In the same region an increase of the partial charge density for Zn could be noticed, resulting from the deposition of zinc together with hydrogen evolution. The shapes of curves 1, 2 and Q_{Zn} respectively show that an increased cathodic current density at more negative potentials is not only caused by hydrogen reduction, but is also accompanied by an increase of Zn deposition. On the other hand, it suggests that the ligand SCN^- is an appropriate (weak) complex agent for Zn^{2+} and it only slightly influences its electrochemical behaviour.

The compositions of thin films depending on the component ratio in the electrolyte are presented in *Figure 3. 28*. In fact, the diagram shows only metal component ratios.

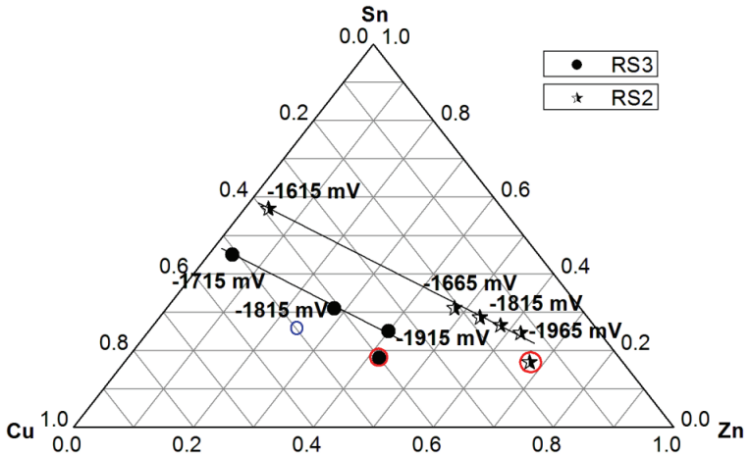

Figure 3. 28 Dependence of CZTS thin films composition on the composition of the electrolyte at different potentials. RS3 and RS2 (in circle) show the composition of electrolytes. The diagram presents metals Cu:Zn:Sn ratio only. The unfilled circle (○) marks the stoichiometric ratio.

Deposited films were about 10% sulphur deficient against stoichiometry of Cu_2ZnSnS_4. As seen in *Figure 3. 28*, the compositions of the films are in line, and with an increased deposition potential the composition tends to approach the initial electrolyte. Slightly higher Sn content in the films is due to presence of Sn in the substrate ITO layer. According to the diagram, the Cu:Sn ratio stays constant when the potential is increased. However, at the same time the Zn content in the films increases. This behaviour is in good compliance with results shown in *Figure 3. 27* where the Cu and Sn content keeps constant while the Zn content increases sharply at elevated cathode potential. These observations guide to a simple rule: the Cu:Sn ratio in the deposited film can be controlled

through preparation of the electrolyte with the desired Cu:Sn ratio, whereas the Zn concentration can be controlled during the deposition process by adjusting the potential.

Sulphur concentration has a strong influence on the mechanical properties of the deposited CZTS layers. It was observed that if sulphur concentration in the electrodeposited layers is close to the stoichiometric value, films are powdery, dendritic, unstable and less receptive to further thermal treatments. Figure 3. 29 presents the dependence of sulphur content in the obtained films on deposition time at a constant potential (-1.865 V). The curve shows that sulphur concentration in the films increases with time of deposition while the ratio of metals content to the total atom content decreases. This phenomenon could be explained with peculiarities of sulphur electrolysis [162]. At initial stages sulphur electrodeposition takes place preferably via the electrochemical mechanism at the SnO_2/SLG substrate, where the overpotential of hydrogen is high. With an increase of the deposition time almost the whole electrode surface area is covered with Cu-Zn-Sn-S. That leads to an increased hydrogen evolution rate and rise of sulphur content in the film by reaction R 3.3.

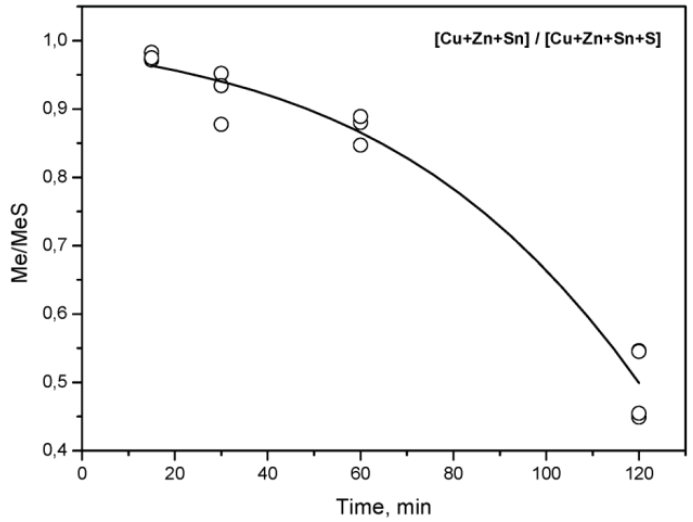

Figure 3. 29 Sulphur concentration in CZTS thin films in dependence on deposition time of the samples (Plating times: 15 minutes, 30 minutes, 60 minutes and 120 minutes at -1.865 V)

3.5.3 Investigation of sulphurised Cu_2ZnSnS_4 compound semiconductor

CZTS films electrodeposited for 60 minutes at -1.865 V contained low sulphur concentration and were, in a second step, annealed in H_2S atmosphere at 550°C for 60 minutes.

There were no noticeable changes in the metal's ratio of the films before and after annealing. Only the sulphur content rose up to the stoichiometric value. The Raman spectrum of the annealed film (*Figure 3. 30 a*) presents a monophase composition of the films. The main vibrations for the kesterite are seen.

The XRD pattern (*Figure 3. 30 b*) for the film annealed at 550°C or for 60 minutes exhibited several peaks corresponding to diffraction lines of the kesterite structure of CZTS. The dominant peak in the XRD pattern of these polycrystalline films correspond to the (112) diffraction line of the kesterite structure of CZTS.

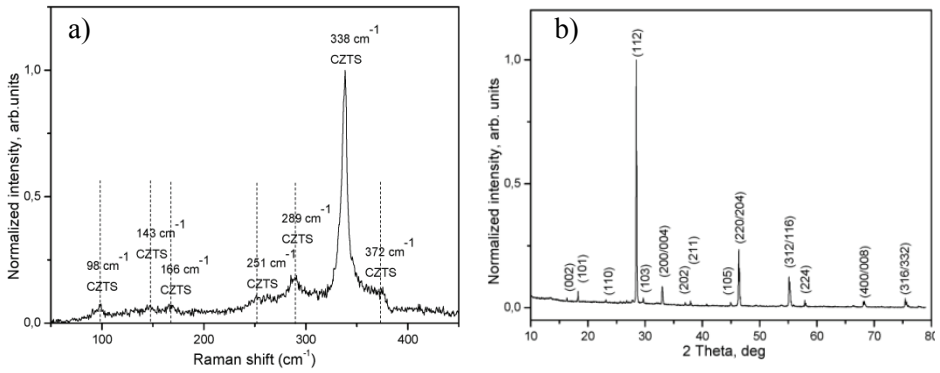

Figure 3. 30 a) Raman spectrum and b) XRD pattern of CZTS film deposited from thiocyanate electrolyte and annealed at 550°C for 1 hour in 5% H_2S:N_2 atmosphere

SEM surface and cross-sectional image of the film annealed at 550°C for 60 minutes is depicted in *Figure 3. 31*. The image shows a typical morphology of CZTS films obtained through this method. The grain size is near 2 – 4 μm, whereas the estimated thickness of the layers is about 1 – 1.5 μm.

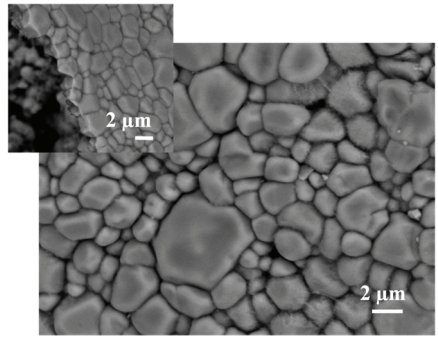

Figure 3. 31 SEM surface and cross-sectional image of CZTS thin film, electrodeposited in thiocyanate electrolyte for 60 minutes and annealed at 550°C for 1 hour in 5% H_2S:N_2 atmosphere

4 CONCLUSIONS

Following the main goal of this work, the technology for producing well-adherent single phase CZTS(Se) thin films by electrochemical deposition of precursor films followed by chalcogenisation was developed.

Different solutions for precursor deposition were elaborated and investigated, including electrodeposition of metallic alloys and/or pure metals and simultaneous electrodeposition of copper, zinc, tin and sulphur. Key findings are:

- Two different complexing agents ($P_2O_7^{4-}$ and $C_6H_5O_7^{3-}$) were used for the deposition of metallic films. It was found that the large difference of stability constants with citrate anions for Cu and Zn leads to a shift of reduction potential for copper in negative direction and allows facile control of metals composition in the alloy. The use of $Na_3C_6H_5O_7$ leads to smoother Cu-Zn alloy deposition. Besides the underpotential deposition of Zn on copper was also observed using $C_6H_5O_7^{3-}$ as a complexing agent.
- The deposition yield when using $C_6H_5O_7^{3-}$ as a complexing agent in the electrodeposition solution was 89% as determined.
- The results from cyclic voltammetry indicate a suitable potential range for simultaneous Cu-Zn, Cu-Sn deposition. Using either trisodium citrate or potassium pyrophosphate in electrolyte the suitable potential for Cu-Zn deposition was between -1.2 and -1.3 V vs. Ag/AgCl. A suitable potential for deposition of Cu-Sn from pyrophosphate ions containing electrolyte was -1.0 to -1.15 V vs Ag/AgCl.
- The dissolution of Zn from the initially deposited Cu-Zn layer in Cu-Sn or pure Sn containing electrolytes results in a need for a very Zn-rich (40–50 at% of Zn) initial Cu-Zn layer in order to get Cu-poor or stoichiometric stacked precursors and subsequently CZTS films.
- It was found that the primary phases formed in thermal annealing of metallic precursor (Cu-Zn-Sn) are Cu_5Zn_8, Cu_6Sn_5, $Cu_{0.7}Zn_{0.3}$ and elemental Sn. The Cu-rich $Cu_{0.7}Zn_{0.3}$ phase arose only after deposition of Sn.
- Thiocyanate ligand allows simultaneous deposition of Cu-Zn-Sn-S thin films. The Cu:Sn ratio in the co-deposited films is controlled through preparation of the electrolyte with the desired Cu:Sn ratio, whereas the Zn concentration is controlled by the applied potential. The sulphur concentration in the co-deposited layers depends on the duration of deposition, but the films are sulphur poor. Lower than stoichiometric concentrations of sulphur in the co-deposited films make thermal annealing in sulphur containing atmosphere compulsory.

Two different regimes for thermal treatment of electrodeposited metallic precursors were performed: Conventional thermal annealing in sealed quartz ampoules as well as rapid thermal annealing in H_2S atmosphere.

- Precursor films selenised for 15 minutes at 530ºC in sealed ampoules led to a well-crystallized $Cu_2ZnSnSe_4$ phase. However, XRD and Raman analyses indicate the presence of additional phases in the films. Films selenised at lower temperature (470ºC) for different durations contain ZnSe phase and Se additionally to a $Cu_2ZnSnSe_4$ phase. Monophase $Cu_2ZnSnSe_4$ film with crystals of large size is observed after 60 minutes of annealing.
- Optimal sulphurisation parameters for rapid thermal annealing were found to be 2°C/s ramp up rate and cooling down to 25°C for 15 minutes at 470ºC. The rapid thermal annealing at 470°C during 8 minutes results in complete sulphurisation of precursors and formation of a CZTS layer.
- The Mo sulphurisation begins after the sulphurisation of precursors and results in appearance of MoS_2 peaks in Raman spectra of these films.

Overall this work has developed suitable approaches and parameters for formation of CZTS(Se) compound by electrochemical deposition and annealing route. The work also identified and described a number of peculiarities of this approach, which will help to inform future research in this field.

AKNOWLEGMENTS

I am deeply thankful to my supervisors Senior Researcher Dr Olga Volobujeva and Professor Enn Mellikov for their great help, support and motivation during the years of my PhD studies. Their encouragement, guidance and lively discussions enabled me to pursue my studies successfully. During these years they also gave me the opportunity to attend conferences, summer schools and other meetings concerning my PhD topic, which helped me in gaining additional experience, extending my knowledge and also in establishing valuable collaborations with partner institutes abroad.

I am also thankful to the Dean of the Faculty of Chemical and Materials Technology and the Director of the doctoral school "Functional materials and technologies" in TUT Professor Andres Öpik for giving me the opportunity to pursue my PhD studies in the faculty in TUT and to participate in the Doctoral school.

I would also like to thank Professor Remigijus Juškenas from the University of Vilnius and Dr Jonathan J. Scragg from the University of Uppsala, for accepting to be opponents at my PhD defense.

Dr Maxim Ganchev I thank for all his contributions to this work: valuable advices, part in writing publications and sharing his ideas and knowledge.

I am grateful to Lead Research Scientist Dr Mare Altosaar, for her kind support and continuous advice, which is much appreciated.

With a big pleasure I thank all my colleagues with who I worked on aspects of this thesis: Dr Maarja Grossberg and PhD student Taavi Raadik for Raman spectroscopy measurements, Dr Rainer Traksmaa and Dr Arvo Mere for the XRD analysis. My thanks also go to Dr Jaan Raudoja for enormous help with annealing experiments and for clarifying equipment related questions. Dr Karin Kerm is thanked for excellent polarography measurements.

Dr Alar Jänes and Dr Jaanus Kruusma from Tartu University are greatly thanked for checking my electrochemical results and for giving advice. My special thanks here also to Dr Julia Kois for her assistance during this work and providing me with the RDE setup. Professor Dieter Meissner I thank for his valuable remarks, advices and discussions on various fields of electrochemistry.

This thesis could not have been completed without great support and advices of my colleagues and friends: Dr Revathi Naidu, PhD students Mihkel Loorits and Jelena Gurevits. Many thanks also to the always positively inspiring colleagues Dr Sergei Bereznev, Dr Tiit Varema and to Professor Jüri Krustok for being ready to help at any time and answer questions that arose during my studies. I am also grateful to all other colleagues from the laboratory for their kind attitude and readiness to help. A big thank also to our secretary Rita Jaaguman for her organizational support.

My profound gratitude I express to my family: my mother Jelena, my grandparents Aleksandra and Nikolay and my husband Franz for their unconditional support and belief they shared with me all these years.

This work was supported by the Estonian Science Foundation grant 8147. The target financing by the Estonian Ministry of Education and Research No. SF0140099s08, Estonian Centre of Excellence in Research “High-technology Materials for Sustainable Development” (project TAR 11059), Estonian governmental program in new energy technologies (projects AR 10128) and graduate school “Functional materials and technologies” are gratefully appreciated

Julia Lehner Tallinn, May 2014

ABSTRACT

Formation of Cu_2ZnSnS_4 and $Cu_2ZnSnSe_4$ by chalcogenisation of electrochemically deposited precursor layers

The aim of the present doctoral thesis was to investigate the formation of Cu_2ZnSnS_4 and $Cu_2ZnSnSe_4$ compounds during chalcogenisation of electrochemically deposited thin layers.

CZTS(Se) is a novel and promising semiconductor-absorber material for the solar cell industry as it consists of earth-abundant and non-toxic elements (except Se). One of the advantages of this quaternary compound is its high absorption coefficient of more than 10^4 cm^{-1}. Additionally, CZTS(Se) has a direct band gap of approximately 1 eV for $Cu_2ZnSnSe_4$ and 1.5 eV for Cu_2ZnSnS_4. The preparation method for precursor films in this study is electrochemical deposition. Benefits of this method include performance at, or near room temperature, cost-efficiency, small chemicals wastage and relatively fast deposition rate. Using non-toxic materials, it can be considered an environmentally friendly production technique. Electrochemical deposition of metals, alloys and compounds can be controlled through some of the electrical parameters of the deposition process, as well as by chemical parameters of the prepared electrolyte (concentration of constituents, pH, complexing agents), and by the duration of the process. Through all these variables composition, morphology and thickness of deposited layers can be regulated.

In the present work, the influence of the initial composition of precursors as well as the influence of different conditions in the chalcogenisation process on the synthesized CZTS(Se) phase and its chemical composition was investigated. Two different approaches for preparation of precursor films were performed and compared: 1) simultaneous co-deposition of elemental Cu-Zn-Sn-S elements and 2) sequential deposition of various stacked alloys (Cu-Zn, Cu-Sn) and metal (Sn). Three different complexing agents (SCN^-, $P_2O_7^{4-}$, $C_6H_5O_7^{3-}$) were applied in order to find best conditions for precursor preparation. The novelty of this work is the electrodeposition of binary compounds to form precursor layers and their subsequent chalcogenisation to form CZTS(Se) thin films.

Electrodeposited precursor layers were annealed in two different ways:

1) isothermal annealing in selenium vapour or
2) sulphurisation in H_2S atmosphere in an infrared furnace (rapid thermal annealing).

The main advantage of rapid thermal annealing is the fast heating and cooling rate that can save time and energy, both of which is important for potential future industrial production. Electrochemically deposited precursors and thermally treated films were investigated with cyclic voltammetry, polarography, SEM, EDX, AFM, XRD and Raman spectroscopy.

It was found that use of a rotating disc electrode leads to formation of precursors with uniform thickness and homogenous structure. The complexing agent $C_6H_5O_7^{3-}$ led to deposition of dense and smooth metallic precursor layers.

The investigations also showed the occurrence of underpotential deposition phenomenon of Zn^{2+} on a primordial copper layer. Deposition of metallic layers using $P_2O_7^{4-}$ as a complexing agent resulted in a yield of 79% and in contrast deposition from the electrolyte containing $C_6H_5O_7^{3-}$ as complexing agent resulted in a yield of 89%. A suitable potential range for simultaneous Cu-Zn deposition was determined through cyclic voltammetry. With citrate ion as the complexing agent the suitable potential for Cu-Zn deposition was found to be in the range of -1.2 to -1.3 V (vs Ag/AgCl). Moreover, it was found that for stacked precursor structures like Cu-Zn/Sn and Cu-Zn/Sn-Cu, Zn tends to dissolve from the initially deposited Cu-Zn layer in copper-tin or pure tin containing electrolytes. It was concluded that very Zn-rich (40 – 50 at% of Zn) initial Cu-Zn layer is required in order to get Cu-poor or stoichiometrically stacked precursors and subsequently CZTS(Se) films. The primary phases formed in metallic precursors (Cu-Zn-Sn) are Cu_5Zn_8, Cu_6Sn_5, $Cu_{0.7}Zn_{0.3}$ and elemental Sn. The Cu-rich phase $Cu_{0.7}Zn_{0.3}$ arose only after deposition of Sn.

Thiocyanate ligand used for deposition of Cu-Zn-Sn-S thin films showed the possibility of simultaneous co-deposition of Cu-Zn-Sn-S compounds. The Cu:Sn ratio in the co-deposited films is controlled through preparation of the electrolyte with the desired Cu:Sn ratio, whereas the Zn concentration is determined by applied potential. The sulphur concentration in the co-deposited layers depends on the duration of deposition, but the films are as a rule sulphur poor and need additional treatment in chalcogen atmosphere. After annealing in H_2S gas CZTS films were formed and XRD and Raman spectroscopy measurements indicated the absence of other phases in the film.

Precursor films selenised for 15 minutes at 530ºC in sealed ampoules exhibited a well-crystallized $Cu_2ZnSnSe_4$ phase. However, XRD and Raman analyses indicate the presence of additional phases in these films. Optimal sulphurisation parameters for rapid thermal annealing were found to be 2°C/s ramp up rate and cooling down to 25°C for 15 minutes at 470ºC. RTA at 470°C for 8 minutes results in complete sulphurisation of precursors and formation of a CZTS layer. The Mo sulphurisation begins after the sulphurisation of precursors and results in appearance of the MoS_2 phase.

KOKKUVÕTE

$Cu_2ZnSnSe_4$ ja Cu_2ZnSnS_4 moodustumine elektrokeemiliselt sadestatud kihtide kalkogeniseerimisel

Käesoleva doktoritöö eesmärgiks oli uurida Cu_2ZnSnS_4 ja $Cu_2ZnSnSe_4$ (CZTS(Se)) sünteesiprotsessi seaduspärasusi õhukeste metallikihtide elektrokeemilisel sadestamisel ja sadestamisele järgnevas kalkogeniseerimise protsessis.

CZTS(Se) on uudne ja perspektiivne pooljuhtühend-absorbermaterjal päikeseenergeetikas, kuna ta koosneb maakoores rohkelt esinevatest mittemürgistest elementidest ning omab kõrget neeldumiskoefitsenti ja optimaalset keelutsooni laiust. Töös kasutatud elektrokeemilise sadestamise meetodi peamisteks eelisteks on protsessi odavus, suhteliselt suur sadestuskiirus ning väike kemikaalide kulu. Elektrokeemiline sadestamine on hästi kontrollitav mitmete sadestusprotsessi elektriliste parameetritega, kasutatava elektrolüüdi keemiliste parameetritega (kontsentratsioon, pH, vabade ioonide kompleksseerimine) ning sadestamise kestvusega, mis võimaldavad reguleerida sadestatavate kilede koostist, morfoloogiat ja paksust.

Antud töös uuriti nii lähtekilede elektrokeemilise sadestusprotsessi parameetrite kui ka kilede kalkogeniseerimisprotsessi erinevate parameetrite mõju CZTS(Se) faasi- ja keemilisele koostisele. Läbiviidud uuringutes kasutati ja võrreldi kahte erinevat lähenemisviisi lähtekilede elektrokeemiliseks sadestuseks: 1) kõikide CZTS koostiselementide üheaegset koos-sadestust ja 2) erinevate metallisulamite järjestikust sadestamist. Töös kasutati kompleksioonide moodustamiseks sadestuslahustes kolme erinevat ligandi. Uurimistöö põhiliseks uudsuseks on binaarsete metallisulamite elektrokeemiline sadestamine CZTS(Se) lähtekiledes ja CZTS(Se) absorberkilede sünteesimine nende lähtekilede kalkogeniseerimise teel.

Elektrokeemiliselt sadestatud prekursorkilesid kuumutati kahel viisil: 1) isotermiliselt seleeni atmosfääris või 2) sulfureerimisel H_2S gaasi keskkonnas, kasutades niinimetatud kiirkuumutuse meetodit. Kasutatud kiirkuumutuse peamiseks eeliseks on koostise ja termotöötluse parameetrite täpsem kontrollimine laias temperatuuride vahemikus. Elektrokeemilise sadestusprotsessi ja sadestatud prekursorkilede, samuti ka kuumutatud õhukeste CZTS(Se) kilede uurimiseks kasutati tsüklilist voltamperomeetriat, Raman-spekroskoopiat, EDX ja XRD, AFM ning SEM meetodeid.

Töö käigus leiti, et prekursorkilede homogeensuse ja ühtlase paksuse tagas pöörleva elektroodi kasutamine. Selgitati välja, et parimate parameetritega metalsed prekursorikiled saadakse, kui kasutada elektrokeemilise sadestamise lahustes ligandina kas $P_2O_7^{4-}$ või $C_6H_5O_7^{3-}$ ioone. Uurimuse tulemusena leiti, et naatriumtsitraadi juuresolekul on võimalik sadestada siledama pinnaga kilesid. Uurimuses määrati elektrokeemilise sadestamisprotsessi saagiseks pürofosfaatses lahuses 79% ja tsitraatses lahuses 89%. Töös leiti erinevate sulamikihtide võimalikud sadestamis-piirkonnad: naatriumtsitraadi juuresolekul

lahuses on Cu-Zn sulami sadestamise piirkond vahemikus -1.2 ja -1.3 V (vs Ag/AgCl). Töös leiti seaduspära, et kihiliste struktuuride Cu-Zn/Sn ja Cu-Zn/Sn-Cu sadestamise puhul läheb tsink pealiskihi sadestamisel Cu-Zn-aluskihist uuesti tina sisaldavasse elektrolüüti. Zn kao kompenseerimiseks sadestati Cu-Zn aluskiht kõrgema Zn kontsentratsiooniga (40 – 50 at% Zn), mis kindlustas pärast sulfureerimist saadavate CZTS kilede stöhhiomeetrilise koostise. Faasikoostise uuringud näitasid, et metalliliste lähtekilede (Cu-Zn-Sn) termiline käsitlus viib esimese etapina Cu_5Zn_8, Cu_6Sn_5, $Cu_{0.7}Zn_{0.3}$ ja elementaarse tina tekkele kiledes.

Koossadestusprotsessi uurimine näitas, et kõigi nelja koostiselemendi Cu-Zn-Sn-S üheaegne koossadestamine on võimalik, kui kasutada sadestamislahuses ligandina tiotsüanaati. Leiti, et Cu:Sn suhet koossadestatud kiledes on võimalik kontrollida sadestamiseks kasutatava elektrolüüdi koostisega (Cu^{2+} ja Sn^{2+} kontsentratsioonidega), kuid Zn kontsentratsioon kiledes on kontrollitav vaid sadestuspotentsiaaliga. Siiski on koossadestusprotsessis saadud CZTS kiled väävlivaesed ning vajavad seetõttu termilist järeltöötlemist kalkogeeni keskkonnas. Pärast koossadestusprotsessil saadud kilede kuumutamist 550ºC juures saadi stöhhiomeetrilised CZTS kiled, kus XRD ja Raman-spektroskoopilised uuringud ei näidanud teiste kõrvalfaaside olemasolu.

Töös näidati, et CZTS kilede saamiseks on võimalik kasutada nii prekursorkilede termilist töötlust evakueeritud kvartsampullides Se juuresolekul kui ka nende ülikiiret kuumutust H_2S voos (inglise keeles rapid thermal annealing - RTA). Selgus, et lähtekilede seleniseerimisel evakueeritud kvartsampullides 530 ºC juures 15 min. jooksul moodustus hästi kristalliseerunud $Cu_2ZnSnSe_4$ kile, mis XRD ja Raman analüüside alusel oli mitmefaasiline. Kiirkuumutus H_2S voos 470 °C juures 8 min. jooksul kasutades optimaalset temperatuuri tõstmise kiirust 2 ºC/s ja 15 minutilist jahutamist toatemperatuurini andis tulemuseks ühefaasilise Cu_2ZnSnS_4 kile. Näidati, et MoS_2 moodustumine Mo-alusklaasil algab kiirkuumutust kasutades alles pärast prekursorkile sulfuriseerumist.

Kokkuvõtvalt võib välja tuua, et antud töös arendatud elektrokeemiliselt sadestatud binaarsete metallisulamite kilede kiirkuumutamine kalkogeeni sisaldavas gaasivoos on uudne ja perspektiivne tehnoloogia ühefaasiliste CZTS(Se) absorberkilede sünteesimiseks

REFERENCES

[1] International Energy Agency, „World Energy Outlook 2013," IEA, 2013.

[2] A. Feltrin and A. Freundlich, "Material considerations for terawatt level deployment of photovoltaics," *Renewable Energy 33,* p. 180, 2008.

[3] IEA PVPS, „PVPS Report: Snapshot of Global PV 1992-2013," 2013.

[4] I. Fraunhofer Institute for Solar Energy Systems, „Photovoltaics Report 7 Nov 2013" 2013.

[5] NREL, „Best Research Cell Efficiencies," 2014. [Online]. Available: http://www.nrel.gov/ncpv/images/efficiency_chart.jpg. [Accessed 07 04 2014].

[6] „Solar Frontier," 2014. [Online]. Available: http://www.solar-frontier.com/eng/news/2014/C031367.html.

[7] IEA PVPS, „Trends 2013 in Photovoltaic Applications," 2013.

[8] W. Wang, M. T. Winkler, O. Gunawan, T. Gokmen, T. Todorov, Y. Zhu and D. B. Mitzi, „Device Characteristics of CZTSSe Thin-Film Solar Cells with 12.6% Efficiency," *Advanced Energy Materials,* 2013 DOI:10.1002/aenm.201301465.

[9] S. Ahmed, K. B. Reuter, O. Gunawan, G. Lubomyr, T. Romankiw and H. Deligianni, „A High Efficiency Electrodeposited Cu_2ZnSnS_4 Solar Cell," *Advanced Energy Materials 2,* p. 253, 2012.

[10] J. Poortmans and V. Arkhipov, Thin Film Solar Cells, Fabrication, Characterization and Applications, Chichester, West Sussex, England: John Wiley & Sons Ltd, 2006.

[11] A. Goetzberger and C. Hebling, „Photovoltaic materials, past, present, future," *Solar Energy Materials & Solar Cells 62,* p. 1, 2000.

[12] K. L. Chopra, P. D. Paulson and V. Dutta, „Thin-Film Solar Cells: An Overview," *Progress in Photovoltaics 12,* p. 69, 2004.

[13] L. Shiozawa, F. Augustine, G. Sullivan, M. Smith and W. Cook, „Clevite Final Report," ARL 69-0155, 1969.

[14] P. Bhat, S. Das, D. Pandya and K. Chopra, „Back illuminated high efficiency thin-film Cu2S/CdS solar cells," *Solar Energy Materials 1,* p. 215, 1979.

[15] A. Goetzberger, J. Luther and G. Willeke, „Solar cells: past, present, future," *Solar Energy Materials & Solar Cells 74,* p. 1, 2002.

[16] R. Birkmire, „Compound polycrystalline solar cells:: Recent progress and Y2 K perspective," *Solar Energy Materials & Solar Cells 65,* pp. 17-28, 2001.

[17] H. Katagiri, K. Jimbo, W. Maw, K. Oishi, M. Yamazaki, H. Araki and A. Takeuchi, „Development of CZTS-based thin film solar cells," *Thin Solid Films 517,* p. 2455, 2009.

[18] M. A. Green, K. Emery, D. L. King, S. Igari and W. Warta, „Solar Cell Efficiency Tables," *Progress in Photovoltaics 9,* p. 55, 2002.

[19] J. J. Scragg, Copper Zinc Tin Sulfide Thin Films for Photovoltaics, Springer-Verlag Berlin Heidelberg, 2011, PhD thesis.

[20] H. Wang and J. M. Bell, „Thin film solar cells based on Cu_2ZnSnS_4 absorber," *In The 5th World Congress on Engineering Asset Management (WCEAM 2010)*, Brisbane, 2010.

[21] H. Flammersberger, *Experimental study of Cu_2ZnSnS_4 thin films for solar cells,* Uppsala, 2010, Master Thesis.

[22] I. Dudchak and L. Piskach, „Phase equilibria in the Cu_2SnSe_3–$SnSe_2$–ZnSe system," *Journal of Alloys and Compounds 351,* p. 145, 2003.

[23] I. Olekseyuk, I. Dudchak and L. Piskach, „Phase equilibria in the Cu_2S-ZnS-SnS_2 system," *Journal of Alloys and Compounds 368,* p. 135, 2004.

[24] T. Gödecke, T. Haalboom and F. Ernst, „Phase equilibria of Cu-In-Se I: stable states and nonequilibrium states of the In_2Se_3-Cu_2Se subsystem," *Zeitschrift für Metallkunde 91,* p. 622, 2000.

[25] S. Siebentritt, „Why are kesterite solar cells not 20% efficient?," *Thin Solid Films 535,* pp. 1-4, 2013.

[26] H. Araki, A. Mikaduki, Y. Kubo, T. Sato, K. Jimbo, W. Maw, H. Katagiri, M. Yamazaki, K. Oishi and A. Takeuchi, „Preparation of Cu_2ZnSnS_4 thin films by sulfurization of stacked metallic layers," *Thin Solid Films 517,* p. 1457, 2008.

[27] T. Schnabel, M. Löw and E. Ahlswede, „Vacuum-free preparation of 7.5% efficient $Cu_2ZnSn(S,Se)_4$ solar cells based on metal salt precursors," *Solar Energy Materials & Solar Cells 117,* p. 324, 2013.

[28] S. M. Pawar, A. I. Inamdar, B. S. Pawarb, K. Gurav, S. W. Shin, X. Yanjun, S. S. Kolekar, J.-H. Lee, J. H. Kim and H. Im, „Synthesis of Cu_2ZnSnS_4 (CZTS) absorber by rapid thermal processing (RTP) sulfurization of stacked metallic precursor films for solar cell applications," *Materials Letters 118,* p. 76, 2014.

[29] C. M. Fella, A. R. Uhl, Y. E. Romanyuk and A. N. Tiwari, „$Cu_2ZnSnSe_4$ absorbers processed from solution deposited metal salt precursors under different selenization conditions," *Physica Status Solidi 209,* p. 1043, 2012.

[30] K. Tanaka, M. Oonuki, N. Moritake and H. Uchiki, „Cu_2ZnSnS_4 thin film solar cells prepared by non-vacuum processing," *Solar Energy Materials & Solar Cells 93,* p. 583, 2009.

[31] K. Tanaka, Y. Fukui, N. Moritake and H. Uchiki, „Chemical

composition dependence of morphological and optical properties of Cu_2ZnSnS_4 thin films deposited by sol–gel sulfurization and Cu_2ZnSnS_4 thin film solar cell efficiency," *Solar EnergyMaterials & SolarCells 95,* p. 838, 2011.

[32] A. Weber, H. Krauth, S. Perlt, B. Schubert, I. Kötschau, S. Schorr and H.-W. Schock, „Multi-stage evaporation of Cu_2ZnSnS_4 thin films," *Thin Solid Films 517,* p. 2524, 2009.

[33] O. Volobujeva, S. Bereznev, J. Raudoja, K. Otto, M. Pilvet and E. Mellikov, „Synthesis and characterisation of $Cu_2ZnSnSe_4$ thin films prepared via a vacuum evaporation-based route," *Thin Solid Films 535,* p. 48, 2013.

[34] K. Maeda, K. Tanaka, Y. Fukui and H. Uchiki, „Influence of H_2S concentration on the properties of Cu_2ZnSnS_4 thin films and solar cells prepared by sol–gel sulfurization," *Solar Energy Materials & Solar Cells 95,* p. 2855, 2011.

[35] S. Mali, P. Shinde, C. Betty, P. Bhosale, Y. Oh and P. Patil, „Synthesis and characterization of Cu_2ZnSnS_4 thin films by SILAR method," *Journal of Physics and Chemistry of Solids 73,* p. 735, 2012.

[36] H. Araki, Y. Kubo, A. Mikaduki, K. Jimbo, W. Maw, H. Katagiri, M. Yamazaki, K. Oishi and A. Takeuchi, "Preparation of Cu_2ZnSnS_4 thin films by sulfurizing electroplated precursors," *Solar Energy Materials and Solar Cells 93,* p. 996, 2009.

[37] K. Jimbo, R. Kimura, T. Kamimura and H. Katagiri, „Cu_2ZnSnS_4-type thin film solar cells using abundant materials," *Thin Solid Films 515,* p. 5997, 2007.

[38] X. Zeng, K. Tai, T. Zhang, C. Ho, X. Chen, A. Huan, T. Sum and L. Wong, „$Cu_2ZnSn(S,Se)_4$ kesterite solar cell with 5.1% efficiency using spray pyrolysis of aqueous precursor solution followed by selenization," *Solar EnergyMaterials & SolarCells 124,* p. 55, 2014.

[39] Z. Zhou, Y. Wang, D. Xu and Y. Zhang, „Fabrication of Cu_2ZnSnS_4 screen printed layers for solar cells," *Solar Energy Materials & Solar Cells 94,* p. 2042, 2010.

[40] C. Platzer-Bjorkman, J. Scragg, H. Flammersberger, T. Kubart and M. Edoff, „Influence of precursor sulfur content on film formation and compositional changes in Cu_2ZnSnS_4 films and solar cells," *Solar energy Materials & Solar Cells 98,* p. 110, 2012.

[41] A. Moholkar, S. Shinde, A. Babar, K.-U. Sim, Y.-b. Kwon, K. Rajpure, P. Patil, C. Bhosale and J. Kim, „Development of CZTS thin films solar cells by pulsed laser deposition: Influence of pulse repetition rate," *Solar Energy 85,* p. 1354, 2011.

[42] N. Carter, W.-C. Yang, C. Miskin, C. Hages, E. Stach and R. Agrawal, „$Cu_2ZnSn(S,Se)_4$ solar cells from inks of heterogeneous

Cu–Zn–Sn–S nanocrystals," *Solar Energy Materials & Solar Cells 123,* p. 189, 2014.

[43] T. Dhakal, C.-Y. Peng, R. Tobias, R. Dasharathy and C. Westgate, „Characterization of a CZTS thin film solar cell grown by sputtering method," *Solar Energy 100,* p. 23, 2014.

[44] J. Li, T. Ma, W. Liu, G. Jiang and C. Zhu, „The $Cu_2ZnSnSe_4$ thin films solar cells synthetized by electrodeposition route," *Applied Surface Science 258,* p. 6261, 2012.

[45] J. J. Scragg, D. M. Berg and P. Dale, „A 3.2% efficient Kesterite device from electrodeposited stacked elemental layers," *Journal of Electroanalytical Chemistry 646,* p. 52, 2010.

[46] H. Araki, Y. Kubo, K. Jimbo, W. Maw and H. Katagiri, „Preparation of Cu_2ZnSnS_4 thin films by sulfurization of co-electroplated Cu-Zn-Sn precursors," *Physica Status Solidi 6,* p. 1266, 2009.

[47] Y. Zhang, C. Liao, K. Zong and H. Wang, „$Cu_2ZnSnSe_4$ thin film solar cells prepared by rapid thermal annealing of co-electroplated Cu–Zn–Sn precursors," *Solar Energy 94,* p. 1, 2013.

[48] N. Moritake, Y. Fukui, M. Oonuki, K. Tanaka and H. Uchiki, „Preparation of Cu_2ZnSnS_4 thin film solar cells under non-vacuum condition," *Physica Status Solidi 6,* p. 1233, 2009.

[49] R. Chalapathy, G. Jung and B. Ahn, „Fabrication of Cu_2ZnSnS_4 films by sulfurization of Cu/ZnSn/Cu precursor layers in sulfur atmosphere for solar cells," *Solar Energy Materials & Solar Cells 95,* p. 3216, 2011.

[50] A. Walsh, S. Chen, S.-H. Wei and X.-G. Gong, „Kesterite Thin-Film Solar Cells: Advances in Materials Modelling of Cu_2ZnSnS_4," *Advanced Energy Materials 2,* pp. 400-409, 2012.

[51] D. Mitzi, O. Gunawan, T. Todorov, K. Wang and S. Guha, „The path towards a high-performance solution-processed kesterite solar cell," *Solar Energy Materials & Solar Cells 95,* p. 1421, 2011.

[52] J. Just, D. Lützenkirchen-Hecht, R. Frahm, S. Schorr and T. Unold, „Determination of secondary phases in kesterite Cu_2ZnSnS_4 thin films by x-ray absorption near edge structure analysis," *Applied Physics Letters 99,* (2011) doi: 10.1063/1.3671994.

[53] J. Ge, Y. Wu, C. Zhang, S. Zuo and J. Jiang, „Comparative study of the influence of two distinct sulfurization ramping rates on the properties of Cu_2ZnSnS_4 thin films," *Applied Surface Science 258,* p. 7250, 2012.

[54] A. Ennaoui, M. Lux-Steiner, A. Weber, D. Abou-Ras, I. Kötschau, H.-W. Schock, R. Schurr, A. Hölzing, S. Jost, R. Hock, T. Voss, J. Schulze and A. Kirbs, „Cu_2ZnSnS_4 thin film solar cells from electroplated precursors: Novel low-cost perspective," *Thin Solid*

Films 517, p. 2511, 2009.

[55] A. Redinger, D. M. Berg, P. J. Dale and S. Siebentritt, „The Consequences of Kesterite Equilibria for Efficient Solar Cells," *Journal of the American Chemical Society 133,* p. 3320, 2011.

[56] A. Weber, R. Mainz, T. Unold, S. Schorr and H.-W. Schock, „In-situ XRD on formation reactions of Cu_2ZnSnS_4 thin films," *Physica Status Solidi 6,* p. 1245, 2009.

[57] B. Shin, O. Gunawan, Y. Zhu, N. Bojarczuk, S. Chey and S. Guha, „Thin film solar cell with 8.4% power conversion efficiency using an earth-abundant Cu_2ZnSnS_4 absorber," *Progress in Photovoltaics 21,* p. 72, 2013.

[58] B. Shin, Y. Zhu, N. Bojarczuk, S. Chey and S. Guha, „Control of an interfacial $MoSe_2$ layer in $Cu_2ZnSnSe_4$ thin film solar cells: 8.9% power conversion efficiency with a TiN diffusion barrier," *Applied Physics Letters 101,* p. 053903, 2012.

[59] H. Katagiri, K. Jimbo, S. Yamada, T. Kamimura, W. Maw, T. Fukano, T. Ito and T. Motohiro, „Enhanced Conversion Efficiencies of Cu_2ZnSnS_4-Based Thin Film Solar Cells by Using Preferential Etching Technique," *Applied Physics Express 1,* p. 041201, 2008.

[60] Solliance / Imomec news item, 4 Jul 2013, http://www.solliance.eu/ [Online].

[61] A. Nandur and B. White, „Growth of Cu_2ZnSnS_4(CZTS) by Pulsed Laser Deposition for Thin film Photovoltaic Absorber Material," *American Physical Society Meeting*, 2014.

[62] C. J. Hibberd, E. Chassaing, W. Liu, D. B. Mitzi, D. Lincot and A. N. Tiwari, „Non-vacuum methods for formation of Cu(In, Ga)(Se, $S)_2$ thin film photovoltaic absorbers," *Progress in Photovoltaics 18,* p. 434, 2010.

[63] D. E. Carlson, *The status and future of the photovoltaics industry,* ppt, 2011.

[64] N. Kamoun, H. Bouzouita and B. Rezig, „Fabrication and characterization of Cu_2ZnSnS_4 thin films deposited by spray pyrolysis technique," *Thin Solid Films 515,* p. 5949, 2007.

[65] Y. Kishore Kumar, G. Suresh Babu, P. Uday Bhaskar and V. Sundara Raja, „Preparation and characterization of spray-deposited Cu_2ZnSnS_4 thin films," *Solar Energy Materials & Solar Cells 93,* p. 1230, 2009.

[66] W. Daranfed, M. S. Aida, N. Attaf, J. Bougdira and H. Rinnert, „Cu_2ZnSnS_4 thin films deposition by ultrasonic spray pyrolysis," *Journal of Alloys and Compounds 542,* p. 22, 2012.

[67] T. Prabhakar and J. Nagaraju, „Device parameters of Cu_2ZnSnS_4 thin film solar cell," *Photovoltaic Specialists Conference (PVSC), 37th IEEE,* p. 001346, 2011.

[68] B. M. C. Stacey F. Bent, „Self-organizing nanostructured solar cells“. Patent US 20090314342 A1, 2009.

[69] M. Cao, L. Li, B. Zhang, J. Huang, L. Wang, Y. Shen, Y. Sun, J. Jiang and G. Hu, „One-step deposition of Cu2ZnSnS4 thin films for solar cells,“ *Solar Energy Materials & Solar Cells 117,* p. 81, 2013.

[70] Н. Федотьев, А. Алабышев, А. Рогинян, И. Вячеславов, П. Животинский and А. Гальнбек, Прикладная электрохимия, ГХИ, 1962.

[71] В. Багоцкий, Основы электрохимии, Химия, 1988.

[72] M. Schwartz, „Deposition from Aqueous Solutions: An Overview,“ *Handbook of Deposition Technologies for Films and Coatings (Second Edition)*, Noyes Publications, 1994.

[73] C. Hering and F. H. Getman: Standard Table of Electrochemical Equivalents and their Derivatives„http://archive.org/stream/standardtableel00getmgoog/standardtableel00getmgoog_djvu.txt,“ [Online].

[74] K.Madhusoodanan: Derivation of current efficiency loss and monitoring energy performance in a membrane cell chlor-alkali electrolyser „http://www.energymanagertraining.com/Book_all/Technical_Pdf/MonitoringEnergyPerformanceChlorAlkali-KMadhusoodanan.doc.,“ [Online].

[75] C. Gougaud, S. Delbos, R. Bodeux, E. Chassaing and D. Lincot, „Synthesis and characterization of kesterite absorbers prepared by co-electrodeposition and annealing in sulphur atmosphere,“ *EMRS Conference*, Strasbourg, 2012.

[76] R. Schurr, A. Hölzing, S. Jost, R. Hock, T. Voss, J. Schulze, A. Kirbs, A. Ennaoui, M. Lux-Steiner, A. Weber, I. Kötschau and H. W. Schock, „The crystallisation of Cu2ZnSnS4 thin film solar cell absorbers from co-electroplated Cu–Zn–Sn precursors,“ *Thin Solid Films 517,* p. 2465, 2009.

[77] R. Juškenas, S. Kanapeckaite, V. Karpaviciene, Z. Mockus, V. Pakstas, A. Selskiene, R. Giraitis and G. Niaura, „A two-step approach for electrochemical deposition of Cu–Zn–Sn and Se precursors for CZTSe solar cells,“ *Solar Energy Materials & Solar Cells 101,* p. 277, 2012.

[78] K. D. Lee, S.-W. Seo, D.-K. Lee and H. Kim, „Preparation of Cu_2ZnSnS_4 thin films via electrochemical deposition and rapid thermal annealing,“ *Thin Solid Films 546,* p. 294, 2013.

[79] Z. Chen, L. Han, L. Wan, C. Zhang, X. Niu and J. Xu, „$Cu_2ZnSnSe_4$ thin films prepared by selenization of co-electroplated Cu–Zn–Sn precursors,“ *Applied Surface Science 257,* p. 8490, 2011.

[80] P. K. Sarswat and M. Free, „A Comparative Study of Co-electrodeposited Cu_2ZnSnS_4 Absorber Material on Fluorinated Tin

Oxide and Molybdenum Substrates," *Journal of Electronic Materials 41,* p. 2210, 2012.

[81] J. J. Scragg, P. J. Dale and L. M. Peter, „Towards sustainable materials for solar energy conversion: Preparation and photoelectrochemical characterization of Cu_2ZnSnS_4," *Electrochemistry Communications 10,* p. 639, 2008.

[82] M. Kurihara, D. Berg, J. Fischer, S. Siebentritt and P. J. Dale, „Kesterite absorber layer uniformity from electrodeposited precursors," *Physica Status Solidi 6,* p. 1241, 2009.

[83] J. J. Scragg, P. J. Dale, L. M. Peter, G. Zoppi and I. Forbes, „New routes to sustainable photovoltaics: evaluation of Cu_2ZnSnS_4 as an alternative absorber material," *Physica Status Solidi 245,* p. 1772, 2008.

[84] G. Ma, T. Minegishi, D. Yokoyama, J. Kubota ja K. Domen, „Photoelectrochemical hydrogen production on Cu_2ZnSnS_4/Mo-mesh thin-film electrodes prepared by electroplating," *Chemical Physics Letters 501,* p. 619, 2011.

[85] T. Kobayashi, K. Jimbo, K. Tsuchida, S. Shinoda, T. Oyanagi and H. Katagiri, „Investigation of Cu_2ZnSnS_4-Based Thin Film Solar Cells Using Abundant Materials," *Japanese Journal of Applied Physics 44,* p. 783, 2005.

[86] L. Thouin and J. Vedel, „Electrodeposition and Characterization of $CuInSe_2$ Thin Films," *Journal of the Electrochemical Society 142,* p. 2996, 1995.

[87] A. Molin and A. Dikusar, „Electrodeposition of $CuInSe_2$ thin films from aqueous citric solutions II. Investigation of macrokinetics of electrodeposition by means of rotating disk electrode," *Thin Solid Films 237,* p. 72, 1994.

[88] M. Oliveira, M. Azevedo and A. Cunha, „A voltammetric study of the electrodeposition of $CuInSe_2$ in a citrate electrolyte," *Thin Solid Films 405,* 2002.

[89] W. Septina, S. Ikeda, A. Kyoraiseki, T. Harada and M. Matsumura, „Single-step electrodeposition of a microcrystalline $Cu_2ZnSnSe_4$ thin film with a kesterite structure," *Electrochimica Acta 88,* p. 436, 2013.

[90] S. M. Pawar, B. S. Pawar, A. V. Moholkar, D. S. Choi, J. H. Yun, J. H. Moon, S. S. Kolekar and J. H. Kim, „Single step electrosynthesis of Cu_2ZnSnS_4 (CZTS) thin films for solar cell application," *Electrochimica Acta 55,* p. 4057, 2010.

[91] B. S. Pawar, S. M. Pawar, S. W. Shin, D. S. Choi, C. J. Park, S. S. Kolekar and J. H. Kim, „Effect of complexing agent on the properties of electrochemically deposited Cu_2ZnSnS_4 (CZTS) thin films," *Applied Surface Science 257,* p. 1786, 2010.

[92] C. P. Chan, H. Lam and C. Surya, „Preparation of Cu_2ZnSnS_4 films by electrodeposition using ionic liquids," *Solar Energy Materials & Solar Cells 94,* p. 207, 2010.

[93] A. Fischereder, „Investigation of Cu_2ZnSnS_4 Formation from Metal Salts and Thioacetamide," *Chemistry of Materials 22,* p. 3399, 2010.

[94] C. M. Fella, A. R. Uhl, C. Hammond, I. Hermans, Y. Romanyuk and A. N. Tiwari, „Formation mechanism of $Cu_2ZnSnSe_4$ absorber layers during selenization of solution deposited metal precursors," *Journal of Alloys and Compounds 567,* p. 102, 2013.

[95] G. M. Ilari, C. M. Fella, C. Ziegler, A. R. Uhl, Y. E. Romanyuk and A. N. Tiwari, „$Cu_2ZnSnSe_4$ solar cell absorbers spin-coated from amine-containing ether solutions," *Solar Energy Materials & Solar Cells 104,* p. 125, 2012.

[96] S. Marchionna, P. Garattini, A. Le Donne, M. Acciarri, S. Tombolato and S. Binetti, „Cu_2ZnSnS_4 solar cells grown by sulphurisation of sputtered metal precursors," *Thin Solid Films 542,* p. 114, 2013.

[97] A. Weber, I. Kötschau, S. Schorr and H. Schock, „Formation of Cu_2ZnSnS_4 and Cu_2ZnSnS_4-$CuInS_2$ Thin Films Investigated by In-Situ Energy Dispersive X-Ray Diffraction," *Materials Research Society Symposium Proceedings,* pp. 1012-Y03-35, 2007.

[98] S. Schorr, A. Weber, V. Honkimäki and H.-W. Schock, „In-situ investigation of the kesterite formation from binary and ternary sulphides," *Thin Solid Films 517,* p. 2461, 2009.

[99] O. Volobujeva, *SEM Study of Selenization of Different Thin Metallic Films,* Tallinn, TUT Press, 2008, PhD thesis

[100] F. Hergert, R. Hock, A. Weber, M. Purwins, J. Palm and V. Probst, „In situ investigation of the formation of $Cu(In,Ga)Se_2$ from selenized metallic precursors by x-ray diffraction," *Journal of Physics and Chemistry of Solids 66,* p. 1903, 2005.

[101] P. Salome, P. Fernandes and A. Cunha, „Morphological and structural characterization of $Cu_2ZnSnSe_4$ thin films grown by selenization of elemental precursor layers," *Thin Solid Films 517,* p. 2531, 2009.

[102] J. Scragg, P. Dale and L. Peter, „Synthesis and characterization of Cu_2ZnSnS_4 absorber layers by an electrodeposition-annealing route," *Thin Solid Films 517,* p. 2481, 2009.

[103] V. Chawla and B. Clemens, „Effect of composition on high efficiency CZTSSe devices fabricated using co-sputtering of compound targets," *Photovoltaic Specialists Conference (PVSC), 2012 38th IEEE*, 2012.

[104] K. V. Gurav, S. M. Pawar, S. W. Shin, M. P. Suryawanshi, J. H. Kim and e. al, „Electrosynthesis of CZTS films by sulfurization of CZT precursor: Effect of soft annealing treatment," *Applied Surface Science 283,* p. 74, 2013.

[105] L. Kaupmees, *Selenization of Molybdenum as Contact Material in Solar Cells,* Tallinn: TUT press, 2011, PhD Thesis.

[106] L. Kaupmees, M. Altosaar, O. Volobujeva and P. Barvinschi, „Study of Mo selenisation process on different Mo substrates,*Materials Research Society Symposium Proceedings*, 2010.

[107] T. Wada, N. Kohara, S. Nishiwaki ja T. Negami, „Characterisation of the Cu(In, Ga)Se_2/Mo interface in CIGS solar cells," *Thin Solid Films 387,* p. 118, 2001.

[108] R. Schwartz and J. Gray, „The use of $CuIn_{1-x}Ga_xSe_2$ layers to improve the performance of $CuInSe_2$ cells," *Proc. 21st IEEE Photovolt. Spec. Conf.,Kissimmee, FL, USA*, 1990, p. 570.

[109] J. Guillemoles, L. Kronik, D. Cahen, U. Rau, A. Jasenek and H.-W. Schock, „Stability Issues of Cu(In,Ga)Se_2-Based Solar Cells," *The Journal of Physical Chemistry 104,* p. 4849, 2000.

[110] I. Repins, C. Beall, N. Vora, C. DeHart, D. Kuciauskas, P. Dippo, B. To, J. Mann, W.-C. Hsu, A. Goodrich and R. Noufi, „Co-evaporated $Cu_2ZnSnSe_4$ films and devices," *Solar Energy Materials & Solar Cells 101,* p. 154, 2012.

[111] S. Siebentritt and S. Schorr, „Kesterites—a challenging material for solar cells," *Progress in Photovoltaics 20,* p. 512, 2012.

[112] S. Ahn, S. Jung, J. Gwak, A. Cho, K. Shin, K. Yoon, D. Park, H. Cheong and J. H. Yun, „Determination of band gap energy (Eg) of$Cu_2ZnSnSe_4$ thin films: on the discrepancies of reported band gap values," *Applied Physics Letters 97,* p. 021905, 2010.

[113] W.-C. Hsu, I. Repins, C. Beall, C. DeHart, G. Teeter, B. To, Y. Yang and R. Noufi, „The effect of Zn excess on kesterite solar cells," *Solar Energy Materials & Solar Cells 113,* p. 160, 2013.

[114] "Encyclopedia entry on Rapid Thermal Processing" „http://en.wikipedia.org/wiki/Rapid_thermal_processing," [Online].

[115] Ulvac, *Infrared Gold Image Furnace,* Japan: Ulvac-Rico, Inc.

[116] Unitronics,Introduction to PID. 29 May 2005, „http://www.unitronics.com/Downloads/Support/Technical%20Library/PID/PID%20Documents/PID_Tips_1.pdf," [Online].

[117] A. J. Cheng, M. Manno, A. Khare, C. Leighton, S. Campbell and E. Aydil, „Imaging and phase identification of Cu_2ZnSnS_4 thin films using confocal Raman spectroscopy," *Journal of Vacuum Science and Technology 29,* p. 051203, 2011.

[118] J. J. Scragg, T. Ericson, X. Fontane, V. Izquierdo-Roca, A. Perez-Rodriguez, T. Kubart, M. Edoff and C. Platzer-Björkman, „Rapid annealing of reactively sputtered precursors for Cu_2ZnSnS_4 solar cells," *Progress in Photovoltaics 22,* p. 10, 2014.

[119] Z. Kamala, Introduction to Polarography and Allied Techniques, New

Age International, 2006.

[120] A. J. Bard and L. R. Faulkner, Electrochemical Methods: Fundamentals and Applications, 2nd Edition, Wiley, 2001.

[121] А. Ямпольский and В. А. Ильин, Краткий справочник гальванотехника, Машиностроение, Ленингр. отд-ние, 1981.

[122] M. Pourbaix, Atlas of Electrochemical Equilibria in Aqueous Solutions, Second English Edition, National Association of Corrosion Engineers, 1974.

[123] A. Pigaga, A. Selskis, R. Juškenas and A. Sveikauskaite, „The Interaction Of Two Ligand Containing Electroplating Solutions. Final Decontamination.," *Ars Separatoria Acta 1,* p. 138, 2002.

[124] J. Watters and A. Aaron, „Spectrophotometric Investigation of the Complexes Formed between Copper and Pyrophosphate Ions in Aqueous Solution," *Journal of the American Chemical Society 75,* p. 611, 1953.

[125] L. Rogers and C. Reynolds, „Interaction of Pyrophosphate Ion with Certain Multivalent Cations in Aqueous Solutions," *Journal of the American Chemical Society 71,* p. 2081, 1949.

[126] Б. Никольский, Справочник Химика, Том 3, Химия, 1965.

[127] C. L. Faust, „Alloy Plating," *Journal of The Electrochemical Society 80,* p. 301, 1941.

[128] J. Vaid and T. L. Rama Char, „Electrodeposition of tin from the Pyrophosphate Bath," *Current Science 21,* p. 300, 1952.

[129] H. Basset, W. L. Bedwell and J. B. Hutchinson, „Studies of phosphates. Part IV. Pyrophosphates of some bivalent metals and their double salt, and solid solutions with sodium pyrophosphate," *Journal of Chemical Society,* p. 1412, 1936.

[130] M. R. Buchner, F. Kraus and H. Schmidbaur, „Pyrophosphate Complexation of Tin(II) in Aqueous Solutions as Applied in Electrolytes for the Deposition of Tin and Tin Alloys Such as White Bronze," *Inorganic Chemistry 51,* p. 8860, 2012.

[131] S. S. Djokic, Electrodeposition and Surface Finishing, Springer New York, 2014.

[132] Ю. Ю. Лурье, Справочник по аналитической химии., Химия, 1971.

[133] R. Juškenas, V. Karpaviciene, V. Pakštas, A. Selskis and V. Kapocius, „Electrochemical and XRD studies of Cu–Zn coatings electrodeposited in solution with D-mannitol," *Journal of Electroanalytical Chemistry 602,* p. 237, 2007.

[134] U. Manz, S. Berger, K. Bronder, K. Leyendecker, B. Weyhmüller and G. Wirth, „Cyanide-Free Electroplating of Cu-Sn Alloys," *NASF Surface Technology White Papers 77,* p. 1, 2013.

[135] E. Chassaing, K. V. Quang and R. Wiart, „Kinetics of copper electrodeposition in citrate electrolytes,“ *Journal of Applied Electrochemistry 16,* p. 591, 1986.

[136] T. Ishizaki, T. Ohtomo, Y. Sakamoto ja A. Fuwa, „Effect of pH on the Electrodeposition of ZnTe Film from a Citric Acid Solution,“ *Materials Transactions 45,* p. 277, 2004.

[137] F. Ferreira, F. Silva, A. Luna, D. Lago and L. Senna, „Response surface modeling and optimization to study the influence of the deposition parameters on the electrodeposition of Cu-Zn alloys in citrate medium,“ *Journal of Applied Electrochemistry 37,* p. 473, 2007.

[138] S. Rode, C. Henninot, C. Vallieres and M. Matlosz, „Complexation chemistry in copper plating from citrate baths,“ *Journal of The Electrochemical Society 151,* p. C405, 2004.

[139] V. Sudha and M. V. Sangaranarayanan, „Underpotential deposition of metals – Progress and prospects in modelling,“ *Journal of Chemical Sciences,* p. 207, (117) 2005.

[140] Y. Gamburg and G. Zangari, Theory and Practice of Metal Electrodeposition, Springer, 2011.

[141] K. N. Tu, „Cu/Sn interfacial reactions; thin film case versus bulk case,“ *Materials Chemistry and Physics 46,* p. 217, 1996.

[142] M. Date ja K. N. Tu, „Interfacial reactions and impact reliability of Sn–Zn solder joints on Cu or electroless Au/Ni(P) bond-pads,“ *Journal of Materials Research 19,* p. 2887, 2004.

[143] F. S. Tehrani, V. Daadmehr, A. T. Rezakhani, R. Hosseini Akbarnejad and S. Gholipour, „Structural, Magnetic, and Optical Properties of Zinc- and Copper-Substituted Nickel Ferrite Nanocrystals,“ *Journal of Superconductivity and Novel Magnetism,* p. 2443, (25) 2012.

[144] P. Balaz, Mechanochemistry in Nanoscience and mineral engineering, Berlin: Springer, 2008.

[145] B. E. Warren, X-Ray Diffraction, Nw York: Dover, 1990.

[146] N. Revathi, P. Prathap, R. W. Miles and K. T. Ramakrishna Reddy, „Annealing effect on the physical properties of evaporated In2S3 films,“ *Solar Energy Materials & Solar Cells 94,* p. 1487, 2010.

[147] T. Yamaguchi, T. Kubo, K. Maeda, S. Niyama, T. Imanishi and A. Wakahara, „Fabrication of Cu_2ZnSnS_4 thin films by sulfurization process from quaternary compound for photovoltaic device applications," *The International Conference on Electrical Engineering*, 2009.

[148] W. Hlaingoo, J. Johnson, A. Bhatia, E. Lund, M. Nowell and M. Scarpulla, „Grain Size and Texture of Cu_2ZnSnS_4 Thin Films

Synthesized by Cosputtering Binary Sulfides and Annealing: Effects of Processing Conditions and Sodium ," *Journal of Electronic Materials 40,* p. 2214, 2011.

[149] K. Maeda, K. Tanaka, Y. Nakano and H. Uchiki, „Annealing Temperature Dependence of Properties of Cu_2ZnSnS_4 Thin Films Prepared by Sol--Gel Sulfurization Method," *Japanese Journal of Applied Physics 50,* p. 05FB08, 2011.

[150] H. C. Ong, A. E. Zhu and G. T. Du, „Dependence of the excitonic transition energies and mosaicity on residual strain in ZnO thin films," *Applied Physics Letters 80,* p. 941, 2002.

[151] W. K. Kim, E. A. Payzant, S. Yoon and T. J. Anderson, „In situ investigation on selenization kinetics of Cu–In precursor using time-resolved, high temperature X-ray diffraction," *Journal of Crystal Growth 294,* p. 231, 2006.

[152] H. W. Schock and U. Rau, „The role of structural properties and defects for the performance of Cu-chalcopyrite-based thin-film solar cells," *Physica B 308,* p. 1081, 2001.

[153] F. A. Kröger, „Cathodic Deposition and Characterization of Metallic or Semiconducting Binary Alloys or Compounds," *Journal of Electrochemical Society 125,* p. 2028, 1978.

[154] M. Kemell, H. Saloniemi, M. Ritala and M. Leskelä, „Electrochemical quartz crystal microbalance study of the electrodeposition mechanisms of Cu2−xSe thin films," *Electrochimica Acta 45,* p. 3737, 2000.

[155] M. G. Ganchev and K. D. Kochev, „Investigation of the electrodeposition process in the Cu-In-Se system," *Solar Energy Materials & Solar Cells 31,* p. 163, 1993.

[156] E. Tzvetkova, N. Stratieva, M. Ganchev, I. Tomov, K. Ivanova and K. Kochev, „Preparation and structure of annealed $CuInSe_2$ electrodeposited films," *Thin Solid Films 311,* p. 101, 1997.

[157] M. Kemell, H. Saloniemi, M. Ritala and M. Leskelä, „Electrochemical Quartz Crystal Microbalance Study of the Electrodeposition Mechanisms of $CuInSe_2$ Thin Films," *Journal of Electrochemical Society 148,* p. C 110, 2001.

[158] R. N. Bhattacharya and A. M. Fernandez, „$CuIn_{1-x}Ga_xSe_2$-based photovoltaic cells from electrodeposited precursor films," *Solar Energy Materials & Solar Cells 76,* p. 331, 2003.

[159] R. Ugarte, R. Schrebler, R. Cordova, E. Dalchiele and H. Gomez, „Electrodeposition of $CuInSe_2$ thin films in a glycine acid medium," *Thin Solid Films 340,* p. 117, 1999.

[160] J. Kois, M. Ganchev, M. Kaelin, S. Bereznev, E. Tzvetkova, O. Volobujeva, N. Stratieva and A. N. Tiwari, „Electrodeposition of Cu–

In–Ga thin metal films for Cu(In, Ga)Se_2 based solar cells," *Thin Solid Films 516,* p. 5948, 2008.

[161] A. Bahta, G. Parker and D. Tuck, „Critical survey of stability constants of complexes of thiocyanate ion," *Pure and Applied Chemistry 69,* p. 1489, 1997.

[162] N. A. Shvab, V. D. Litovchenko and L. M. Rudkovskaja, „Mechanism of Reduction of Thiosulfate Ions on the Cathode," *Russian Journal of Applied Chemistry 80,* p. 1852, 2007.

[163] M. Grossberg, J. Krustok, K. Timmo and M. Altosaar, „Radiative recombination in $Cu_2ZnSnSe_4$ monograins studied by photoluminescence spectroscopy," *Thin Solid Films 517,* p. 2489, 2009.

[164] M. Ishii, K. Shibata and H. Nozaki, „Anion Distributions and Phase Transitions in $CuS_{1-x}Se_x$(x = 0-1) Studied by Raman Spectroscopy," *Journal of Solid State Chemistry 105,* p. 504, 1993.

[165] G. Perna, M. Lastella, M. Ambrico and V. Capozzi, „Temperature dependance of the optical properties of ZnSe films deposited on quartz substrate," *Applied Physics A 83,* p. 127, 2006.

[166] M. Grossberg, J. Krustok, J. Raudoja and T. Raadik, „The role of structural properties on deep defect states in Cu_2ZnSnS_4 studied by photoluminescence spectroscopy," *Applied Physics Letters 101,* p. 102102, 2012.

[167] L. Price, I. Parkin, A. Hardy and R. Clark, „Atmospheric Pressure Chemical Vapor Deposition of Tin Sulfides (SnS, Sn_2S_3, and SnS_2) on Glass," *Chemistry of Materials 11,* p. 1792, 1999.

[168] D. Papadimitriou, N. Esser and C. Xue, „Structural properties of chalcopyrite thin films studied by Raman spectroscopy," *Physica Status Solidi 242,* p. 2633, 2005.

[169] G. Frey, R. Tenne, M. Matthews, M. Dresselhaus and G. Dresselhaus, „Raman and resonance Raman investigation of MoS_2 nanoparticles," *Physical Review B 60,* p. 2883, 1999.

[170] Encyclopedia entry on Carcinogen „http://en.wikipedia.org/wiki/Carcinogen," [Online].

[171] Y. Lin, S. Ikeda, W. Septina, Y. Kawasaki, T. Harada and M. Matsumura, „Mechanistic aspects of preheating effects of electrodeposited metallic precursors on structural and photovoltaic properties of Cu_2ZnSnS_4 thin films," *Solar Energy Materials & Solar Cells 120,* p. 218, 2014.

APPENDIX A

Article I

J. Lehner, M. Ganchev, M. Loorits, N. Revathi, T. Raadik, J. Raudoja, M. Grossberg, E. Mellikov, O. Volobujeva; Structural and compositional properties of CZTS thin films formed by rapid thermal annealing of electrodeposited layers, *Journal of Crystal Growth*, Vol. 380 (2013), p. 236-240

Journal of Crystal Growth 380 (2013) 236–240

Contents lists available at SciVerse ScienceDirect

Journal of Crystal Growth

journal homepage: www.elsevier.com/locate/jcrysgro

Structural and compositional properties of CZTS thin films formed by rapid thermal annealing of electrodeposited layers

J. Lehner [a,*], M. Ganchev [b], M. Loorits [a], N. Revathi [a], T. Raadik [a], J. Raudoja [a], M. Grossberg [a], E. Mellikov [a], O. Volobujeva [a]

[a] Tallinn University of Technology, Department of Materials Science, Ehitajate tee 5, Tallinn 19086, Estonia
[b] Central Laboratory of Solar Energy-Bulgarian Academy of Sciences, 72 Tzarigradsko shaussee, 1784 Sofia, Bulgaria

ARTICLE INFO

Article history:
Received 18 April 2013
Received in revised form
3 June 2013
Accepted 10 June 2013
Communicated by R. Kern
Available online 4 July 2013

Keywords:
A1. Surface structure
B1. Metals, alloys
B2. Semiconducting quaternary alloys
B3. Solar cells

ABSTRACT

In this work Cu_2ZnSnS_4 (CZTS) thin films were formed by rapid thermal annealing (RTA) of sequentially electrodeposited Cu–Zn and Sn films in 5% H_2S containing atmosphere. Six different thermal profiles were used in the experiments. In three of these, the temperature ramping up was varied, while the variable in the other three profiles was the cooling down rate. The optimising parameters for RTA of electrodeposited films were found and annealed films were characterised by X-ray diffraction (XRD), micro-Raman spectroscopy, scanning electron microscopy and energy dispersive X-ray spectroscopy (SEM+EDS). The material parameters such as lattice strain and crystallite size were also determined and the influence of annealing temperature and heating rate on these parameters was discussed.The pathway of MoS_2 formation was investigated.

1. Introduction

PV accounted for only 0.1% of global electricity generation in 2009 (20 TWh of 20 PWh); however, to provide a realistic chance to limit the global temperature increase to 2 °C, PV would need to provide more than 6% (2.6 PWh of 41 PWh) of global electricity consumption in 2050 [1]. This implies a tremendous growth of two orders of magnitude within a 40 years' timeframe.

In 2011, 85% of the PV market belonged to crystalline silicon solar cells followed by CdTe thin films at 8% and amorphous silicon thin films at 3%; CIS/CIGS thin films grew rapidly from 1% in 2009 to 3% in 2011 [2]. Conversion efficiencies of 17.3% for CdTe and 20.3% for CIS/CIGS have achieved in research labs, but efficiency of commercially available CdTe and CIS/CIGS PV panels reach only 12–13% [3,4] while their crystalline silicon based counterparts achieve already close to 20% [5] efficiency. However, these concepts have the downside of using one or several expensive and potentially scarce materials (tellurium, indium and gallium) which may hamper the strong growth of PV as outlined above. In addition, CdTe and CIS/CIGS require the use of toxic elements such as cadmium or selenium which, arguably, disqualify them as 'clean' technologies. The development of Cu_2ZnSnS_4 (CZTS) solar cells can eliminate both constraints at the same time. CZTS is a quaternary compound, where compared to its close relative CIGS indium and gallium are substituted by two non-toxic and earth abundant elements, zinc and tin. Furthermore, selenium is replaced by sulphur. Moreover CZTS has a suitable band gap of 1.5 eV (CZTS) [6] and a high absorption coefficient of 10^{-4} cm^{-1}. The record efficiency of 10.1% for (selenium containing) CZTSSe absorbers was recently achieved by the group of Barkhouse [7]. However, in this approach a highly toxic and unstable hydrazine is used as a solvent.

Reducing of the complexity of industrial productions processes in the thin film solar cell industry is crucial to achieve further cost reductions. In this respect, non-vacuum processes are highly desired as they can supersede expensive machinery and reduce operation and maintenance cost in production plants. Electrochemical deposition could be used as one of the low cost method for precursor preparation. Scragg et al. prepared CZTS films by sequential electrodeposition of constituent metals followed by annealing in elemental sulphur atmosphere [8,9]. The given approach with improved precursor stack (Cu/Sn/Cu/Zn) has given device efficiency 3.2% [10]. The group of Ahmed [11] demonstrated an efficiency of 7.3%, which is the record for electrodeposited Cu_2ZnSnS_4 solar devices. The high performance of the device underlines the suitability of electrodeposition of precursor layers and following annealing as viable low-cost processes for solar cell fabrication based on to earth-abundant materials.

Annealing of precursors at high temperatures is an essential second step of most all approaches for obtaining a well crystallised

* Corresponding author. Tel.: +372 5813 1064.
E-mail address: jullenok@gmail.com (J. Lehner).

0022-0248/$ - see front matter © 2013 Elsevier B.V. All rights reserved.
http://dx.doi.org/10.1016/j.jcrysgro.2013.06.012

and single phase absorber material. Annealing has been performed for different durations and in different atmospheres (argon, nitrogen, vacuum, chalcogen containing atmosphere). The chalcogen containing atmosphere sulphur (or selenium) could be formed in the chamber (ampoule) inserting a piece of sulphur (or selenium) into chamber or by hydrogen sulphide gas flowing through a tube into the chamber.

It was shown for Cu_2ZnSnS_4 compounds that the chemical path of material formation and its properties strongly depend on the rate of temperature rise [12]. Necessity to avoid the formation stable mediate compounds and to produce single-phase materials leads to the development of rapid thermal annealing (RTA). Scragg et al. [13] used rapid thermal annealing for sputtered stacked Cu–Zn–Sn precursors and this resulted in the cell efficiency of 4.6%.

In this work we present our preliminary results in searching for suitable conditions for rapid thermal annealing (RTA) of electrodeposited stacked precursor layers. Precursors for our study consist of copper zinc alloy and metallic tin stacked films. Six different thermal annealing profiles were used in our experiments. In three of these, the temperature ramping up was varied, while the variable in the other three profiles was the rate of cooling down. The main challenge was in preventing peeling off molybdenum from the glass substrate after sulphurisation. Calculation of crystallite size and strains in films depending on the annealing temperature and heating rate was done in order to follow the thin film formation and crystal growth. The pathway of formation of MoS_2 was investigated.

2. Experimental

Cu–Zn alloy and tin stacked precursor layers for CZTS compound formation were prepared by sequential electrodeposition in potentiostatic conditions. The setup consisted of a conventional three-electrode cell configuration with Ag/AgCl as a reference electrode and platinum gauze as a counter electrode. A rotating disk electrode with Mo-coated soda lime glass (15×15 mm^2) was used as a substrate and working electrode, respectively. Prior to electrodeposition, substrates were cleaned in ethanol and rinsed in distilled water. Deposition was carried out at room temperature using a Gamry 3000 potentiostat. The electrolyte for Cu–Zn electrodeposition had the composition 0.1 M $Na_3C_6H_5O_7$, 0.02 M $CuSO_4 \cdot 5H_2O$ and 0.02M $ZnSO_4 \cdot 7H_2O$. The tin electrolyte consisted of a saturated sodium pyrophosphate solution and 0.02 M $SnCl_2 \cdot 2H_2O$. The electrodeposition potentials vs. Ag/AgCl electrode was -1.22 V for the Cu–Zn layer and -0.9 V for the Sn layer. Metallic precursor layers were applied in the following sequence: Mo/Cu–Zn alloy/Sn. Depositing of the layers in reverse order led to poor adhesion of Sn on the Mo surface.

The sulphurisation process was carried out at 470 °C and 500 °C in a tubular furnace in H2S+N2 atmosphere with a H2S concentration of 5%. The heating rate was varied between 2 °C/sec and 3.3 °C/sec. The samples reached temporary a temperature of 520 °C during their rapid annealing at 500 °C. After annealing, samples were cooled down to 25 °C during 5, 8 or 15 min. In the second set of experiments, the duration of annealing was 5, 8 and/or 15 min at 470 °C, while samples reached a maximum temperature of 490 °C.

Precursor and sulphurized films were analysed through high resolution scanning electron microscopy and energy dispersive X-ray analysis (EDS) using a Zeiss ULTRA 55 with Bruker EDS detector. The room temperature micro Raman spectra were recorded by a Horiba LabRam 800 high-resolution spectrometer equipped with a multichannel CCD detection system on back-scattering regime providing a spectral resolution of 0.5 cm^{-1}. The light source for micro Raman was a green (532 nm) and a red (633 nm) laser focused to a spot of at least 10 μm diameter. X-Ray diffraction measurements were performed using a Bruker D5005 diffractometer (Bragg-Brentano geometry) and Cu $K\alpha_1$ radiation with $\lambda = 1.5406$ Å at 40 kV, 40 mA.

3. Results and discussion

Sequentially electrodeposited Cu–Zn alloy and Sn layers with total thickness around 650 nm were prepared and used as precursors for sulphurisation. In Fig. 1 morphologies of electrodeposited CuZn (a) and CuZn–Sn (b) layers are depicted. The initial CuZn alloy film consists of small densely packed crystals and was mirror bright showing a gold-like colour. The Sn layer deposited onto Cu–Zn alloy layer consisted of crystals sized 0.2–0.5 μm with prolonged equally distributed holes between them. Initial composition of sequential electrodeposited precursors was tin rich in order to compensate tin loss during the annealing (Table 1). Two types of precursor with different duration of tin deposition were prepared.

3.1. Sulphurisation in IR furnace

Six different thermal treatment regimes were applied in order to find suitable conditions for rapid thermal annealing of electrodeposited precursors. At first the speed of raising temperature up to 470 °C was varied between 3.3 °C/sec and 2 °C/sec (Fig. 2a) and samples were cooled down to room temperature (25 °C) within

Table 1
Elemental composition of stacked precursor layers determined by EDS as a function of tin electrodeposition time.

Duration of tin deposition (sec)	Cu (at%)	Zn (at%)	Sn (at%)	Cu/(Zn+Sn)	Zn/Sn
200	42.18	19.51	38.31	0.73	0.51
170	45.97	22.32	32.14	0.84	0.70

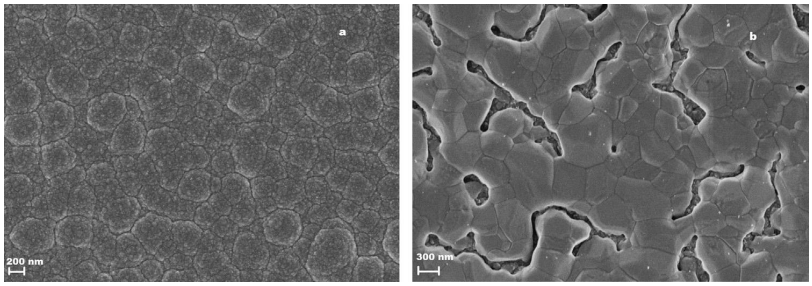

Fig. 1. (a) SEM image of electrodeposited CuZn layer (b) CuZn-Sn layer.

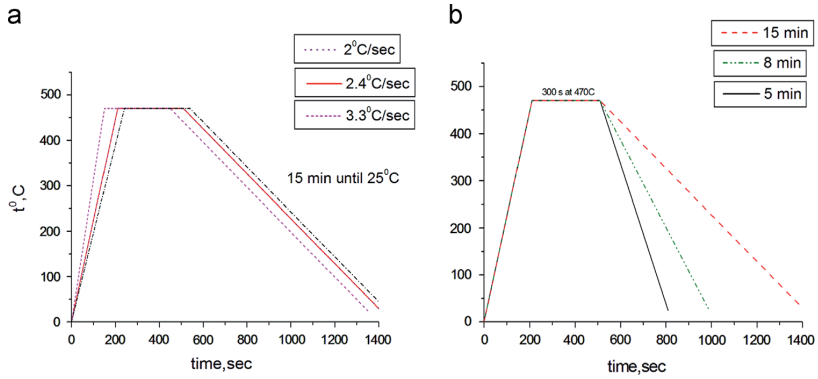

Fig. 2. Thermal profiles with the three distinct heating (a) and cooling (b) rates.

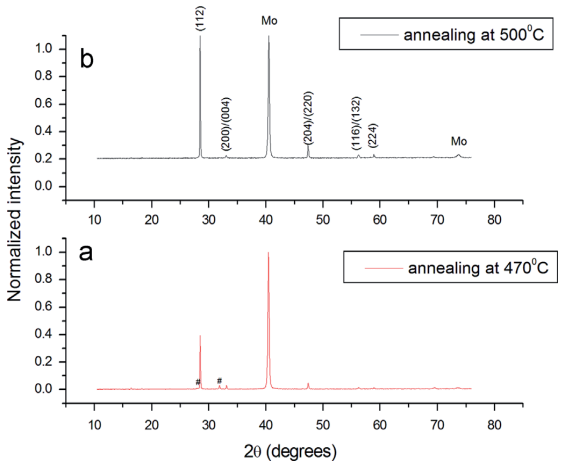

Fig. 3. XRD spectra of annealed films at 500 °C and 470 °C.

15 min. Precursor films that were annealed under fastest used temperature rise (3.3 °C/sec, fast ramp) contained a large number of cracks in the film and in some cases, the glass substrate was found split up after annealing. It makes these films not suitable for further investigations. The films sulphurised under temperature rise of 2.4 °C/sec showed diminished amount of cracks. Films obtained under "slow" temperature rising (2 °C/sec) were smooth and continuous. The thermal profile in Fig. 2b was used in experiments with variable cooling durations (from 5 to 15 min). The speed of temperature rise was kept constant and was equal to 2 °C/sec. The films with fast and medium cooling rate (cooling down to 25 °C during 5 or 8 min) tend to peel off from the substrate. This is probably due to the strain in films resulting from the difference of thermal coefficients of substrates and film. Only cooling for 15 min resulted in CZTS layers with good adhesion to the substrate. Therefore, the optimised heating and cooling parameters were found to be ramp up 2 °C/sec and cooling down to 25 °C during 15 min.

The XRD patterns (Fig. 3) for the films annealed at 470 °C or 500 °C for 8 min exhibited several peaks corresponding to diffraction lines of the kesterite structure of CZTS (PDF Card-04-003-8920). Dominant peak of XRD pattern of these polycrystalline films respond to the (112) diffraction line of the kesterite structure of CZTS. Additional small peaks in XRD pattern were attributed to the appearance of separate Sn_3S_4 phase (JCPDS# 27-0900) (Sn_2S_3+SnS) [14]. The presence of a Sn containing secondary phases in used films explains the determined by EDS excess of Sn in precursor films (see Table 1).

Table 2
Calculated crystallite size and strain values for films annealed at 470 °C and 500 °C with different heating rates.

t (°C)	Crystallite size (nm)	Heating, (°C/sec)	Strain
500	84	2	−0.4019
470	71	2	−0.3067
470	61	2.4	0.0345

It was reported in literature [15] that crystallites larger in size led to the improved efficiency of the solar cell. Crystallite size of CZTS films was calculated with Debye Scherrer formula [16] using full width at half maximum (FWHM) of the (112) peak. The evaluated crystallite size of the films annealed at 470 °C was equal to 71 nm whereas the crystallite size increased to 84 nm at 500 °C, which might be due to the higher thermal energy of the atoms at 500 °C [17]. The analogous results for annealed CZTS thin films were demonstrated by Yamaguchi et al. [18]. The CZTS films annealed with moderate heating rate (2.4 °C/sec) showed smaller crystallite size of 61 nm than those which are produced with the slowest heating rate (71 nm) (see Table 2).

The strain in films was calculated using the relation [19], where c is the lattice constant evaluated from the XRD data and c_o is the bulk lattice constant. The strain in the films was found to be compressive and found to be lower for slow heating rate when compared to faster heating rates. This infers that decrease of strain could enhance the crystallinity of the films.

The SEM surface and cross-sectional images of the films annealed at 470 °C for 8 and 15 min are shown in Fig. 4. Films bear a surface resemblance to each other. However SEM cross sectional image on Fig. 4 (d) for a film annealed for 15 min allows to discern a very thin layer of MoS_2 (around 70 nm) on the interface between the substrate and the CZTS film. The thickness of the sulphurised films was measured by SEM in randomly chosen places and there is no big difference between the thickness of CZTS layers annealed for 8 or 15 min. Films annealed for shorter and longer periods are in average 1.33 μm and 1.45 μm thick respectively. EDS presents composition close to stoichiometry for both layers (see Table 3); however, the signal at 2.308 keV (sulphur) in the EDS spectra was higher than stoichiometrically desired. This probably occurs due overlapping energy peaks for sulphur and Mo in EDS spectra, namely Mo Lα and S Kα. The reaction pathway of sulphurisation and formation of MoS_2 seems to be similar to the

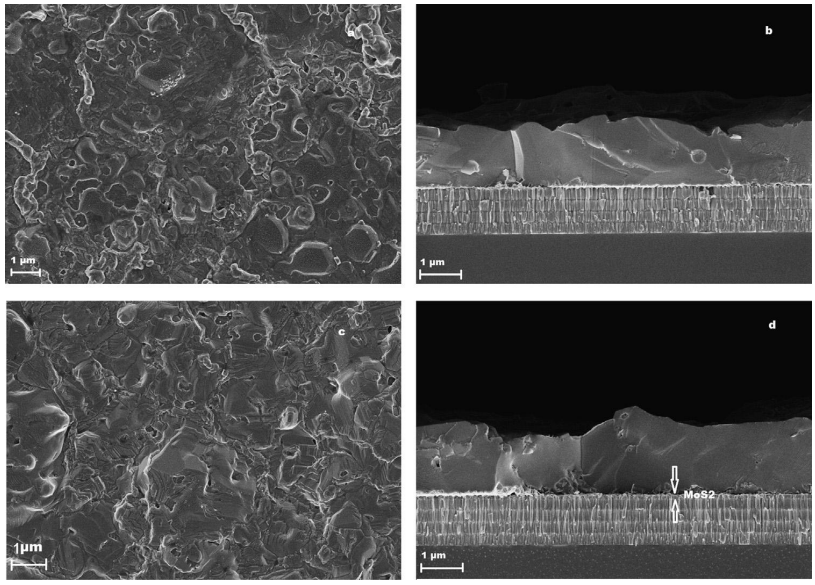

Fig. 4. SEM surface and cross-sectional images of the film annealed at 470 °C for 8 min (a - b) and (c - d) for 15 min.

Table 3
Elemental composition of CZTS layer after RTA.

Time of tin deposition (sec)	Sulphurisation, t ,c	Cu	Zn	Sn	S	Cu/(Zn+Sn)	Zn/Sn
200	470 °, 15 min	22.94	10.25	12.37	54.43	1	0.83
170	470 °, 8 min	22.35	11.1	12.05	54.5	0.96	0.92
170	500 °, 8 min	21.54	10.97	11.02	56.47	0.98	0.99

pathway reported by Kim et al. [20] for formation of $CuInSe_2$ in the selenisation process. The detailed observation of XRD data by Kim shows that $MoSe_2$ begins to form above 450 °C, after the completion of CISe formation. Taking into account thicknesses and EDS results of the films we assume, that 8 min of sulphurisation at 470 °C leads to the complete formation of the CZTS layer and later on Mo begins to sulphurise forming MoS_2. In case of $CuInSe_2$, it is reported by many groups [21,22] that formation of a thin $MoSe_2$ layer is beneficial for cell performance. On the contrary the latest report for CZTS compound of Shin [23] suggests that a reverse correlation between device performance and $MoSe_2$ thickness exists, showing the best efficiency for solar cells with almost no $MoSe_2$ layer. Therefore it is crucial to control MoS_2 formation through optimising of sulphurisation parameters.

To identify the chemical nature of separate binary or ternary phases which could also be present in the formed CZTS, films were analysed by Raman spectroscopy. The Raman spectra in Fig. 5 represent our results for films annealed at 470 °C for 5, 8 and 15 min. All spectra are characterised by the presence of two strong peaks at about 286 and 337 cm^{-1}, that are identified with the main vibrational A1 symmetry modes from CZTS [24,25]. The spectra also have weaker peaks at about 96 and 166 cm^{-1} which could be identified as E and/or B symmetry modes of CZTS [26]. Peaks at 474 and 142 cm^{-1}, in spectrum for sample annealed for 5 min, could be assigned to separate CuS phase [27], suggesting the partial incompleteness of CZTS formation reaction within 5 min of sulphurisation. Spectra for the film annealed for 15 min show additional dominant peaks at 380 and 408 cm^{-1} that are

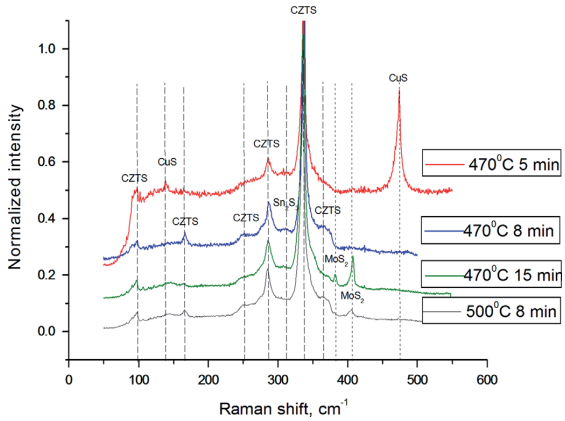

Fig. 5. Raman spectra for the films sulphurised for different temperatures and durations.

connected with the formation of an interfacial MoS_2 phase [25]. This result is consistent with the results obtained from cross-sectional SEM images. Almost all peaks in Raman spectra of precursor films sulphurised at 500 °C for 8 min could be attributed to CZTS phase except small peaks at 380 and 408 cm^{-1} that are assigned to MoS_2. This indicates that sulphurisation reaction of precursors goes faster at 500 °C and as a result the CZTS layer could be obtained already in less than 8 min of sulphurisation. The only additional small peak at 308 cm^{-1} present in Raman spectra of the film sulphurised during 8 min at 470 °C could be attributed to main characterisation mode of the Sn_2S_3 phase [28].

4. Conclusions

Electrodeposited metallic precursor layers were sulphurised by rapid thermal annealing and six regimes with different cooling

and heating up rates were applied. The optimised sulphurisation parameters for RTA (2 °C/s ramp up rate and cooling down to 25 °C for 15 min at 470 °C) results in smooth and dense films with a good adhesion to the substrate. The annealing at 470 °C during 8 min results in the complete sulphurisation of precursors, in the formation of a CZTS layer. The Mo sulphurisation begins after the sulphurization of precursors and results in appearance of MoS_2 peaks in Raman spectra of these films.

References

[1] Navigant Consulting Inc., Presentation by Paula Mints at Solar in the Future Energy Mix NCCACS, May 14, 2012. Available from: ⟨http://www.avsusergroups.org/pag_pdfs/2012_5mints.pdf⟩ (accessed 27.07.12).

[2] NREL Best Research—Cell Efficiencies. National Renewable Energy Laboratory, ⟨http://www.nrel.gov/ncpv/images/efficiency_chart.jpg⟩ (accessed 27.07.12).

[3] News item on solarserver.com, ⟨http://www.solarserver.com/solar-magazine/solar-news/current/2012/kw25/stion-reaches-148-aperture-area-efficiency-with-cigs-modules.html⟩ (accessed 27.07.12).

[4] News item on solarserver.com. Available from: ⟨http://www.solarserver.com/solar-magazine/solar-news/current/2012/kw03/first-solar-announces-another-world-record-for-cdte-pv-144-percent-total-module-area-efficiency-confirmed-by-nrel.html⟩ (accessed 27.07.12).

[5] Solar Server (2012) PV research, ⟨http://www.solarserver.com/solar-magazine/solar-news/current/2011/kw08/pv-research-20-percent-efficiency-in-sight-for-silicon-solar-cells-processed-at-near-industry-conditions.html⟩.

[6] K. Ito, T. Nakazawa, J. Appl. Phys. 27 (1988) 2094–2097.

[7] D.A.R. Barkhouse, O. Gunawan, T. Gokmen, T.K. Todorov, D.B. Mitzi, Prog. Photovoltaics Res. Appl. (2011), http://dx.doi.org/10.1002/pip.1160, n/a.

[8] J.J. Scragg, et al., Eletrochem. Commun. 10 (2008) 639.

[9] J.J. Scragg, Thin Solid Films 517 (2009) 2481–2484.

[10] J.J. Scragg, et al., J. Electroanal. Chem. 646 (2010) 52.

[11] S. Ahmed, K.B. Reuter, O. Gunawan, L.G. Lubomyr, T. Romankiw, H. Deligianni, Adv. Energy Mater. 2 (2012) 253–259.

[12] J. Ge, Y. Wu, C. Zhang, S. Zuo, J. Jiang, J. Ma, Appl. Surf. Sci. (2012) 7250–7254.

[13] J.J. Scragg, T. Ericson, X. Fontané, V. Izquierdo-Roca, Prog. Photovoltaics Res. Appl. (2012), http://dx.doi.org/10.1002/pip 2265, n/a.

[14] P.e.t.e.r. Balaz, Mechanochemistry in Nanoscience and mineral engineering, Springer- Verlag, Berlin Heidelberg66.

[15] T. Tanaka, D. Kawasaki, M. Nishio, Phys. Status Solidi 3 (2006) 2844–2847.

[16] B.E. Warren, X-ray Diffraction, Dover, New York253.

[17] N. Revathi, P. Prathap, K.T.Ramakrishna Reddy, Solar Energy Mater. Solar Cells 94 (2010) 1487.

[18] T. Yamaguchi, T. Kubo, K. Maeda, S. Niiyama, T. Imanishi, and A. Wakahara, The International Conference on Electrical Engineering 2009, ⟨www.icee-con.org/papers/2009/pdf/1.03_I9FP0235_E.Pdf⟩.

[19] H.C. Ong, A.X.E. Zhu, G.T. Du, Appl. Phys. Lett. 80 (2002) 941.

[20] W.K. Kim, E.A. Payzant, S. Yoon, T.J. Anderson, J. Cryst. Growth 294 (2006) 231–235.

[21] T. Wada, N. Kohara, S. Nishiwaki, T. Negami, Thin Solid Films 387 (2001) 118–122.

[22] W. Schock, U. Rau, Physica B 308–310 (2001) 1081–1085.

[23] B. Shin, Y. Zhu, N.A. Bojarczuk, S. Jay Chey, S. Guha, Appl. Phys. Lett 101 (2012) 053903, http://dx.doi.org/10.1063/1.4740276.

[24] M. Altosaar, J. Raudoja, K. Timmo, M. Danilson, M. Grossberg, J. Krustok, E. Mellikov, Phys. Status Solidi 205 (2008) 167–170.

[25] X. Fontane, V. Izquierdo-Roca, E. Saucedo, S. Schorr, J. Alloys and Compd. 539 (2012) 190–194.

[26] X. Fontane, L. Calvo-Barrio, V. Izquierdo-Roca, E. Saucedo, A. Perez-Rodriguez, Appl. Phys. Lett. (2011), http://dx.doi.org/10.1063/1.3587614.

[27] D. Papadimitriou, N. Esser, C. Hue, Phys. Status Solidi 242 (2005) 2633–2643.

[28] P. Fernandes, P. Salome, A. Cunha, J. Alloys and Compd. 509 (2011) 7600–7606.

APPENDIX A

Article II

J. Iljina, O. Volobujeva, T. Raadik, N. Revathi, J. Raudoja, M. Loorits, R. Traksmaa, E. Mellikov; Selenisation of sequentially electrodeposited Cu–Zn and Sn precursor layers, *Thin Solid Films,* Vol. 535 (2013), p. 14-17

Thin Solid Films 535 (2013) 14–17

Contents lists available at SciVerse ScienceDirect

Thin Solid Films

journal homepage: www.elsevier.com/locate/tsf

Selenisation of sequentially electrodeposited Cu–Zn and Sn precursor layers

J. Iljina *, O. Volobujeva, T. Raadik, N. Revathi, J. Raudoja, M. Loorits, R. Traksmaa, E. Mellikov

Tallinn University of Technology, Department of Materials Science, Ehitajate tee 5, Tallinn 19086, Estonia

ARTICLE INFO

Available online 7 January 2013

Keywords:
$Cu_2ZnSnSe_4$
Solar cells
Electrodeposition
Raman

ABSTRACT

$Cu_2ZnSnSe_4$ (CZTSe) thin films were produced through the selenisation of sequentially electrodeposited Cu–Zn and Sn stacked films. The micro-structural and compositional properties of the precursor stacked and selenised films were characterised using scanning electron microscopy/energy dispersive spectroscopy, X-ray diffraction and Raman spectroscopy. The electrodeposited Cu–Zn layers had a high concentration of zinc to compensate for the loss of zinc that occurred during the following deposition of the tin layer. It was observed that a Cu/Zn ratio equal to 1.1 in the electrodeposited Cu–Zn layers is optimal and provides the desired ratio of all the metallic components in selenised CZTSe films. Selenisation for 60 min resulted in highly crystalline CZTSe films with a grain size of 1.5–4 μm. In addition, the influence of the Cu–Zn ratio in the electrodeposited stacked layers on the morphology and the elemental and phase compositions of the CZTSe films was investigated.

1. Introduction

Within the photovoltaic (PV) sector, material concepts based on abundant and less costly elements has attracted increasing attention. Compounds that can possibly replace the indium-containing $CuInSe_2$ absorbers have been introduced in a variety of reports. These compounds include $CuSbS(Se)_2$ [1], Cu_2CoSnS_4 [2] and SnS [3–5]. However, the absorber material that has attracted the greatest attention is $Cu_2ZnSnSe(S)_4$ (CZTSe(S)) due to its tolerable band gap from 1 eV [6,7] to 1.5 eV [8,9] and its high absorbance coefficient that is greater than 10^4 cm^{-1}. The best PV device produced to date, with an efficiency of 10.1%, was produced from materials using a hybrid solution-particle slurry method [10]. However, in this approach, highly toxic and unstable hydrazine is used as a solvent, which could lead to limitations for this method. The development of the electrodeposition-annealing route for producing CZTSe absorbers is one of the most promising steps towards obtaining inexpensive solar cells. The current best efficiency value for solar cells was obtained using electroplated Cu_2ZnSnS_4, and this value is 7.3% [11]. In this study, metal precursor layers were sequentially electrodeposited and the influence of the composition of the electrodeposited Cu–Zn layer on the microstructure, morphology and composition of the CZTSe absorber layers was investigated. Additionally, the study seeks to investigate the peculiarities of crystal growth during the selenisation process.

2. Experimental details

The Cu–Zn alloy and Sn precursor layers were prepared by sequential electrodeposition under potentiostatic conditions. The experimental setup consisted of a conventional three-electrode cell configuration with Ag/AgCl as a reference-electrode and platinum gauze as a counter-electrode. A rotating disc electrode (Radiometer Analytical) with Mo-coated soda lime glass with dimension of 15×15 mm was used as a substrate and working electrode. Before the electrodeposition process, the substrates were cleaned in ethanol and rinsed with distilled water. The deposition was performed at room temperature using a Gamry 3000 potentiostat. Two series of precursor layers, named Sol A and Sol B, were prepared and used for selenisation. For both series, the Cu/Zn ratio was varied: in Sol A, the Cu/Zn ratio was equal to 1.7; and in Sol B, the Cu/Zn ratio was equal to 1.1. The precursors for Sol A were prepared from an electrolyte that contained 0.1 M $Na_3C_6H_5O_7$, 0.02 M $CuSO_4 \cdot 5H_2O$ and 0.015 M $ZnSO_4 \cdot 7H_2O$ with an electrodeposition potential of −1.23 V. In the electrolyte for the preparation of the Sol B precursors, an increased concentration of $ZnSO_4 \cdot 7H_2O$ (0.02 M) was used while the concentrations of copper and sodium citrate were unchanged. The electrodeposition potential for the preparation of the Sol B precursors was increased to −1.24 V. Tin was deposited for the same duration and at the same potential −1.3 V vs Ag/AgCl electrode on both series of the initial CuZn layers. The tin electrolyte was composed of a saturated sodium pyrophosphate solution and 0.02 M $SnCl_2 \cdot 2H_2O$. In this investigation, we used a rotating disc electrode, which allowed us to improve the uniformity of the electrodeposited precursor layers in contrast to our previous experiments [12]. A 300 rpm rotation speed was used for the electrodeposition. The total thickness of precursor films was around 650 nm. The metallic precursor layers were applied in the same sequence as in [12] for the Mo/Cu–Zn alloy/Sn. The reverse deposition sequence of layers leads to poor adhesion of Sn to the Mo surface.

The stacked precursors were placed in evacuated quartz ampoules (1.3 Pa) and subsequently heated isothermally at 470 °C for 20, 40 and 60 min. A piece of selenium (30 mg) was inserted into the ampoule before it was sealed.

* Corresponding author.
E-mail address: jullenok@gmail.com (J. Iljina).

0040-6090/$ – see front matter
http://dx.doi.org/10.1016/j.tsf.2012.12.085

Table 1
Compositions of the precursors and selenised films of Sol A and Sol B.

Type	Cu (at.%)	Zn (at.%)	Sn (at.%)	Se (at.%)	Cu/Zn
Metallic precursors					
Sol A-1	62.6	37.4	–	–	1.7
Sol B-1	53.1	46.9	–	–	1.1
Sol A-2	51.4	21.9	27.2	–	2.3
Sol B-2	43.1	23.9	33	–	1.8
Selenized films					
Experiment 1					
Sol A	24.7	10.7	13.3	51.4	2.3
Sol B	21.3	12.3	14.9	51.4	1.7
Experiment 2					
470 °C/20 min	20	11.6	15.6	52.8	1.7
470 °C/40 min	21.3	11.5	15.4	51.7	1.8
470 °C/60 min	22.4	12.7	12.6	52.4	1.8

The precursor and selenised films were analysed using high resolution-scanning electron microscopy (HR-SEM Zeiss ULTRA 55). Measurements were made at operating voltage 2.5 kV and the chemical composition of films as well as the distribution of their components was determined via energy dispersive X-ray analysis (EDS), equipped with Röntec EDX-XFlash detector, at 20 kV. Room temperature micro-Raman spectra were recorded on a Horiba LabRam 800 high-resolution spectrometer equipped with a multichannel CCD detection system in the backscattering regime, which provided a spectral resolution of 0.5 cm^{-1}. The light source for the micro-Raman measurements was a green laser with a 532 nm wavelength focused on a spot that was at least 10 μm in diameter. X-ray diffraction (XRD) measurements were performed using a Bruker D5005 diffractometer (Bragg–Brentano geometry) and Cu $K\alpha_1$ radiation with $\lambda =$ 1.5406 Å at 40 kV, 40 mA.

3. Results and discussion

3.1. Dependence of the composition and morphology of the selenised films on the composition of the electrodeposited CuZn layer

Based on the composition of $Cu_2ZnSnSe_4$, the ratio of metals in the electrodeposited Cu/Zn alloy must be approximately two to obtain a stoichiometric atomic ratio of metals in the final $Cu_2ZnSnSe_4$ films. According to the literature, changes in the concentrations of the metals (except tin) before and after thermal treatment do not occur. However, many groups have reported a significant loss of tin during annealing due to its high volatility [13,14]. Therefore, we electrodeposited Sn with a greater concentration than that required by stoichiometry (see Table 1).

CuZn layers with a 1.7 ratio were electrodeposited for 5 min from the Sol A electrolyte. The EDS analysis indicated that after the electrodeposition of tin, there was a loss of zinc from the precursors and the ratio of Cu/Zn changed from the initial 1.7 to 2.3. The results are presented in Table 1. The possible explanation for this loss of Zn in final precursor films can be attributed to the dissolution of Zn in the $SnCl_2$ electrolyte before and during the electrodeposition of Sn. Zinc, which is a more active metal than Sn or Cu, reacts with the $SnCl_2$ electrolyte and a displacement reaction consequently occurs.

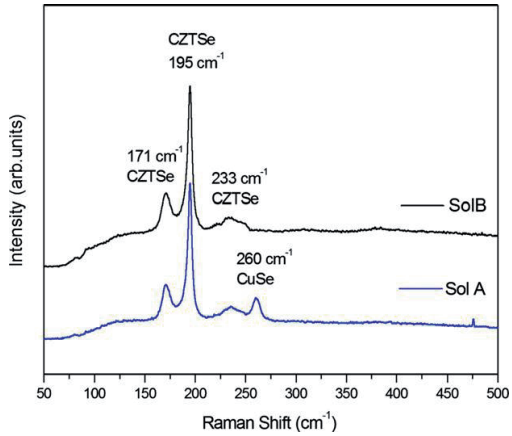

Fig. 2. Raman spectra of $Cu_2ZnSnSe_4$ thin layers selenised at 470 °C for 40 min.

The initial CuZn layer with a 1.1 ratio was obtained by increasing both the zinc concentration in the electrolyte to 0.02 M and the deposition potential to −1.24 V. For convenience, this type of precursor was called Sol B. After the electrodeposition of tin, the Cu/Zn ratio increased to 1.8 (see Table 1).

For the first experiment, the Sol A and Sol B precursors were used. The stacks of precursors were selenised at 470 °C for 40 min in sealed quartz ampoules in a selenium atmosphere. The compositions of the resulting CZTSe films are presented in Table 1. Films from both series are tin rich; however, in the Sol B-type CZTSe films, the content of zinc is higher and the composition of Zn is closer to that required by stoichiometry. A decrease in the copper concentration is also observed (see Table 1). SEM images of the surfaces of the selenised precursor films (Fig. 1) indicate that the use of the Sol B-type precursors results in a uniform and smooth CZTSe layer with small-sized crystals, which have different shapes with round edges. However, the use of the Sol A-type precursors resulted in non-homogenous and non-uniform CZTSe films. Large formations with a hexagonal shape of approximately 4 μm were detected on the surfaces of these films. The EDS analyses allowed to determine that these formations are separate CuSe crystals ([Cu] = 49%, [Se] = 51%). The formed CZTSe layer exhibits a “wrinkled”

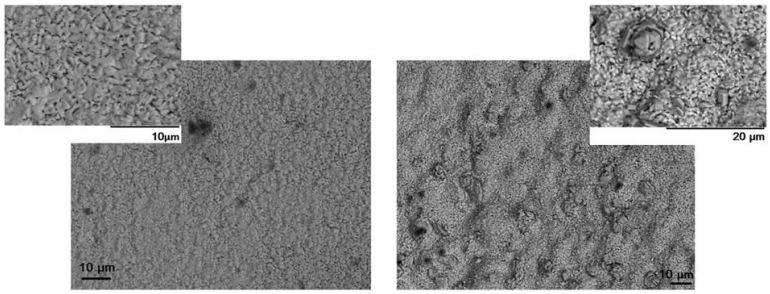

Fig. 1. SEM surface images of the films selenised at 470 °C for 40 min.

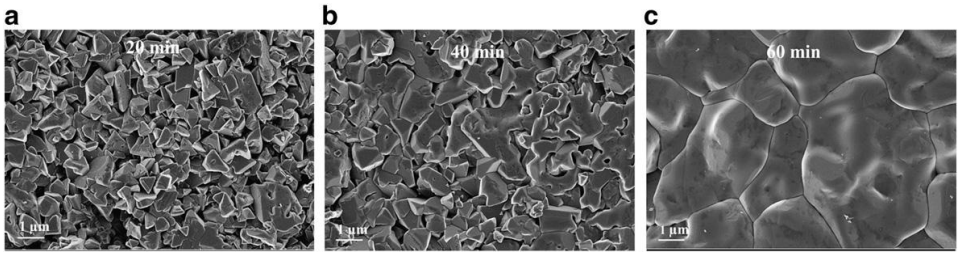

Fig. 3. SEM surface images of CZTSe films annealed for (a) 20 min, (b) 40 min and (c) 60 min at 470 °C.

structure, which indicates the loss of their contact with Mo substrate; the formed films easily peeled off of the Mo substrate.

The Raman scattering spectra from the surface of the CZTSe thin films from both series of precursors are depicted in Fig. 2, which provides evidence for the presence of foreign phases in the selenised films. The peaks at 171 cm^{-1}, 195 cm^{-1}, and 233 cm^{-1}, which correspond to CZTSe, are dominating features in both graphs [12]. However, it is clearly seen that in the spectrum for the Sol A-type films, there is an additional peak at 260 cm^{-1} that is related to the separate CuSe phase [12]. These results are in a good agreement with the EDS results.

3.2. Influence of the duration of selenisation on the $Cu_2ZnSnSe_4$ films

Only precursor stacks of the Sol B composition were used for these investigations. The surface of the films that were selenised for 20 min at 470 °C consists of a mixture of small triangular crystals with a size less than 0.7 μm and medium-sized rectangular crystals (Fig. 3). The formed crystals are densely packed and have sharp angles. The presence of separate phases and elements in the films was indicated by the Raman measurements. The Raman peaks at 237 cm^{-1} and 250 cm^{-1} can be attributed to pure Se and ZnSe phases, respectively (see Fig. 4) [15,16]. However, the primary peak of CZTSe at 196 cm^{-1} is already present after the shortest selenisation time.

When the selenisation duration was increased to 40 min, the size of the crystals increased (Fig. 3(b)). Grain growth continues, which implies that the small crystallites grow together to form larger agglomerates. The intensity of the peaks at 250 cm^{-1} and 237 cm^{-1} decreases, which indicates the lower content of ZnSe and elemental Se in the CZTSe layer. The Raman spectrum exhibits a broad peak in the region beginning from 231 cm^{-1} to 250 cm^{-1}.

Large crystals with a size of 1.5 to 4 μm are observed in the films annealed for 60 min in Fig. 3(c). The Raman spectra do not reveal presence of other phases; all peaks belong to the CZTSe compound (see Fig. 4). The full-width at half-maximum of the primary CZTSe peaks at 171 and 196 cm^{-1} becomes narrower, which indicates improved crystallinity. An additional peak appears at 233 cm^{-1}, which could be referred to as the third CZTS peak.

The composition of the CZTSe films becomes Zn-rich (see Table 1, experiment 2) when the annealing duration increases. This compositional change most likely occurs due to the loss of Sn during the longer selenisation times. However, note that no Sn-deficient films were observed, even after 60 min of annealing, by EDS (Sn = 12.6 at.%).

Almost all the peaks in the XRD pattern of a film selenised at 470 °C for 60 min in Fig. 5 are attributed to the CZTSe phase. Additional small and broad peaks at 13°, 31° and 56° are attributed to the selenisation of the Mo substrate and to the presence of the $MoSe_2$ phase — drysdallite. Because there is a difference in band gaps between the absorber and the $MoSe_2$ layers, the latter could be used a mirror for the electrons to reduce back-surface recombination [17].

4. Conclusions

Two series of metal stacked precursor Cu–Zn and Sn layers were electrodeposited and selenised. It was observed that the deposited precursors with a Cu/Zn ratio of 1.8 tend to form smooth and uniform films after selenisation. The CZTSe films prepared from precursors with a Cu/Zn ratio of 2.3 have CuSe crystals on their surfaces after annealing for 40 min at 470 °C. Furthermore, these films have a "wrinkled" and non-uniform morphology, which could lead to poor performance in future applications.

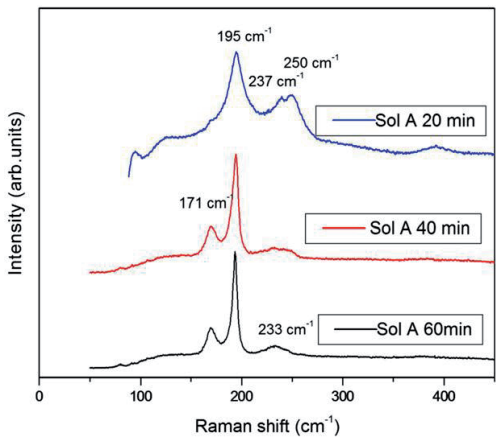

Fig. 4. Raman spectra of CZTSe films selenised at 470 °C for different duration.

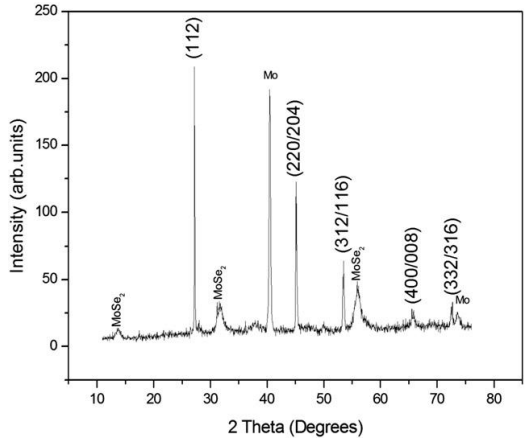

Fig. 5. XRD pattern of the film selenised for 60 min at 470 °C.

In the second experiment, only the precursors with a Cu/Zn ratio of 1.8 were used. The precursors were selenised for different durations. The presence of pure selenium and a ZnSe phase was detected in the Raman spectra of the films that were annealed for 20 min. The CZTSe films that were selenised for 60 min exhibited an increased grain size and the presence of secondary phases; however, the presence of $MoSe_2$ was not observed.

Acknowledgements

Estonian Centre of Excellence in Research Project TK117T "High-technology Materials for Sustainable Development", Estonian Energy Technology Programme (project AR 10128), Estonian Ministry of Higher Education and Science (targeted project T099) and Estonian Science Foundation (G8147) are acknowledged for the financing of the research.

References

[1] D. Colombara, L.M. Peter, K.D. Rogers, J.D. Painter, S. Roncallo, Thin Solid Films 519 (2011) 7438.
[2] M. Benchikri, O. Zaberca, R. El Ouatib, B. Durand, F. Oftinger, A. Balocchi, J.Y. Chane-Ching, Mater. Lett. 68 (2012) 340.
[3] Chengwu Shi, Zh.u. Chen, Gaoyang Shi, Renjie Sun, Xiaoping Zhan, Xinjie Shen, Thin Solid Films 520 (2012) 4898.
[4] B. Subramanian, C. Sanjeeviraja, M. Jayachandran, Sol. Energy Mater. Sol. Cells 79 (2003) 57.
[5] K.T. Ramakrishna Reddy, N. Koteswara Reddy, R.W. Miles, Sol. Energy Mater. Sol. Cells 90 (2006) 3041.
[6] T.M. Friedlmeier, N. Wieser, T. Walter, H. Dittrich, H.W. Schock, Proc. 14th European Photovoltaic Science and Engineering Conference, 1997, p. 1242.
[7] M. Grossberg, J. Krustok, K. Timmo, M. Altosaar, Thin Solid Films 517 (2009) 2489.
[8] G.S. Babu, Y.B. Kishore Kumar, P.U. Bhaskar, V.S. Raja, J. Phys. D: Appl. Phys. 41 (2008) 205.
[9] H. Matsushita, T. Ichikawa, A. Katsui, J. Mater. Sci. 40 (2005) 2003.
[10] D.A.R. Barkhouse, O. Gunawan, T. Gokmen, T.K. Todorov, D.B. Mitzi, Prog. Photovolt. 20 (2012) 6.
[11] Shafaat Ahmed, Kathleen B. Reuter, Oki Gunawan, Lian Guo, Lubomyr T. Romankiw, Hariklia Deligianni, Adv. Energy Mater. 2 (2012) 253.
[12] M. Ganchev, J. Iljina, L. Kaupmees, T. Raadik, O. Volobujeva, A. Mere, M. Altosaar, J. Raudoja, E. Mellikov, Thin Solid Films 519 (2011) 7394.
[13] J.J. Scragg, Phillip J. Dale, Diego Colombara, L.M. Peter, Chem. Phys. Chem. 13 (2012) 3035.
[14] Kyoo-Ho Kim, Ikhlasul Amal, Electron. Mater. Lett. 7 (2011) 225.
[15] V. Poborchii, A.V. Kolobov, K. Tanaka, Appl. Phys. Lett. 72 (1998) 1167.
[16] G. Perna, M. Lastella, M. Ambrico, V. Capozzi, Appl. Phys. A 83 (2006) 127.
[17] L. Kaupmees, PhD thesis, Tallinn University of Technology, Estonia, 2011, p 17.

APPENDIX A

Article III

J. Iljina, R. Zhang, M. Ganchev, T. Raadik, O. Volobujeva, M. Altosaar, R. Traksmaa, E. Mellikov; Formation of Cu_2ZnSnS_4 absorber layers for solar cells by electrodeposition-annealing route, *Thin Solid Films*, Vol. 537 (2013), p. 85-89

Thin Solid Films 537 (2013) 85–89

Contents lists available at SciVerse ScienceDirect

Thin Solid Films

journal homepage: www.elsevier.com/locate/tsf

Formation of Cu_2ZnSnS_4 absorber layers for solar cells by electrodeposition-annealing route

J. Iljina [b], R. Zhang [b], M. Ganchev [a,b,*], T. Raadik [b], O. Volobujeva [b], M. Altosaar [b], R. Traksmaa [b], E. Mellikov [b]

[a] Cental Laboratory of Solar Energy & New Energy Source, Bulgarian Academy of Sciences,78 Tzarigradsko shaussee, 1784 Sofia, Bulgaria
[b] Department of Materials Science, Tallinn Technical University, Ehitajate tee 5, Tallinn 19086, Estonia

ARTICLE INFO

Article history:
Received 20 March 2012
Received in revised form 11 April 2013
Accepted 12 April 2013
Available online 25 April 2013

Keywords:
Electrodeposition
thin films
kesterite
reactive annealing

ABSTRACT

This study investigates the electrodeposition process of quaternary copper–zinc–tin–sulfur (CZTS) thin films with a focus on the ability of ligands to bring deposition potentials of the individual elements closer to each other. Our results show that thiocyanate ions (CNS^-) can be used as a suitable complexant for the electrodeposition of Cu_2ZnSnS_4 from aqueous solutions. A complex electrolyte was developed and the composition measurements showed a large potential interval for the deposition of the CZTS thin film material with an appropriate metal ratio. The layers recrystallized in stoichiometric kesterite structure after annealing at 550 °C in H_2S atmosphere for 60 min.

1. Introduction

Electrodeposition is a promising method for formation of compound absorber films for photovoltaic applications. In an industrial setup, this approach could enable fast deposition of large areas at reasonable production costs. The electrodeposited layers are annealed in a second process step to form the final semiconductor. This approach can provide remarkable efficiencies for completed photovoltaic (PV) devices and results in a better cost and efficiency ratio for the final product compared to expensive vacuum processes used in the industry today. However, significant research on understanding of the individual process steps is still required to access this cost reduction potential. While finding the appropriate electrolyte composition is the key question in the electrodeposition step, the challenge in the annealing step is the development of suitable process conditions with respect to the peculiarities of the produced thin film material. Electrodeposition of compound thin films is based on Kroger's findings [1]. A simple example for PV applications is the binary compound CdTe, for which an epitaxial effect through electrodeposition was achieved. Peculiarities of the electrodeposition of metal alloys are discussed extensively by A. Brenner [2]. To electrodeposit thin layer material with the desired solid-state properties, it is essential to follow certain thermodynamic conditions in the process. In case of multicomponent compound deposition, the relevant thermodynamic characteristics are the equilibrium potentials of the constituents and the free energy of compound formation (Gibbs free energy). In case of metal alloys, where deposition takes place under negligible variation in the free energy, the more important condition is the relative location of the standard electrode potentials of the elements. To deposit compounds with considerable free energy of formation, the approach by Kroger should be applied [1]. According to those, in electrodeposition of CdTe, as an example, it should be kept into account the difference in relative concentrations of the active ions and an appropriate range of deposition potentials or the particular properties of electrolyte [3]. Furthermore, in case of multicomponent compounds' deposition, the order and relative disposition of standard electrode potentials for each metal constituents have to be considered [4]. For example, for $CuInSe_2$ the equilibrium potentials of metals could be manipulated by introducing an appropriate ligand [5] whereas the equilibrium potential of the non-metal element depends on the concomitant water splitting reaction, and therefore depends on the acidity of the solution [6]. When all these considerations are taken into account, the electrodeposition of ternary $CuInSe_2$ compounds could be performed by two different regimes: (a) by induced codeposition mechanism [7] and (b) under the conditions of diffusion limitations [8–10]. In case (a), the deposition reaction takes place close to the equilibrium and therefore allows more appropriate arrangement of the complete structure. In this case the speed of deposition is slow and the composition of the deposit remains constant over large interval of deposition potentials although being slightly different from the desired components ratio. In case (b), the obtained structure is again imperfect but the growth speed is higher compared to case (a) and the composition and the components ratio can be controlled by simple process parameters such as applied potential, concentration of elements in the electrolyte, temperature, agitation, and so forth [11].

* Corresponding author at: Department of Materials Science, Tallinn Technical University, Ehitajate tee 5, Tallinn 19086, Estonia. Tel.: +359 878736008; fax: +359 28754016.
E-mail address: mganchev@abv.bg (M. Ganchev).

0040-6090/$ – see front matter © 2013 Elsevier B.V. All rights reserved.
http://dx.doi.org/10.1016/j.tsf.2013.04.038

Since deposits are amorphous in both cases and additional annealing treatments are compulsory, the variant (b) appears to be favorable, since it results in more efficient PV devices [8–10]. Next generation diamante-like multicomponent compounds for PV application are kesterite (Cu_2ZnSnS_4 or CZTS), stannite ($Cu_2ZnSnSe_4$ or CZTSe) and their mixtures ($Cu_2ZnSn(S,Se)_4$). There are a few investigations covering direct electrodeposition in aqueous electrolytes of the quaternary compounds $Cu_2ZnSnSe_4$ [12] and Cu_2ZnSnS_4 [12,13]. Work [12] presents an extensive investigation on kinetics of electrodeposition of Cu, Zn, and Sn alloys and their chalcogenide derivatives. The history of research and development of electrodeposition approaches for simultaneous deposition of Cu, Zn and Sn are treated in details. As a result a suitable formulation of pyrophosphate metal salts, complexant, buffer and other additives are combined for direct deposition of CZTSe. CZTS was formed by co-electrodeposition of Cu–Zn–Sn alloy followed by sulfurization. Obtained layers are completed to solar cells. Work [13] suggests a popular complexant formulation of mixed citrate and tartaric ions for codeposition Cu–Zn–Sn with thiosulfate in order to obtain stoichiometric Cu–Zn–Sn–S precursors.

Presented research introduces a new electrodeposition route for formation of layers of copper, zinc, tin and sulfur which after reactive annealing in H_2S atmosphere result in stoichiometric Cu_2ZnSnS_4 layers.

2. Experimental details

Electrodeposition was carried out potentiostatically in a conventional three-electrode electrochemical cell with a mercury sulfate electrode as the reference electrode. The substrate electrodes were indium–tin oxide (ITO) covered glasses in size 2 × 1 cm^2 disposed vertically against platinum gauze used as auxiliary electrode.

The electrolyte consisted of 4 M potassium thiocyanate (KCNS) in a 0.4 M acetic buffer (pH 5) with dissolved chloride compounds of Cu^+, Zn^{2+} and Sn^{2+} in addition of $Na_2S_2O_3$ in total concentration of 10 mM. Scanning electron microscopy and energy dispersive X-ray analysis (EDAX) were performed on a Hitachi TM 1000 unit supplied with an X-ray source and a detector with an accelerating voltage of 15.0 kV and acquisition time of 90 s.

X-ray diffraction (XRD) measurements were performed using a Bruker D5005 diffractometer (Bragg–Brentano geometry) and Cu $K\alpha_1$ radiation with λ = 1.5406 Å at 40 kV and 40 mA. The room temperature micro Raman spectra were recorded by a Horiba LabRam 800 high-resolution spectrometer supplied with a multichannel detector in backscattering regime. A green laser with 532 nm wavelength served as light source and was focused on a spot area of at least 10 μm diameter, providing a spectral resolution of 0.5 cm^{-1}.

Reactive annealing was carried out in a tubular quartz reactor under the flow of a gas mixture of 5% H_2S in N_2 at atmospheric pressure. The tube was heated by direct infrared (IR) irradiation from xenon lamps. The desired temperature profile was maintained by an IR Ulvac-Rico heating system coupled with a computer controller setup. After annealing, the reactor volume was rinsed for 5 min with a N_2 stream. The actual temperature profile is depicted in Fig. 1.

3. Preliminary considerations

In our previous studies the ability of thiocyanate ions (CNS^-) as appropriate ligands for simultaneous electrodeposition of Cu, In and Se was investigated [5,6]. Following these results, we focus in this paper on verifying the thiocyanate ions as suitable ligands for electrodeposition of Cu, Zn, Sn and S.

The criterion determining the suitability of a ligand for simultaneous electrodeposition of a few elements is the interrelation of stability constants of their respective compounds. On the one hand, ligands must fix stronger the elements with the most positive standard electrode potentials and at the same time to form weak complexes towards the elements with more negative standard electrode

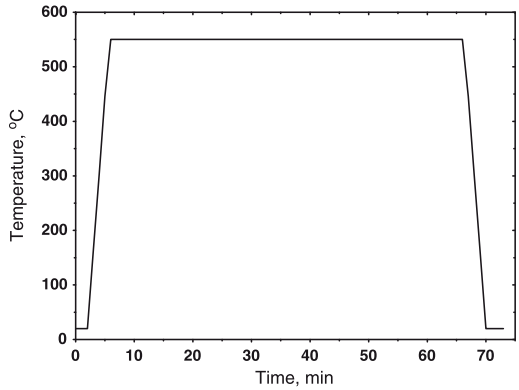

Fig. 1. Temperature profile for thermal processing of as-deposited Cu–Zn–Sn–S thin films in atmosphere of 5% H_2S in N_2.

potentials. Relative positions of standard electrode potentials (vs. NHE) of involved metal elements are the following [14]:

$$Cu^+ + e^- = Cu0.522V \quad (1)$$

$$Sn^{2+} + 2e^- = Sn{-}0.136V \quad (2)$$

$$Zn^{2+} + 2e^- = Zn{-}0.762V \quad (3)$$

Table 1 shows the negative logarithms of the stability constant values for thiocyanate complexes with Cu^+, Zn^{2+} and Sn^{2+} [15]. Stability constants for the element with most positive standard electrode potential (Cu) have high values (around 12.7) whereas Sn and Zn ions are under weak influence of the thiocyanate and their complexes are much lower in magnitude (near 1.2 and 2.3 respectively). This means that the deposition potential of copper is moved in negative direction, whereas Sn and Zn are not bound as strong to the ligand. Therefore deposition potential of copper shifts closer to the potentials of metals with more negative standard electrode potentials.

As far as sulfur deposition is concerned, thiocyanate is indifferent. In our case the sulfur supply is provided by a cathodic reduction of thiosulfate ion — $S_2O_3{}^{2-}$. Reduction of thiosulfate is elucidated in details in [16]. Following their conclusions the thiosulfate undergoes reduction by two ways. The first one is direct reduction with two electrons near the potential of the zero charge of the surface:

$$S_2O_3^{2-} + 2e^- = S^{2-} + SO_3^{2-} \quad (4)$$

At more negative potentials reduction goes through nascent hydrogen evolved on cathode:

$$S_2O_3^{2-} + H + OH^- = S^{2-} + SO_3^{2-} + H_2O \quad (5)$$

Table 1
Thiocyanate complex stability constants by critical survey of stability constants of complexes of thiocyanate ion [15].

	$-\lg\beta^1$	$-\lg\beta^2$	$-\lg\beta^3$	$-\lg\beta^4$
Cu^+	12.7	11.0	11.6	12.02
Sn^{2+}	1.2	1.8		1.7
Zn^{2+}	1.46	2.16	2.33	2.01

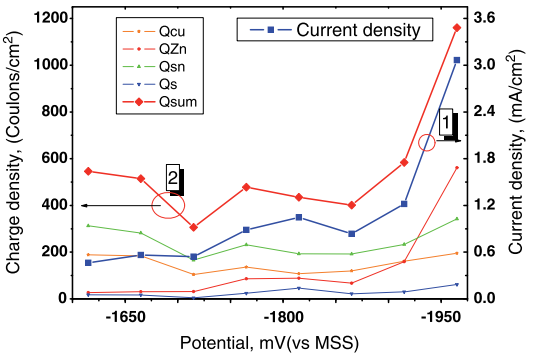

Fig. 2. Dependence of cathodic current density, charge density and partial charge densities for electrodeposition of Cu–Zn–Sn–S thin films from thiocyanate electrolyte 4 M KCNS in 0.4 M acetic buffer (pH 5.0); $[Cu^{+}]:[Zn^{2+}]:[Sn^{2+}]:[S_2O_3^{2-}] = 3.6:3.2:1.2:1$ mM.

Following these data the general equation for electrodeposition of Kesterite could be described as

$$2Cu^{+} + Zn^{2+} + Sn^{2+} + 4S_2O_3^{2-} + 14e^{-} \Rightarrow Cu_2ZnSnS_4 + 4SO_3^{2-} \quad (6)$$

4. Results and discussion

The electrolyte was stable long enough to enable the deposition of Cu–Zn–Sn–S thin films with different component ratios. Films that contained high sulfur concentrations were powdery, whereas films with low sulfur content were more compact and stable, allowing further processing.

Fig. 2 presents current and surface charge density in dependence on cathode potential (curves 1 and 2). Both curves give information about the current related efficiency of the electrodeposition process depending on the cathode potential. Curves for a partial charge of individual components Cu, Sn, Zn and S are depicted in Fig. 2 as well. Current density was calculated by the established value of the current after 15 min plating time related to the active surface of the electrode. Charge density and respective partial charge densities for the elements are derived by weight measurements of electrodeposited layers and data for the composition by EDAX, following the Faraday's law:

$$Q_i = F \cdot m_i / (z_i \cdot M_i) \quad (7)$$

where Q_i is the partial charge density for the ith element (either Cu, Zn, Sn or S), F is the Faraday's constant ($F = 96{,}485$ C mol^{-1}), m_i is the average mass of the component (Cu, Zn, Sn or S), obtained by related weight percent concentration multiplied to the total mass of the film, z_i is the electrons number for reducing of the related element and M_i is its atomic mass weight. Total charge density is the sum of partials densities, while the hydrogen evolved is not taken into calculations. In order to increase reliability of the calculations they are performed by triple independent EDAX measurements at different points on the electrode.

At initial deposition potentials the shapes of curves 1 and 2 as the partial curves of the components show the same tendency without drastic changes. The sharp rise of curves 1 and 2 begins from −1865 mV and could be explained by beginning hydrogen evolution. In the same region an increase of the partial charge density for Zn could be noticed, resulting from the deposition of metal Zn together with hydrogen evolution. The shapes of curves 1, 2 and 2.3 respectively show that an increased cathodic current density at more negative potentials is not only caused by H^{+} reduction, but is accompanied by an increase of Zn deposition. On the other hand, it suggests that the ligand CNS^{-} is an appropriate (weak) complex agent for Zn^{2+} and it could only slightly influence its electrochemical behavior.

The compositions of thin films depending on the component ratio in the electrolyte are presented in Fig. 3. In fact, the diagram presents only metal component ratios.

As deposited films were about 10% sulfur deficient against stoichiometry of Cu_2ZnSnS_4. As seen in Fig. 3, the compositions of the films are in line, and with an increased deposition potential the composition tends to approach the initial electrolyte. Slightly higher Sn content in the films is due to the presence of tin in the substrate ITO layer. According to the diagram, the Cu–Sn ratio stays constant when the potential is increased. However, at the same time, Zn content in the films increases. This behavior is in good compliance with Fig. 2 where Cu and Sn content keeps constant while the Zn content increases sharply at elevated cathode potential. These observations are guide to a simple rule: The Cu–Sn ratio in the deposited film can be controlled through preparation of the electrolyte with the desired Cu–Sn ratio,

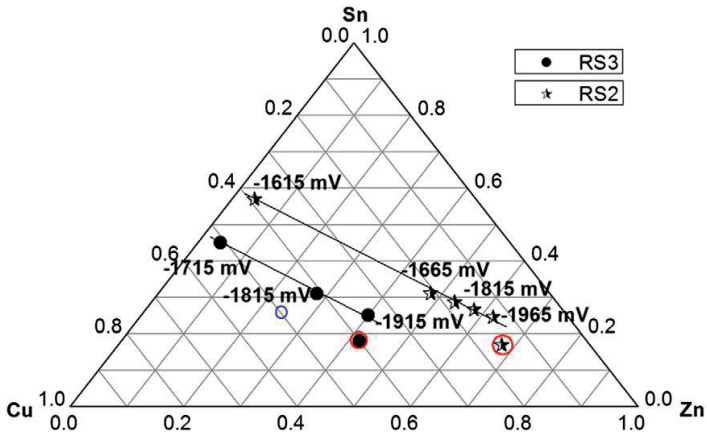

Fig. 3. Dependence of thin film CZTS composition on composition of the electrolyte at different potentials. RS3 and RS2 (in red circle) show the composition of electrolytes. Diagram presents metals Cu–Zn–Sn ratio only. ○ shows the stoichiometric ratio.

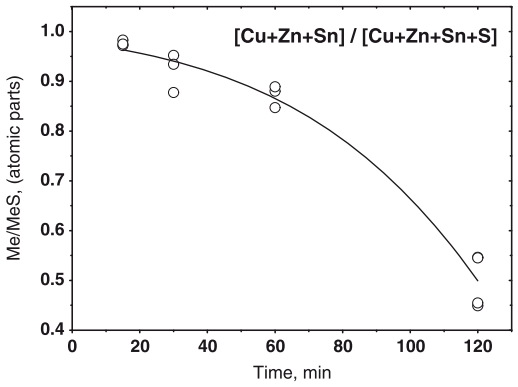

Fig. 4. Sulfur concentration in CZTS thin films in dependence on deposition time of the samples (plating times: 15 min, 30 min, 60 min and 120 min at −1915 mV).

whereas the Zn concentration can be controlled during the deposition process by adjusting the potential. Sulfur concentration has strong influence on the mechanical properties of the deposited CZTS layers. It was observed that if sulfur concentration in the electrodeposited layers is close to the stoichiometric one, films are powdery, dendritic, unstable and less receptive to further thermal treatments. Fig. 4 presents the dependence of the sulfur content in the obtained films on the deposition time at a constant potential (−1915 mV). The curve shows that sulfur concentration in the films increases with the time of deposition and ratio of metal content to the total atom content decreases. This phenomenon could be explained with special features of sulfur electrolysis [16]. At initial stages sulfur electrodeposition takes place preferably by the electrochemical mechanism at the ITO glass substrate, where the over-potential of hydrogen is high. With an increase of the deposition time almost the whole electrode surface area is covered with Cu–Zn–Sn–S. That leads to the increased hydrogen evolution rate and rise of sulfur content in the film by reaction 5. Electrodeposited for 60 min CZTS films at −1915 mV contained low sulfur concentration and in the second step were annealed in H_2S atmosphere at 550 °C for 60 min.

There were no noticeable changes in the metal's ratio of the films before and after annealing. Only sulfur content rose up to the stoichiometric value. For example the sample SR3s1 as deposited had a composition of 51.91 at.% Cu–22.12 at.% Zn–20.89 at.% Sn and 5.06 at.% S while after annealing the composition was 22.61 at.% Cu–13.00 at.% Zn–13.07 at.% Sn and 51.31 at.% S.

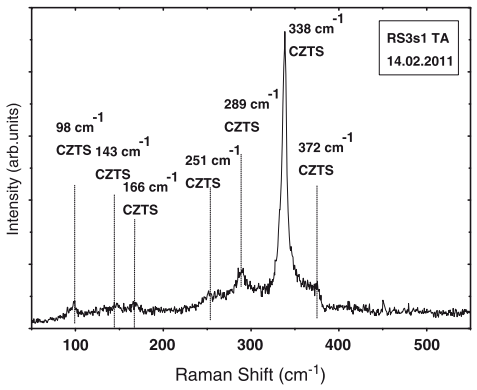

Fig. 5. Raman shift for sample thin film CZTS, deposited from thiocyanate electrolyte and annealed at 550 °C for 1 h in 5% H_2S:N_2 atmosphere.

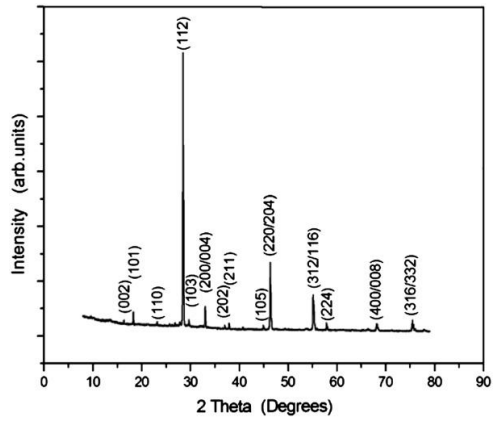

Fig. 6. XRD pattern of CZTS film annealed at 550 °C for 1 h.

Raman spectra of annealed films (Fig. 5) present a monophase composition of the films. The main vibrations for kesterite at 338 cm^{-1}, 289 cm^{-1}, 251 cm^{-1}, 372 cm^{-1}, 166 cm^{-1}, 143 cm^{-1} and 98 cm^{-1} are seen [17].

The XRD pattern (Fig. 6) for the film annealed at 550 °C for 60 min exhibited several peaks corresponding to diffraction lines of the kesterite structure of CZTS (PDF Card —04-003-8920). Dominant peak of the XRD pattern of these polycrystalline films responds to the (112) diffraction line of the kesterite structure of CZTS.

SEM image surface of the film annealed at 550 °C for 60 min is depicted in Fig. 7 and presents a typical morphology of CZTS films obtained through this method. The grain size is near 2–4 μm whereas the estimated thickness of the layers is about 1–1.5 μm.

5. Conclusions

In this study the suitability of thiocyanate as an appropriate ligand for one-step electrodeposition of Cu–Zn–Sn–S thin films was investigated. Basic current–potential dependencies for electrodeposition process using thiocyanate are presented as well. The sulfur concentrations in the as-deposited layers depend on the duration of deposition. Layers with high sulfur concentration resulted in dendritic and

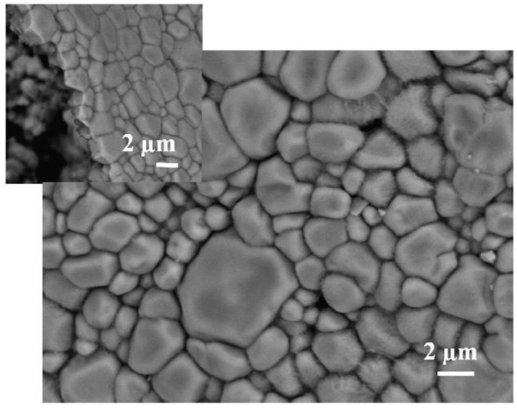

Fig. 7. SEM surface and cross-sectional (inset) images of sample CZTS thin film, electrodeposited in the thiocyanate electrolyte for 60 min and annealed at 550 °C for 1 h in 5% H_2S:N_2 atmosphere.

powdery structures and were not appropriate for further treatment. It was shown that electrodeposited layers did not change metal's Cu–Zn–Sn ratio after annealing in a reactive H_2S atmosphere and formed monophase Cu_2ZnSnS_4 layers. The grain size of the layers formed in such a way was as large as 2–4 μm, whereas the thickness of the layers was much lower, near 1.5 μm.

Acknowledgments

The authors thank Dr. J. Raudoja and Dr. T. Varema for their kind assistance. Collaboration agreement between the Bulgarian Academy of Sciences and the Estonian Academy of Sciences as well as the European Researcher's Mobility Program of Estonian National Science Foundation under Contract JD 98 are gratefully acknowledged.

References

[1] F.A. Kröger, J. Electrochem. Soc. 125 (1978) 2028.
[2] A. Brenner, Electrodeposition of alloys, Academic press, 1963. , (Repr. 1991).
[3] D. Lincot, A. Kampmann, B. Mokili, J. Vedel, R. Cortes, M. Froment, Appl. Phys. Lett. 67 (1995) 2355.
[4] M. Kemell, H. Saloniemi, M. Ritala, M. Leskela, Electrochim. Acta 45 (2000) 3737.
[5] M.G. Ganchev, K.D. Kochev, Sol. Energy Mater. Sol. Cells 31 (1993) 163.
[6] E. Tzvetkova, N. Stratieva, M. Ganchev, I. Tomov, K. Ivanova, K. Kochev, Thin Solid Films 311 (1997) 101.
[7] M. Kemell, H. Saloniemi, M. Ritala, M. Leskela, J. Electrochem. Soc. 148 (2001) C110.
[8] D. Lincot, J.F. Guillemoles, S. Taunier, D. Guimard, J. Sicx-Kurdi, A. Chomont, O. Roussel, O. Ramdani, C. Hubert, J.P. Fauvarque, N. Bodereau, L. Parissi, P. Panheleux, P. Fanouillere, N. Naghavi, P.P. Grand, M. Benfarah, P. Mogensen, O. Kerrec, Sol. Energy 77 (2004) 725.
[9] R.N. Bhattacharya, A.M. Fernandez, Sol. Energy Mater. Sol. Cells 76 (2003) 331.
[10] R. Ugarte, R. Schrebler, R. Córdova, E.A. Dalchiele, H. Gómez, Thin Solid Films 340 (1999) 117.
[11] J. Kois, M. Ganchev, M. Kaelin, S. Bereznev, E. Tzvetkova, O. Volobujeva, N. Stratieva, A.N. Tiwari, Thin Solid Films 516 (2008) 5948.
[12] H. Kuhnlein, PhD Thesis, Technical University, Dresden, 2007 (in German).
[13] S.M. Pawar, B.S. Pawar, A.V. Moholkar, D.S. Choi, J.H. Yun, J.H. Moon, S.S. Kolekar, J.H. Kim, Electrochim. Acta 55 (2010) 4057.
[14] A.J. Bard, R. Parsons, J. Jordan, Standard Potentials in Aqueous Solutions, M. Dekker Inc., New York, 1985.
[15] A. Bahta, G. Parker, D. Tuck, Pure Appl. Chem. 69 (7) (1997) 1489.
[16] N.A. Shvab, V.D. Litovchenko, L.M. Rudkovskaya, Russ. J. Appl. Chem. 80 (11) (2007).
[17] X. Fontane, V. Izquierdo-Roca, E. Saucedo, S. Schorr, J. Alloys Compd. 539 (2012) 190.

APPENDIX A

Article IV

M**.** Ganchev, **J**. **Iljina,** L. Kaupmees, J. Raudoja, T. Raadik, O. Volobujeva, E. Mellikov, M. Altosaar; Phase Composition of selenized $Cu_2ZnSnSe_4$ thin films by XRD and Raman studies, *Thin Solid Films*, Vol. 519 (2011), p. 7394-7398

Thin Solid Films 519 (2011) 7394–7398

Contents lists available at ScienceDirect

Thin Solid Films

journal homepage: www.elsevier.com/locate/tsf

Phase composition of selenized $Cu_2ZnSnSe_4$ thin films determined by X-ray diffraction and Raman spectroscopy

M. Ganchev *, J. Iljina, L. Kaupmees, T. Raadik, O. Volobujeva, A. Mere, M. Altosaar, J. Raudoja, E. Mellikov

Department of Materials Science, Tallinn University of Technology, Ehitajate tee 5, 19086 Tallinn, Estonia

ARTICLE INFO

Available online 4 March 2011

Keywords:
$Cu_2ZnSnSe_4$
Stannite
Thin films

ABSTRACT

Thin layers of Sn onto Cu–Zn alloy with different component ratios were processed at different temperatures. Scrupulous comparative analyses were performed by room temperature Raman spectroscopy and X-ray-diffractometry. An excess of tin on the surface results in isothermal selenization at 450 °C in the hexagonal residuals of unstable $SnSe_2$ in the well-crystallized Stannite — $Cu_2ZnSnSe_4$. In similar selenization conditions, copper-rich layers as precursors result in the Stannite phase with micro-immersions of CuSe. Low-temperature photoluminescence spectra of selenized films indicated to two Gaussian shaped bands at 0.81 and 1.16 eV.

1. Introduction

Thin film chalcopyrites and in particular the compounds based on abundant elements of Cu, Zn and Sn have strengthened their position in photovoltaics [1]. Solar cells on mixed sulfur–selenium $Cu_2ZnSn(S,Se)_4$ layers have been reported to show a record efficiency of 9.66% [2], confirming their potential to play a serious role in photovoltaics through the cost–efficiency ratio in material diversification. The first thin film CZTSe device grown by evaporation has shown a 2% efficiency [3].Thin $Cu_2ZnSnSe_4$ (CZTSe) layers have been formed also by pulsed laser ablation [4], selenization of one-step RF sputtered [5] or sequentially deposited substrates [6] as well as by synthesis from melts [7]. CZTSe single crystals were first formed by [8] and compound materials have been shown to crystallize in the Stannite structure with direct band gap near 1.44 eV and a high absorption coefficient tending to 10^4 cm^{-1} [9].

This study analyzes in detail the phase composition of CZTSe layers with different metals ratios selenized under gradual temperature conditions.

2. Experimental details

Substrate layers were deposited electrochemically in potentiostatic conditions using the classic three-electrode cell configuration. Working electrodes were 2×1 cm^2 sized molybdenum covered soda lime glasses positioned against platinum gauze and a saturated mercury sulfate (MSE) reference electrode (0.6151 V vs. SHE). Electrolytes for electrodeposition of Cu–Zn alloy and Sn layers were aqueous pyrophosphate solutions of the sulfate salts of Cu^{2+}, Zn^{2+} and Sn^{2+}. Selenization was performed in isothermal conditions at sealed quartz ampoules placed into the tubular furnace. A cooling-down process procedure was followed, that ensure extra selenium vapors to be condensed in the external empty part of the ampoule far away of the samples. Configurations and regimes were the same as described elsewhere [10].

Routine scanning electron microscopy and energy dispersive X-ray analysis (EDAX) was performed on Hitachi TM 1000 unit supplied with an X-ray source and detector equipment with an accelerating voltage of 15.0 kV and acquisition time of 90 s. Film morphology was examined by Zeiss ULTRA 55 at an accelerating voltage 1.74 kV.

In the X-ray diffraction (XRD) analysis a Rigaku Ultima IV diffractometer with Cu–Kα radiation ($\lambda = 1.5418$ Å) at 40 kV accelerating voltage was used. The diffracted beam was scanned in steps by 0.01° for 2 s in an angular range from 10 to 80° 2Θ.

Qualitative phase analysis was performed on PDXL Rigaku's ICDD PDF2 phase research platform [11]. The room temperature (RT) micro Raman spectra was recorded on Horiba LabRam 800 high-resolution spectrometer equipped with a multichannel detector on backscattering regime. Light source was a green laser with a 532 nm wavelength focused at least on 10 μm spot diameter, providing a spectral resolution of 0.5 cm^{-1}. Photoluminescence measurements were carried out in a closed-cycle He cryostat at 15 K. The PL excitation was done by 441 nm He–Cd laser line and registered with a SPM2 Carl Zeiss Jena monochromator and InGaAs detector.

3. Results and discussion

The influence of the initial composition of the films was studied for Cu-rich, stoichiometric and Cu-poor layers selenized at 450 °C. Temperature dependence experiments were conducted at temperatures

* Corresponding author. Tel.: +372 6203374; fax: +372 6203367.
E-mail address: mganchev@abv.bg (M. Ganchev).

0040-6090/$ – see front matter © 2011 Elsevier B.V. All rights reserved.
doi:10.1016/j.tsf.2011.01.388

Table 1
Temperature of annealing, elemental composition and components ratio of thin CZTSe films, formed by isothermal selenization of sequential Cu + Zn and Sn layers.

N	T, °C	Cu, a%	Zn, a%	Sn, a%	Se, a%	Cu/(Zn + Sn)	Zn/Sn	Me/CZTSe
Samp1	450	22.7	16.7	10.9	49.7	0.8	1.5	0.5
Samp2	450	20.9	17.4	11.9	49.8	0.7	1.5	0.5
Samp3	450	26.4	12.9	11.8	48.9	1.1	1.1	0.5
Samp4	450	28.6	10.7	12.1	48.6	1.2	0.9	0.5
Samp5	490	15.4	25.0	10.8	48.8	0.4	2.3	0.5
Samp6	530	19.9	17.5	13.4	49.2	0.5	1.3	0.5
Samp7	560	13.5	20.7	9.1	56.7	0.5	2.2	0.4

450 °C, 490 °C, 530 °C and 560 °C only for copper-poor samples. XRD analysis was also carried out in addition to the Raman backscattering analysis for comparative investigations of the phase composition of the CZTSe layers.

All samples were Sn-poor ([Zn]/[Sn]>1) after selenization with the exception of the samples prepared using Cu-rich precursors only. The composition of the layers and selenization parameters for all the samples used are summarized in Table 1.

The XRD patterns of CZTSe samples with different [Cu]/{[Zn] + [Sn]} ratios are shown in Fig. 1. Phase composition of the samples as determined by XRD analysis is presented in Table 2. The stannite — $Cu_2ZnSnSe_4$ [11] is recognizable by the main reflections at 27.16°, 45.1° and 53.52° and other minor peaks which are marked in Fig. 1 with s. In addition there are reflections of Mo [11] at 40.2° and 73.5° and three other peaks at 11.5°, 31.6° and 56.0° attributable to $MoSe_2$ [11] (d) — the phase formed by the selenization. Detailed analysis confirmed the existence of $Cu_{1.8}Se$ [11] (marked as b) — with reflections at 27.2°, 45.1° and 56.1°. Also a possible phase is ZnSe [11] — (z) the main peaks of which coincide or lie very close to those of Stannite at 27.16°, 45.1° and 53.5°. The XRD pattern for the Cu-poor sample presents (0,0,1), (0,0,2), (0,0,3) and (0,0,4) reflections of the $SnSe_2$ phase [11] — (T)at angles of 14.44°, 29.09°, 44.25° and 60.29, respectively, resulting in a dominant growth in the polar c-plane orientation. Increased copper concentration provokes a preferable growth of CuSe [11], marked with k, indicated by minor peaks at 26.6°, 28.1°, 31.2° and 50°. In addition the detailed analysis revealed several other phases. The layers Samp3 and Samp4 were shown also to contain ternaries Cu_2SnSe_3 [11] (cts) and Cu_2SnSe_4 [11] (dctts); in addition, Samp3 contain of SnSe (t) [11].

Fig. 2 shows the XRD patterns of layers formed by annealing of Cu–Zn/Sn films in selenium vapors at different temperatures — Samp1 – at 450 °C, Samp5 – 490 °C, Samp6 – 530 °C and Samp7 – at 560 °C, respectively. All samples were Cu-poor, with phase content as shown in Table 2. At the initial temperature, the representative pattern is the same as in the previous description for the Cu-poor case (Samp1). As the temperature rises the main dominant phases are again $Cu_2ZnSnSe_4$, $Cu_{1.8}Se$ and ZnSe. Minor presence of CuSe was registered also but their intensity decreases sharply with the temperature increasing. Respective phases are denoted in Fig. 2 with the same codes s, b, z and k. The most intense peaks are at angles 2Θ — 27.2°, 45.1° and 53.3°. As it was mentioned, the reflections are composite (attributable to many phases: CZTSe, $Cu_{1.8}Se$, ZnSe) with no indication to qualitative distribution. In addition, the phases of $SnSe_2$ and SnSe are also noticeable. The group of ternary Cu_2SnSe_3 is seen

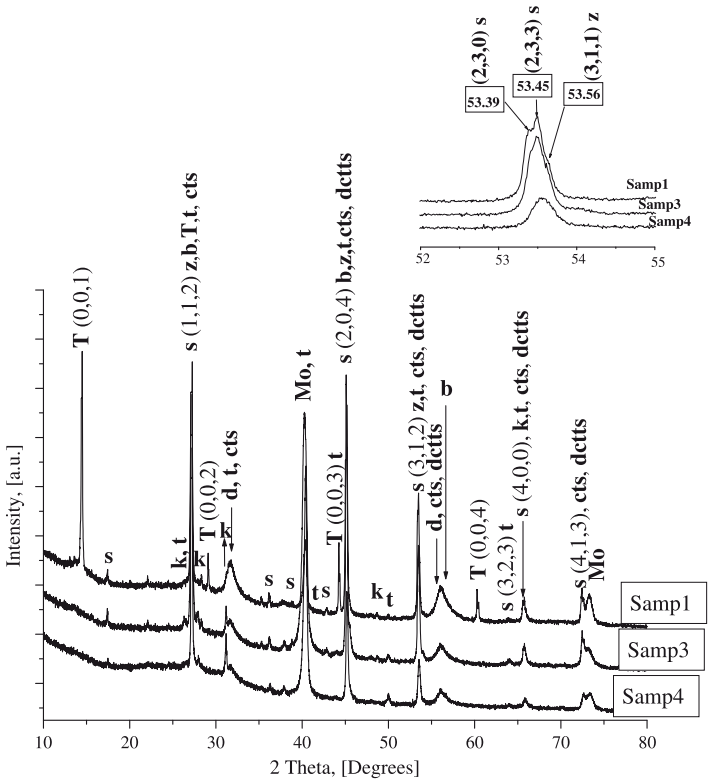

Fig. 1. XRD patterns of Cu-poor (Samp1), Stoichiometric — Cu = (Zn + Sn) (Samp3) and Cu-rich (Samp4) CZTSe thin films, obtained by isothermal selenization at 450 °C of metal Cu–Zn/Sn layers onto Mo covered soda lime glass substrates. Phase symbols: s—$Cu_2ZnSnSe_4$; z—ZnSe; b—$Cu_{1.8}Se$; k—CuSe; t—SnSe; T—$SnSe_2$; d—$MoSe_2$; cts—Cu_2SnSe_3; dctts—Cu_2SnSe_4; Mo—Molybdenum. Inset present the pattern in interval 52°–55° for distinct of CZTSe and ZnSe.

Table 2
Phases, detected by XRD in the samples CZTSe, selenized in isothermal condition according to Table 1: * – existing phase; o – not detected phase.

N	T,	$Cu_2ZnSnSe_4$	Cu_2SnSe_3	Cu_2SnSe_4	$SnSe_2$	$Cu_{1.8}Se$	CuSe	ZnSe	SnSe
	°C	s	cts	dctts	T	b	k	z	t
Samp1	450	*	o	*	*	*	*	*	o
Samp2	450	*	o	*	o	*	*	*	*
Samp3	450	*	*	*	o	*	*	*	*
Samp4	450	*	*	*	o	*	*	*	o
Samp5	490	*	*	*	*	*	*	*	o
Samp6	530	*	*	*	o	*	*	*	o
Samp7	560	*	*	*	*	*	*	*	o

accompanied with Cu_2SnSe_4. When the temperature increases, the signal of the substrate fades and reflections from the layer becomes dominant. CZTSe and ZnSe phases can be distinguished in the vicinity of 53°–54°[12]. Here CZTSe presents twins at 53.39° (2,3,0) and 53.45° (2,3,3) whereas ZnSe presents (3,1,1) peak at 53.56°. As can be seen at the inset of Fig. 2, at lower and higher temperatures (Samp4 and Samp7) ZnSe exists as a minor compound and its crystallinity improves at 530 °C. The same trend can be seen in the crystallization of the phase $Cu_2ZnSnSe_4$. It is also interesting to follow the dependence of CZTSe–ZnSe peaks ratio through the Cu compositional gradient. As can be seen from the inset of Fig. 1, twin peak corresponding to CZTSe dominates and ZnSe is present as a trace in the layers.

Fig. 3 shows the Raman spectra of samples selenized at 450 °C with different Cu concentrations — Cu-poor, stoichiometric CZTSe ($Cu_2ZnSnSe_4$) and Cu-rich CZTSe (Samp2, Samp3 and Samp4, respectively) and samples annealed at different temperatures — Samp5@490 °C; Samp6@530 °C and Samp7@560 °C (in accordance with Table 1). In all samples CZTSe is the dominant phase presenting main vibrations at 79 cm^{-1}, 171 cm^{-1}, 194 cm^{-1}, 231 cm^{-1} and 390 cm^{-1}. For the Cu-rich and stoichiometric samples resonance at 262 cm^{-1} was recorded and taken together with those at 91 cm^{-1} assigned to CuSe (k). In the spectra for Samp2 a signal near 250 cm^{-1} was detected. We attributed it to the phase ZnSe, in accordance with the phase distribution, evidenced in Fig. 1. When the temperature rose from 450 °C to 560 °C, a dominating signal had arisen at the same wave number (250 cm^{-1}), indicating preferential crystallization of ZnSe.

Fig. 4 exhibits the morphology of the quaternary CZTSe films. The micrographs present the surface image of Samp6 (Table 1) annealed at 530 °C (image a) and its cross-section view (image b). The layer is uniform, dense and well crystallized with grain size near 1 μm. On the border of the grains small hexagonal crystals of impurity phases (marked in circles) are seen.

Amongst recognized phases here, CuSe and $SnSe_2$ are hexagonal. As is shown elsewhere [10], ZnSe sets usually on the bottom whereas preferable distribution of copper selenides is on the surface and

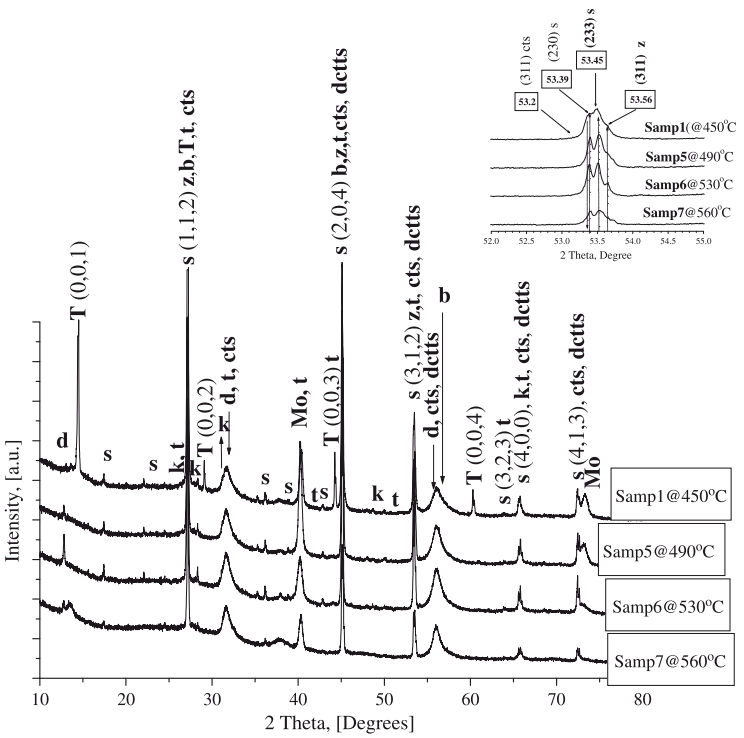

Fig. 2. XRD pattern of CZTSe samples formed by isothermal reactive annealing in Se vapors of Cu–Zn/Sn metal layers at different temperatures: Samp1 — 450 °C; Samp5 — 490 °C; Samp6 — 530 °C and Samp7 — 560 °C. The layers are Cu-poor. For phase symbols refer Fig. 1. Inset presents the pattern in 2Θ interval 52°–55° to gain distinction of CZTS and ZnSe.

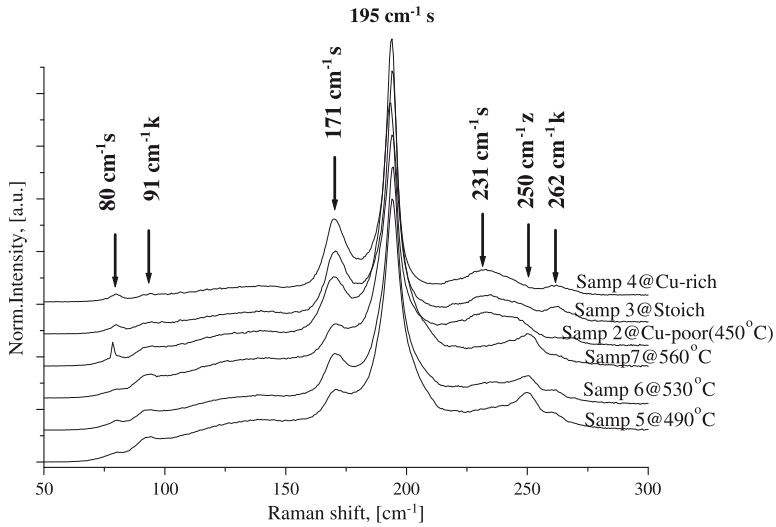

Fig. 3. Raman spectra for thin CZTSe layers: with different Cu concentration annealed at different temperatures. For phase symbols refer Fig. 1. (See also Table 1 and text).

among grain borders of the layer. It was shown above that even copper-poor layers contain separate copper selenide phases.

The low-temperature (T = 15 K) photoluminescence spectra of the annealed CZTSe (Samp1) film are presented in Fig. 5. The PL spectrum of that sample consists of two Gaussian-shaped PL bands at 0.81 and 1.16 eV, respectively. The first one has been recognized already in the monophase CZTSe [13], where temperature and excitation power dependences defined it as a BI-emission. The second band is caused obviously by CuSe contaminants. Previous investigations [10] have shown similar dominating PL emission in the presence of CuSe.

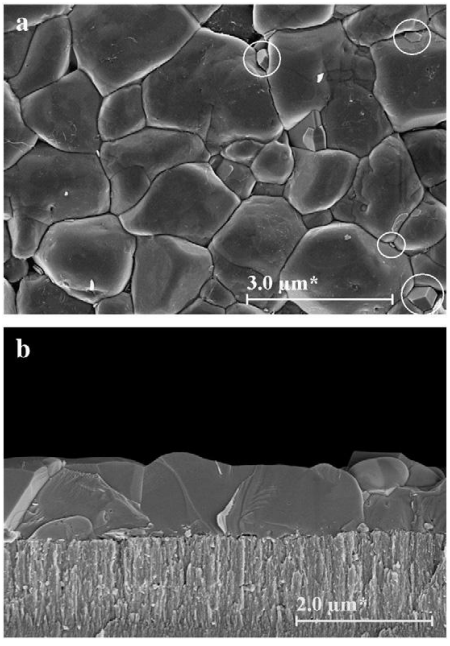

Fig. 4. High resolution SEM micrograph of thin layer CZTSe (Samp6) (a), selenized at 530 °C for 30 min in closed isothermal conditions and (b) — cross section of the film. With circles are marked surface hexagonal impurities on the grain borders.

To complete the overview on the reaction pathway, the inferences made in ref. 12 should be taken into considerations. Results show that at temperatures 200 °C the synthesis of binaries (Cu_2Se, CuSe, SnSe, and ZnSe) takes place. When the temperature rises up to 450 °C, the binary forms the ternary Cu_2SnSe_3, which adsorb ZnSe and form the quaternary $Cu_2ZnSnSe_4$.

$$Sn + 2Se \rightarrow SnSe_2 \quad (1)$$

$$Cu + 2Se \rightarrow Cu_2Se \quad (2)$$

$$Cu + Se \rightarrow CuSe \quad (3)$$

$$Zn + Se \rightarrow ZnSe \quad (4)$$

$$Cu_2Se + SnSe_2 \rightarrow Cu_2SnSe_3 \quad (5)$$

$$Cu_2SnSe_3 + ZnSe \rightarrow Cu_2ZnSnSe_4 \quad (6)$$

$$Cu_2Se + 2SnSe_2 \rightarrow Cu_2SnSe_4 + SnSe \quad (7)$$

$$SnSe_2 \leftrightarrow SnSe + Se \quad (8)$$

Sequence of Reactions 1, 2, 4, 5 and 6 on analogy with [14] gives an interaction chains to form the quaternary CZTSe compound. Obviously Reactions 5 and 6 do not pass up to the last and together with Reaction 3 give an idea of how to explain the phase composition, revealed by XRD and partially by Raman backscattering analyses. The phase of Cu_2SnSe_4 could be formed at higher concentrations of $SnSe_2$, e.g. by Reaction 7. This interaction could give an insight into the SnSe assumed by XRD.

Reaction 7 gives an idea of SnSe in the films but SnSe could come from another interaction, which should be taken into consideration. Equilibrium of tin compounds with selenium depends on the temperature and respectively on the pressure of the selenium vapors by equilibrium 8.

As it follows from equilibrium 8 according to the Le Chatelier–Braun principle, at high temperatures selenium vapor pressure is high and reaction equilibrium is moved on the left, keeping tin in the high

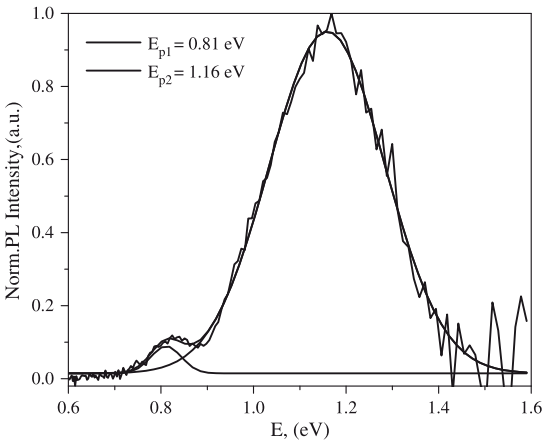

Fig. 5. Low temperature (15 K) photoluminescence spectra of thin CZTSe film (Samp1), annealed in closed isothermal conditions.

valence form. Samples in the ampoule are cooled down to ensure selenium to be moved to condensate preferably away from the sample. The samples should be held in a comparatively warmer part of the ampoule, in fact, to stimulate the decay of $SnSe_2$ in the layers.

Precise phase research analysis, performed by the PDXL software platform and the appropriate methodology for the experiments provides also an insight into the relative phase distribution and copper fraction in the grown films. For example, the composite reflection in Fig. 1 at 27.2° could be consistent with Stannite(s), Zinc Selenide (z), $Cu_{1.8}Se$ (b), $SnSe_2$ (T), SnSe — (t) and Cu_2SnSe_3 — (cts). About ZnSe an inset is added, which can provide an imagination of its part. $SnSe_2$ disposes individual reflections at 14.4°, 29.4°, 44.4° and 60.4° and the set of diffractograms shows that it consists only at the lower temperature 450 °C for copper poor sample (Samp1). The low valent form SnSe has individual reflections at 42° and 50.1° beside those at 26.4°, 31.6°, 40.3°, 45.5°, 48.6°, 53.5°, 64° and 65.7°. The set of curves presents an increase in the reflection height at 50.1°, its role being additionally described with the set of proposed formation reactions. Berzellianite ($Cu_{1.8}Se$ — b) disposes individually at 56.8° near the reflection of Drysdallite — ($MoSe_2$ — d) at 56.0°. The set of diffractograms shows that it appears at the copper-rich sample as a little shoulder, which could be recognized as an indication of presence in traces only at copper rich samples. Cu_2SnSe_3 disposes reflections at 27.16°, 31.6°, 45.1°, 53.5°, 56°, 65.7° and 72.5°, corresponding to the planes (1,1,1), (2,0,0), (2,2,0), (3,1,1), (2,2,2), (4,0,0) and (3,3,1) respectively. Cu_2SnSe_4(dctts) [11] presents at 45.2°, 53.4°, 55.95°, 65.8° and 72.5° from the respective planes (2,2,0), (3,1,1), (2,2,2), (4,0,0) and (3,3,1). Cu_2SnSe_3 appears together with SnSe, $Cu_2ZnSnSe_4$ and ZnSe at 31.6° close to the large reflection of $MoSe_2$ at 31.8° and after the reflection of the CuSe (k) at 31.2°. The lack of another visible shoulder besides the reflection of CuSe on the large reflection of $MoSe_2$ (keeping in mind the considerations for SnSe) would suggest a presence of Cu_2SnSe_3 as very small part. The same considerations could be made for reflections at 45.1° and 53.5°, respectively and to conclude that the main phase is Stannite ($Cu_2ZnSnSe_4$) and all other phases present as minorities or traces.

4. Conclusions

The study adds insights into the thermal interactions of metals Cu, Zn and Sn with Se at the temperature interval of 450 °C–560 °C for samples with a deficiency of Cu against stoichiometry of $Cu_2ZnSnSe_4$. Features of the phase composition depending on the relative Cu concentration at 450 °C were revealed for quaternary compound samples $Cu_2ZnSnSe_4$.

Acknowledgments

Authors would like to thank Dr J. Krustok and K. Timmo for discussions on PL and XRD. Estonian National Science Foundation under Contract JD 98, grants G-8147 and G-6954 and HTM (Estonia) under the project No. SF0140099s08 are gratefully acknowledged.

References

[1] H. Katagiri, K. Jimbo, W.S. Maw, K. Oishi, M. Yamazaki, H. Araki, A.Takeuchi, Thin Solid Films 517 (2009) 2455–2460.
[2] T. Todorov, K. Reuter, D. Mitzi, Adv. Mater. 22 (2010) 1.
[3] T.M. Friedlmeier, H. Dittrich, H.W. Schock, Inst. Phys. Conference Ser. No. 152, Proc. 11th ICTMC (Salford) P 345, 1997.
[4] R.A. Wibowo, E.S. Lee, B. Munir, K.H. Kim, Phys. Status Solidi A 204 (2007) 3373.
[5] R.A. Wibowo, W.S. Kim, E.S. Lee, B. Munir, K.H. Kim, J. Phys. Chem. Solids 68 (2007) 1908.
[6] O. Volobujeva, J. Raudoja, E. Mellikov, M. Grossberg, S. Bereznev, R. Traksmaa, J. Phys. Chem. Solids 70 (2009) 567.
[7] M. Altosaar, J. Raudoja, K. Timmo, M. Danilson, M. Grossberg, J. Krustok, E. Mellikov, Phys. Status Solidi A 205 (2008) 167.
[8] H. Hahn, H. Schulze, Naturwissenshaften 52 (1965) 426.
[9] L. Guen, W.S. Glaunsinger, A. Wold, Mater. Res. Bull. 14 (1979) 463.
[10] M. Ganchev, L. Kaupmees, J. Iliyna, J. Raudoja, O. Volobujeva, H. Dikov, M. Altosaar, E. Mellikov, T. Varema, Physics Procedia 2 (2010) 65.
[11] International Center for Diffraction Data: CZTSe – 10708930; MoSe2 – 30653481; SnSe – 10890232; SnSe2 – 10893197; ZnSe – 10715978; CuSe – 10728417; Cu1.8Se – 10882043; Cu2SnSe3 – 30654145; Cu2SnSe4 – 10780600; Mo – 10714645.
[12] P.M.P. Salomé, P.A. Fernandez, A.F. da Cunha, Thin Solid Films 517 (2009) 2531.
[13] J. Krustok, K. Timmo, M. Altosaar, Thin Solid Films 517 (2009) 2489.
[14] R. Schurr, A. Hölzing, S. Jost, R. Hock, T. Voß, J. Schulze, A. Kirbs, A. Ennaoui, M. Lux-Steiner, A. Weber, I. Kotschau, H.-W. Schock, Thin Solid Films 517 (2009) 2465.

APPENDIX A

Article V

M. Ganchev, L. Kaupmees, **J. Iliyna,** J. Raudoja, M. Altosaar, O. Volobujeva, E. Mellikov, T. Varema, H. Dikov; Formation of $Cu_2ZnSnSe_4$ thin films by selenization of electrodeposited stacked binary alloy layers, *Energy Procedia,* Vol. 2 (2009), p. 65-70

Available online at www.sciencedirect.com
ScienceDirect
Energy Procedia 2 (2010) 65–70
Energy Procedia
www.elsevier.com/locate/procedia

E-MRS Spring Meeting 2009, Symposium B

Formation of $Cu_2ZnSnSe_4$ thin films by selenization of electrodeposited stacked binary alloy layers

M.Ganchev[a]*, L.Kaupmees[a], J.Iliyna[a], J.Raudoja[a], O. Volobujeva[a], H. Dikov[b], M.Altosaar[a], E.Mellikov[a], T.Varema[a]

[a]*Materials Science Institute, Tallinn University of Technology, Ehitajate tee 5, 19086 Tallinn, Estonia*
[b]*Central Laboratory of Solar Energy-Bulgarian Academy of Sciences, 72 Tzarigradsko shaussee, 1784 Sofia, Bulgaria*

Received 1 June 2009; received in revised form 1 December 2009; accepted 20 December 2009

Abstract

Brass-Bronze thin-stacked layers electrodeposited in Potentiostatic conditions were selenized in an iso-thermal quartz tubular reactor. The ratio of metal components in selenized films was adjusted through appropriate choice of composition and thickness of the constituent layers. Focus is on the influence of annealing conditions on crystalline structure, phase composition, surface morphology and optical properties of the obtained $Cu_2ZnSnSe_4$ (CZTSe) thin films and pecularities of formation CZTSe thin films.

Electrodeposition, Precursor selenisation, $Cu_2ZnSnSe_4$

1. Introduction

Future development of thin film photovoltaics depends on the deployment of low cost and easily up scalable deposition methods for abundant and non-toxic compounds [1]. Ternary chalcopyrites $CuInS_2$ (CIS) and $Cu(In,Ga)Se_2$ were a promising solution but increasing prices of the rare metals In and Ga have affected the cost-efficiency ratio. Replacement of III group metals with cheap and widespread Zinc and Tin serve as another opportunity for diversification and industrialization of compound thin film photovoltaics [2]. $Cu_2ZnSnSe_4$ (CZTSe) is a structure analog of CIS where III group (Indium or Gallium) atoms are exchanged with Zinc and Tin. CZTSe is a prospective material with a direct band gap near 1.44 eV, close to the optimum for the solar irradiation spectra and a high absorption coefficient ranging to 10^4 cm^{-1} [3].

* Corresponding author. Tel.: +37 25 637 9736; fax: +37 26 203 367.
E-mail address: mganchev@abv.bg.

1876-6102 © 2010 Published by Elsevier Ltd
doi:10.1016/j.egypro.2010.07.012

There are numerous investigations on the sulfur compound Cu_2ZnSnS_4 developed by atom beam sputtering [4], thermal evaporations [5] and electron beam evaporated precursors processed in H2Satmosphere [6]. Later, electrodeposition routes [7,8] for the formation of substrate metallic precursors subjected subsequently to sulfurization were explored. Abou-Ras et al. [7] studied Electrodeposition route developed specifically by the formation of metallic alloy Cu-Zn-Sn precursor layers [9] to build solar cells.
The Selenium compound CZTSe thin layer absorbers were grown by pulsed laser ablation [10], one step RF magnetron sputtering [11] or with sequential selenization [12] as well as synthesis from melts [13]. The monograin thin film $Cu_2ZnSnSe_4$ solar cell recently developed has given Voc = 422 mV, J= 21.3 mA/cm^2 and FF 44 % with an overall efficiency of 2.16% [14].
This article focuses on the formation of $Cu_2ZnSnSe_4$ absorber layers by sequential electrodeposition of the Cu-Zn alloy and Cu-Sn stacked precursors, followed by reactive annealing in the atmosphere of selenium vapors.

2. Experimental details

Electrodeposition of precursor layers was performed in a potentiostatic condition with Wenking Bank PGstat 3440 in a three-electrode configuration at room temperature (20^{o}C). Reference was a Saturated Silver Chloride electrode (Ag/AgCl: 3M KCl) and Platinum gauze with much higher active surface than the cathode served as a counter electrode. The working electrodes were molybdenum covered (near 1 μm thick) soda-lime glass substrates sized approximately 1 X 2.5 cm^2 or molybdenum foils with the same dimensions. Solutions for deposition Cu-Zn and Cu-Sn layers contained 0.6M Potassium Pyrophosphate and salts of Cu^{2+}, Zn^{2+} and Sn^{2+} following formulations in [15]. Due to the oxidizing ability of Sn^{2+} on the anode or by the oxygen from air, the electrolytic cell for the deposition of Bronze layers was divided and the anode compartment was isolated ?through an Ion (Na^+) selective membrane. Anolyte was 0.2M Na_2CO_3 and to keep constant cation equilibrium concentrations for the membrane the catolyte contained 0.2M $Na_4P_2O_7$ and 0.4M $K_4P_2O_7$ as well as 0.1M Hydroquinone as an antioxidant.
Substrate layers Cu-Zn/Cu-Sn were selenized under isothermal conditions in evacuated 5-cm long quartz ampoules at 530^{o}C – 560^{o}C during 15 minutes at a 1.5-m thermal tubular reactor. In order to perform the thermal annealing samples with ampoules were placed in a preliminary preheated quartz holder pipe with wall thickness of 2mm, length of 60 cm and with inner diameter of 2.5 cm. After that the pipe with the ampoule inside was comparatively slowly moved out for cooling down to near 50 ^{o}C for another 20 minutes. Estimated annealing temperature profile is shown schematically in Fig.1. Other annealing experiments were performed for 1 h at 400^{o}C preliminary preheating in a vacuum of 150 Torr for metal alloy sublayer homogenization and reactive selenization for 1 h at 560^{o}C. Some singles, high temperature experiments, were performed at 750^{o}C for 2 hours with alloy substrate samples deposited onto molybdenum foil.

Fig.1. Scheme of time-temperature profile for fast annealing experiments

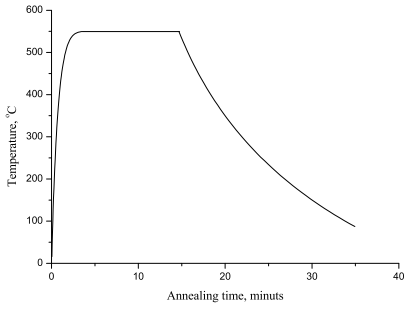

Fig.1. Thermal profile for selenization of thin alloy Brass – Bronze layers

Scanning electron microscopy investigations and EDX composition measurements were performed on Hitachi TT1000 unit supplied with X-ray source and detector equipment with accelerating voltage 15.0 kV and acquisition time 90 sec. High resolution micrograms and fine impurities composition measurements were done on Zeiss

ULTRA 55 at accelerating voltage 1.74 kV through an In lens. The room temperature (RT) micro – Raman spectra were recorded by Horiba LabRam 800 high-resolution spectrometer equipped with a multichannel detection system on backscattering configuration. The spectrometer operated by Green 532 nm wavelength laser focused within a 1 μm spot diameter providing the incident light with a spectral resolution of 0.5 cm^{-1}.
X – ray diffraction analysis (XRD) was performed on Rigaku Ultima IV with Cu - Kα radiation (λ=1.5418Å) and 4 kV accelerating voltage. The diffracted beam was scanned in steps by 0.01° for 2 sec in an angular range from 10 to 80 degrees in 2Θ. A comparison with JCDPS file cards [16] was made to assign the observed peaks. Phases manifested at least with three reflexes are taken into considerations. Optical investigations for determining the type and width of the band gap were carried out on UV-VIS-NIR spectrophotometer JASCO V-670 in the range of 200 to 2500 nm.

3. Results and discussion

Metal substrate layers were formed by two-step electrodepositing of alloys Brass (Cu-Zn) and Bronze (Cu-Sn) films, respectively. Final total film composition depends on the ratio of metals in the pair sublayers and its relative thickness. Total metal film thickness is defined by the sum of the thickness of the partial layers. The sequence of depositing Cu-Sn onto Cu-Zn was followed but an opposite order is possible as well. A 40-minute electrodeposition of Brass layer was followed by a 3-minute electrodeposition of Bronze layer to ensure formation of 1.5 – 2 μm thick CZTSe layer after selenization.

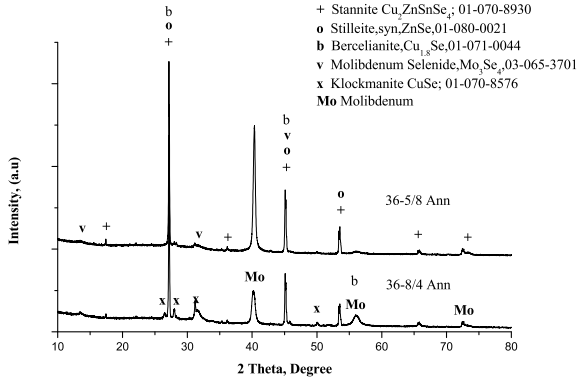

Fig.2. X-Ray diffraction patterns of thin layer $Cu_2ZnSeSe_4$ annealed in different regimes: Sample 36-5/8 – selenization of 15 minutes at 530 °C and 20 minutes slow cooling down; 36-8/4 – 1 hour annealing in vacuum and 1 hour selenization at 560°C

Fig.2 presents XRD patterns of samples 36-8/4 and 36-5/8. The first one had passed preliminary homogenization annealing in vacuum for 1 hour at 400°C, followed by reactive isothermal annealing in Selenium vapors for 1 hour at 560°C. The other sample had been treated for a short time (15 minutes) at 530°C and slow cooling down, following the procedure described by Fig.1. In both cases typical main reflexes of CZTSe at 45.1°, 27.16° and 53.52° in scale 2Θ as well as minorities at 17.44°, 36.25°, 65.98° and 72.65° can be seen. Signals are strong and sharp indicating a well-crystallized Stannite – JCDPS 01-070-8930. Well-defined reflexes from the Molybdenum substrate layer at 40.18°, 56.03° and 72.45° in units 2Θ were detected. There are other peaks, which could be attributed to the Molybdenum substrate as well - reflexes at 11.54° and 31.66°. If we assume the tall peak at 45.1° as a compound caused not only by the Stannite, there is obviously Mo_3Se_4 (JCDPS 03-06503701) - a product of selenization of the substrate. Detailed structural analysis has revealed non-monophase thin film materials in both cases. There are minor but well distinguished reflexes at 26.58°, 28°, 31.2° and 50.02° obviously related to CuSe (Klockmanite – 01-070-8576). Further, following the thesis for a compound character of the XRD pattern, another issue should be

mentioned. Probably it is possible that a thin film material consists of a cubic ZnSe (Stilleite – JCDPS 01-080-0021) the pattern of which coincides with the Stannite one at 27.16°, 45.1° and 53.52° in 2Θ scale. In addition, a scrupulous analysis supposes the existence of another phase – $Cu_{1.8}Se$ (Bercelianite – JCDPS 01-071-0044) with reflexes at 27.16°, 45.1° and 56.03°.

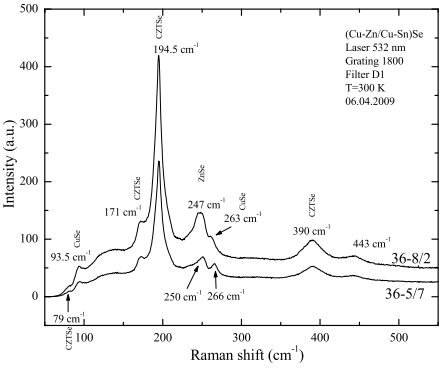

Fig.3. Room temperature Raman spectra of Cu2ZnSnSe4 thin layers

Fig.3 shows the RT Raman spectra of samples 36-8/2 and 36-5/7 deposited and annealed in the same conditions as sample 36-5/8 in Fig.2. The patterns present defined spectra for the well-formed Stannite by almost all important vibrations at 79 cm^{-1}, 173 cm^{-1}, 196 cm^{-1}, 231 cm^{-1} and 390 cm^{-1}, respectively. There are two peaks that could be attributed to CuSe – at 94 cm^{-1} and near 263 cm^{-1}. Another signal at 247 cm^{-1} was registered, which may be due to the cubic ZnSe. The weak vibration at 443 cm^{-1} could be attributed to the bond Si-O-Si from the substrate [17]. As the samples are similar in composition and are annealed in the same conditions, the differences in signal intensities in the spectra should be related to the differences in layer thickness.

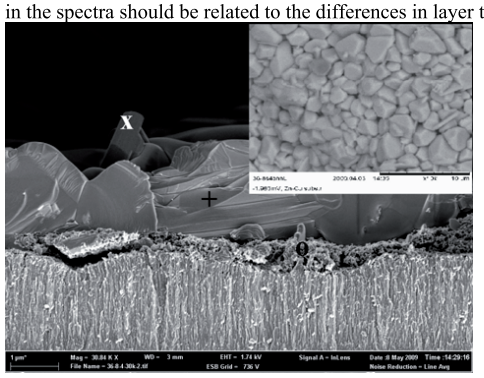

Fig.4. SEM cross section microgram of the CZTSe thin film, annealed in vacuum for 1 hour, followed by a selenization at 560°C for 1 hour. Insertion presents the surface morphology image of the same film.

Fig.4 presents a SEM microgram of sample 36-8/4 preliminarily annealed in vacuum for 1 hour at 400°C and selenized at 560°C for 1 hour. As we could take insights from the XRD and Raman spectra, the CZTSe thin layer was found to consist of large grains sized more than 1μm. More detailed observations revealed fine grains situated

mainly on the large grain boundaries at the bottom of the layer and flat hexagonal well-formed crystals situated mainly on the surface of the layer. High definition EDX allowed us to determine the composition peculiarities of the described objects. Large grain composition (measured at point +) indicates to slightly Tin rich CZTSe (23.77 at% Cu- 11.30 at% Zn- 13.67 at% Sn – 51.25 at% Se) thin film material. Fine powder crystallites on the interface Mo - CZTSe indicated as **o** shows a composition of 52.65 at% Zn – 47.35 at% Se that corresponds to the Stilleite phase presented in Fig.2. Flat plate crystal grains on the surface – indicated as **x** were defined to correspond to the Klockmanite (Fig.2), giving 47.48 at% Cu – 52.52 at% Se.

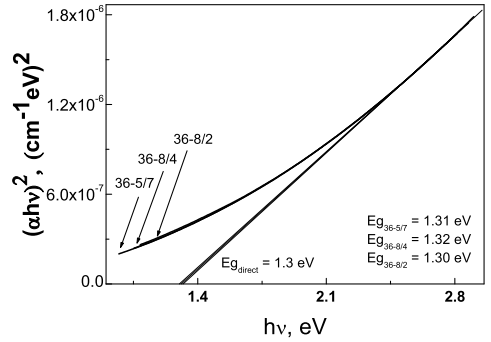

Fig.5. Plot for determining the band gap of $Cu_2ZnSnSe_4$ films selenized in different conditions: 36-8/4 -1 hour at 400°C in vacuum +1 hour at 560°C and 36-8/2&36-5/7 for 10 minutes at 530 °C. The analysis is based on the assumption that CZTSe is a direct band gap material.

Fig.5 shows the dependence of the curves of $(\alpha h\nu)^2$ on the dropping optical light energy hν for layers CZTSe deposited in similar conditions but annealed both by fast (10 minutes selenization at 530°C -36-8/2&36-5/7) or through preliminary metal alloy homogenization at 400°C for 1 hour and 1 hour selenization at 560°C – sample 36-8/4. The direct optical band gap was approximated by plotting $(\alpha h\nu)^2$ versus the energy in eV and extrapolating the linear part of the spectrum $(\alpha h\nu)^2 = f(h\nu)$ to zero. Thus, the band gap of the CZTSe thin films was estimated to be 1.31 eV ± 0.01 eV. This value is much lower than those reported earlier [3,5] 1.44 eV and 1.56 eV. It seems closer to those close to 1 eV proposed recently in the investigations of monograin materials [18]
Comparison of the data in Fig.2 enables to conclude that a longer annealing time acts favourably to the formation of well-crystallized Stannite $Cu_2ZnSeSe_4$ and different binaries (Klockmanite - CuSe and Stilleite - ZnSe) as well as those for thicker under-layer of Mo_3Se_4.

4. Conclusions

Electrodeposition of alloys Brass and Bronze substrate layers followed by selenization results in successful formation of well-crystallized Stannite thin film structures. Shorter annealing time may lead to favorable formation of Stannite thin films but the system is still not a perfect mono phase. All thin layer materials showed similar optical properties and a band gap near 1.31 eV.

5. Acknowledgements

European Researcher's Mobility Program of Estonian Science Foundation under Contract JD 98 is gratefully acknowledged.

6. References

1. A Vision for Photovoltaic Technology for 2030 and Beyond, European Commission, 2004.
2. Feltrin, A. Freindlich, Material considerations for terawatt level deployment of photovoltaics, Renew. Energy 33 (2008) 180–185.
3. H.Matsushita, T.Maeda, A.Katsui and T.Takadzawa, J.Cryst.Growth 208, 416 (2000).
4. K. Ito, T. Nakazawa, Jpn. J. Appl. Phys. 27 (1988) 2094
5. Th. M. Friedlmeier, N. Wieser, T. Walter, H. Dittrich, H.-W. Schock, Proceedings of the 14th European Conference of Photovoltaic Solar Energy Conference and Exhibition, Belford, 1997, p. 1242.
6. H. Katagiri, K. Jimbo, K. Moriya, K. Tsuchida, Proceedings of the 3rd World Conference on Photovoltaic Solar Energy Conversion, Osaka, 2003, p. 2874.
7. Ennaoui A., Lux-Steiner M., Weber A., Abou-Ras D., Kotschau I., Schock H.-W., Schur R., Holzing A., Jost S., Hock R., Voss T., Schulze J., Kirbs A., Thin Solid Films, xxx (2008) xxx-xxx
8. Scragg J., Dale P., Peter L., Electrochemistry Communications 10 (2008) 639-642
9. H. Kühnlein, J. Schulze, T. Voß, Metal plating composition and method for the deposition of copper–zinc–tin suitable for manufacturing thin film solar cell, Patent WO2007134843, Nov. 29, 2007.
10. R.A.Wibowo, E.S.Lee, B.Munir, K.H.Kim, Pulsed laser deposition of quaternaryCu2ZnSnSe4 thin films, Phys. Status Solidi (a)204(2007) 3373–3379.
11. R.A.Wibowo,W.S.Kim,E.S.Lee,B.Munir,K.H.Kim,Single step preparation of quaternary Cu2ZnSnSe4 thin films by RF magnetron sputtering from binary chalcogenide targets, J.Phys.Chem.Solids68(2007)1908–1913
12. O.Volobijeva, J.Raudoja, E.Mellikov, M.Grossberg, S. Bereznev, R.Traksmaa, Cu2ZnSnSe4 films by selenization of Sn-Zn-Cu sequential films, Journal of Physics and Chemistry of Solids, 2009
13. M.Altosaar, J.Raudoja, K.Timmo, M.Danilson, M.Grossberg, J.Krustok, E. Mellikov, Cu2Zn1_x Cdx Sn(Se1_y Sy)4 solid solutions as absorber materials for solar cells, Phys. Status Solidi (a)205(2008)167–170.
14. Mellikov E., Meissner D., Varema T., Altosaar M., Kauk M., Volobujeva O., Raudoja J., Timmo K., Danilson M., Monograin materials for solar cells, Sol. Energy Mater.Sol.Cells, 93,1(2009), 65-68
15. Ямпольский А.М., Ильин В.А., Краткий Справочник Гальванотехника, Ленинград “Машиностроение”, 1981
16. Powder Diffraction File, Joint Committee on Powder Diffraction Standards, American Society for Testing and Materials, Philadelphia, Pa, 1967, PDF 40-1487.
17. Instrument Engineers' Handbook: Process measurement and analysis, Béla G. Lipták,Edition: Published by CRC Press, 2003; ISBN 0849310830, 9780849310836.
18. Grossberg M., Krustok J., Timmo K., Altosaar M., Radiative recombination in Cu2ZnSnSe4 monograins studied by photoluminescence spectroscopy, Thin Solid Films 517, 7 (2009), 2489-2492

APPENDIX B

PDF cards used in this work for interpretation of phase composition of films from XRD measurements

Phase	JCPDS-ICDD number
$Cu_2ZnSnSe_4$	01-070-8930
Cu_2SnSe_3	03-065-4145
Cu_2SnSe_4	01-078-0600
CuSe	01-072-8417
$Cu_{1.8}Se$	01-088-2043
ZnSe	01-071-5978
SnSe	01-089-0232
$MoSe_2$	03-065-3481
Cu_2ZnSnS_4	04-003-8920
Sn_3S_4	00-027-0900
ZnS	04-006-0807
Cu_2SnS_4	01-089-4714
Mo	04-004-8671
Sn	04-004-6229
Cu_5Zn_8	04-013-7094
$Cu_{0.7}Zn_{0.3}$	04-006-2621
CuZn	04-002-3142
Cu_6Sn_5	04-007-2658
CuSn	03-065-3434

Interpretation of Raman shifts

Phase	Raman shifts (cm^{-1})	Reference
$Cu_2ZnSnSe_4$	167, 173, 196, 231, 245	[163]
CuSe	263	[164]
ZnSe	202, 252	[165]
Cu_2ZnSnS_4	98, 142, 168, 252, 263, 288, 339, 347, 355, 365	[166]
Sn_2S_3	307, 251, 234, 183, 71, 60, 52	[167]
CuS	62, 142, 267, 474	[168]
MoS_2	380, 408	[169]

APPENDIX B

Elulookirjeldus

1. Isikuandmed

Ees- ja perekonnanimi	Julia Lehner (Iljina)
Sünniaeg ja -koht	15.09.1986, Sillamäe
Kodakondsus	Eesti
E-posti aadress	jullenok@gmail.com

2. Hariduskäik

Õppeasutus (nimetus lõpetamise ajal)	Lõpetamise aeg	Haridus (eriala/kraad)
Tallinna Tehnikaülikool	2010	Loodusteaduste magister
Tallinna Tehnikaülikool	2008	Toidutehnoloogia insener
Sillamäe Kannuka Keskkool	2005	Keskharidus

3. Keelteoskus (alg-, kesk- või kõrgtase)

Keel	Tase
Vene keel	emakeel
Eesti keel	kesktase
Inglise keel	kesktase
Saksa keel	kesktase
Prantsuse keel	algtase

4. Täiendusõpe

Õppimise aeg	Täiendusõppe korraldaja nimetus
September 2009 – juuli 2013	Doktorikool "Funktsionaalsed materjalid ja tehnoloogiad", Tartu Ülikool ja Tallinna Tehnikaülikool
September 2012	Central Laboratory of Solar Energy and New Energy Sources, Sofia, Bulgaria,
September 2011	International Summer School on Photovoltaics and

	New Concepts of Quantum Solar Energy Conversion (Quantsol), Hirschegg, Austria
Aprill-mai 2011	Center for Physical Sciences and Technology, Vilnius University, Faculty of Chemistry, Vilnius, Lithuania

5. Teenistuskäik

Töötamise aeg	Tööandja nimetus	Ametikoht
2011-täna	Tallinna Tehnikaülikool	Nooremteadur
2008-2010	Tallinna Tehnikaülikool	Insener

6. Teadustegevus, sh tunnustused ja juhendatud lõputööd

- Tänukiri 2010. a üliõpilaste teadustööde riiklikul konkursil
- Juhendatud magistritöö Mihkel Loorits – "Thermal treatment of Cu_2ZnSnS_4 and SnS thin films in H_2S ambient" (Defense 06/2013)

APPENDIX B

Curriculum vitae

1. Personal data

Name	Julia Lehner (née Iljina)
Date and place of birth	15.09.1986, Sillamäe
E-mail address	jullenok@gmail.com

2. Education

Educational institution	Graduation year	Education (field of study/degree)
Tallinn University of Technology	2010	Master of Science in Natural Sciences
Tallinn University of Technology	2008	Bachelor of Science in Engineering
Sillamäe Kannuka school	2005	High school education

3. Language competence/skills (fluent, average, basic skills)

Language	Level
Russian	Native
Estonian	Fluent
English	Fluent
German	Basic knowledge
French	Elementary knowledge

4. Special courses

Period	Educational or other organisation
September 2009 – July 2013	Graduate School "Functional Materials and Technologies" University of Tartu and Tallinn University of Technology
September 2012	Central Laboratory of Solar Energy and New Energy Sources, Sofia, Bulgaria

September 2011	International Summer School on Photovoltaics and New Concepts of Quantum Solar Energy Conversion (Quantsol), in Hirschegg, Austria
April – May 2011	Center for Physical Sciences and Technology, Vilnius University, Faculty of Chemistry, Vilnius, Lithuania

5. Professional employment

Period	Organisation	Position
09/2011 – present	Tallinn University of Technology	Early stage researcher
09/2008 – 07/2010	Tallinn University of Technology	Engineer

6. Research activity, including honours and thesis supervised

- Gratitude letter on the National Student Research Competition, 2010
- Supervision of master thesis of Mihkel Loorits – "Thermal treatment of Cu_2ZnSnS_4 and SnS thin films in H_2S ambient" (Defense 06/2013)

LIST OF PUBLICATIONS

1. N. Revathi, S. Bereznev, **J. Lehner**, M. Safonova, E. Mellikov, O. Volobujeva; Tin monosulfide thin films by PVD method for solar cell applications, *Journal of Materials and Technology, Accepted [to be published in issue 2/2015]*
2. **J. Lehner**, M. Ganchev, M. Loorits, N. Revathi, T. Raadik, J. Raudoja, M. Grossberg, E. Mellikov, O. Volobujeva; Structural and compositional properties of CZTS thin films formed by rapid thermal annealing of electrodeposited layers, *Journal of Crystal Growth*, *380* (*2013*), p. *236-240*
3. N. Revathi, S. Bereznev, **J. Iljina**, M. Safonova , E. Mellikov, O. Volobujeva; PVD grown SnS thin films onto different substrate surfaces, *Journal of Materials Science: Materials in Electronics, 24 (2013), p. 4739-4744*
4. **J. Iljina**, R. Zhang, M. Ganchev, T. Raadik, O. Volobujeva, M. Altosaar, R. Traksmaa, E. Mellikov; Formation of Cu_2ZnSnS_4 absorber layers for solar cells by electrodeposition-annealing route, *Thin Solid Films*, *537 (2013)*, *p. 85-89*
5. **J. Iljina**, O. Volobujeva, T. Raadik, N. Revathi, J. Raudoja, M. Loorits, R. Traksmaa, E. Mellikov; Selenisation of sequentially electrodeposited Cu–Zn and Sn precursor layers, *Thin Solid Films, 535 (2013), p. 14-17*
6. E. Mellikov, D. Meissner, M. Altosaar, M. Kauk, J. Krustok, A. Öpik, O. Volobujeva, **J. Iljina**, K. Timmo, I. Klavina, J. Raudoja, M. Grossberg, T. Varema, K. Muska, M. Ganchev, S. Bereznev, M. Danilson; CZTS monograin powders and thin films, *Advanced Materials Research 222 (2011), p. 8-13*
7. M. Ganchev**, J. Iljina**, L. Kaupmees, T. Raadik, O. Volobujeva, A. Mere, M. Altosaar, J. Raudoja, E. Mellikov: Phase Composition of selenized $Cu_2ZnSnSe_4$ thin films by XRD and Raman studies, *Thin Solid Films*, *519 (2011), p. 7394-7398*
8. M. Ganchev**,** L. Kaupmees, **J. Iliyna**, J. Raudoja, O. Volobujeva, H. Dikov, M. Altosaar, E. Mellikov, T.Varema; Formation of $Cu_2ZnSnSe_4$ thin films by selenization of electrodeposited stacked binary alloy layers, *Energy Procedia, 2 (2009), p. 65-70*

DISSERTATIONS DEFENDED AT
TALLINN UNIVERSITY OF TECHNOLOGY ON
NATURAL AND EXACT SCIENCES

1. **Olav Kongas**. Nonlinear Dynamics in Modeling Cardiac Arrhytmias. 1998.
2. **Kalju Vanatalu**. Optimization of Processes of Microbial Biosynthesis of Isotopically Labeled Biomolecules and Their Complexes. 1999.
3. **Ahto Buldas**. An Algebraic Approach to the Structure of Graphs. 1999.
4. **Monika Drews**. A Metabolic Study of Insect Cells in Batch and Continuous Culture: Application of Chemostat and Turbidostat to the Production of Recombinant Proteins. 1999.
5. **Eola Valdre**. Endothelial-Specific Regulation of Vessel Formation: Role of Receptor Tyrosine Kinases. 2000.
6. **Kalju Lott**. Doping and Defect Thermodynamic Equilibrium in ZnS. 2000.
7. **Reet Koljak**. Novel Fatty Acid Dioxygenases from the Corals *Plexaura homomalla* and *Gersemia fruticosa.* 2001.
8. **Anne Paju**. Asymmetric oxidation of Prochiral and Racemic Ketones by Using Sharpless Catalyst. 2001.
9. **Marko Vendelin**. Cardiac Mechanoenergetics *in silico*. 2001.
10. **Pearu Peterson**. Multi-Soliton Interactions and the Inverse Problem of Wave Crest. 2001.
11. **Anne Menert**. Microcalorimetry of Anaerobic Digestion. 2001.
12. **Toomas Tiivel**. The Role of the Mitochondrial Outer Membrane in *in vivo* Regulation of Respiration in Normal Heart and Skeletal Muscle Cell. 2002.
13. **Olle Hints**. Ordovician Scolecodonts of Estonia and Neighbouring Areas: Taxonomy, Distribution, Palaeoecology, and Application. 2002.
14. **Jaak Nõlvak**. Chitinozoan Biostratigrapy in the Ordovician of Baltoscandia. 2002.
15. **Liivi Kluge**. On Algebraic Structure of Pre-Operad. 2002.
16. **Jaanus Lass**. Biosignal Interpretation: Study of Cardiac Arrhytmias and Electromagnetic Field Effects on Human Nervous System. 2002.
17. **Janek Peterson**. Synthesis, Structural Characterization and Modification of PAMAM Dendrimers. 2002.
18. **Merike Vaher**. Room Temperature Ionic Liquids as Background Electrolyte Additives in Capillary Electrophoresis. 2002.
19. **Valdek Mikli**. Electron Microscopy and Image Analysis Study of Powdered Hardmetal Materials and Optoelectronic Thin Films. 2003.
20. **Mart Viljus**. The Microstructure and Properties of Fine-Grained Cermets. 2003.
21. **Signe Kask**. Identification and Characterization of Dairy-Related *Lactobacillus.* 2003
22. **Tiiu-Mai Laht**. Influence of Microstructure of the Curd on Enzymatic and Microbiological Processes in Swiss-Type Cheese. 2003.
23. **Anne Kuusksalu**. 2–5A Synthetase in the Marine Sponge *Geodia cydonium*. 2003.
24. **Sergei Bereznev**. Solar Cells Based on Polycristalline Copper-Indium Chalcogenides and Conductive Polymers. 2003.

25. **Kadri Kriis**. Asymmetric Synthesis of C_2-Symmetric Bimorpholines and Their Application as Chiral Ligands in the Transfer Hydrogenation of Aromatic Ketones. 2004.
26. **Jekaterina Reut**. Polypyrrole Coatings on Conducting and Insulating Substracts. 2004.
27. **Sven Nõmm**. Realization and Identification of Discrete-Time Nonlinear Systems. 2004.
28. **Olga Kijatkina**. Deposition of Copper Indium Disulphide Films by Chemical Spray Pyrolysis. 2004.
29. **Gert Tamberg**. On Sampling Operators Defined by Rogosinski, Hann and Blackman Windows. 2004.
30. **Monika Übner**. Interaction of Humic Substances with Metal Cations. 2004.
31. **Kaarel Adamberg**. Growth Characteristics of Non-Starter Lactic Acid Bacteria from Cheese. 2004.
32. **Imre Vallikivi**. Lipase-Catalysed Reactions of Prostaglandins. 2004.
33. **Merike Peld**. Substituted Apatites as Sorbents for Heavy Metals. 2005.
34. **Vitali Syritski**. Study of Synthesis and Redox Switching of Polypyrrole and Poly(3,4-ethylenedioxythiophene) by Using *in-situ* Techniques. 2004.
35. **Lee Põllumaa**. Evaluation of Ecotoxicological Effects Related to Oil Shale Industry. 2004.
36. **Riina Aav**. Synthesis of 9,11-Secosterols Intermediates. 2005.
37. **Andres Braunbrück**. Wave Interaction in Weakly Inhomogeneous Materials. 2005.
38. **Robert Kitt**. Generalised Scale-Invariance in Financial Time Series. 2005.
39. **Juss Pavelson**. Mesoscale Physical Processes and the Related Impact on the Summer Nutrient Fields and Phytoplankton Blooms in the Western Gulf of Finland. 2005.
40. **Olari Ilison**. Solitons and Solitary Waves in Media with Higher Order Dispersive and Nonlinear Effects. 2005.
41. **Maksim Säkki**. Intermittency and Long-Range Structurization of Heart Rate. 2005.
42. **Enli Kiipli**. Modelling Seawater Chemistry of the East Baltic Basin in the Late Ordovician–Early Silurian. 2005.
43. **Igor Golovtsov**. Modification of Conductive Properties and Processability of Polyparaphenylene, Polypyrrole and polyaniline. 2005.
44. **Katrin Laos**. Interaction Between Furcellaran and the Globular Proteins (Bovine Serum Albumin β-Lactoglobulin). 2005.
45. **Arvo Mere**. Structural and Electrical Properties of Spray Deposited Copper Indium Disulphide Films for Solar Cells. 2006.
46. **Sille Ehala**. Development and Application of Various On- and Off-Line Analytical Methods for the Analysis of Bioactive Compounds. 2006.
47. **Maria Kulp**. Capillary Electrophoretic Monitoring of Biochemical Reaction Kinetics. 2006.
48. **Anu Aaspõllu.** Proteinases from *Vipera lebetina* Snake Venom Affecting Hemostasis. 2006.
49. **Lyudmila Chekulayeva**. Photosensitized Inactivation of Tumor Cells by Porphyrins and Chlorins. 2006.

50. **Merle Uudsemaa**. Quantum-Chemical Modeling of Solvated First Row Transition Metal Ions. 2006.
51. **Tagli Pitsi**. Nutrition Situation of Pre-School Children in Estonia from 1995 to 2004. 2006.
52. **Angela Ivask**. Luminescent Recombinant Sensor Bacteria for the Analysis of Bioavailable Heavy Metals. 2006.
53. **Tiina Lõugas**. Study on Physico-Chemical Properties and Some Bioactive Compounds of Sea Buckthorn (*Hippophae rhamnoides* L.). 2006.
54. **Kaja Kasemets**. Effect of Changing Environmental Conditions on the Fermentative Growth of *Saccharomyces cerevisae* S288C: Auxo-accelerostat Study. 2006.
55. **Ildar Nisamedtinov**. Application of ^{13}C and Fluorescence Labeling in Metabolic Studies of *Saccharomyces* spp. 2006.
56. **Alar Leibak**. On Additive Generalisation of Voronoï's Theory of Perfect Forms over Algebraic Number Fields. 2006.
57. **Andri Jagomägi**. Photoluminescence of Chalcopyrite Tellurides. 2006.
58. **Tõnu Martma**. Application of Carbon Isotopes to the Study of the Ordovician and Silurian of the Baltic. 2006.
59. **Marit Kauk**. Chemical Composition of $CuInSe_2$ Monograin Powders for Solar Cell Application. 2006.
60. **Julia Kois**. Electrochemical Deposition of $CuInSe_2$ Thin Films for Photovoltaic Applications. 2006.
61. **Ilona Oja Açik**. Sol-Gel Deposition of Titanium Dioxide Films. 2007.
62. **Tiia Anmann**. Integrated and Organized Cellular Bioenergetic Systems in Heart and Brain. 2007.
63. **Katrin Trummal**. Purification, Characterization and Specificity Studies of Metalloproteinases from *Vipera lebetina* Snake Venom. 2007.
64. **Gennadi Lessin**. Biochemical Definition of Coastal Zone Using Numerical Modeling and Measurement Data. 2007.
65. **Enno Pais**. Inverse problems to determine non-homogeneous degenerate memory kernels in heat flow. 2007.
66. **Maria Borissova**. Capillary Electrophoresis on Alkylimidazolium Salts. 2007.
67. **Karin Valmsen**. Prostaglandin Synthesis in the Coral *Plexaura homomalla*: Control of Prostaglandin Stereochemistry at Carbon 15 by Cyclooxygenases. 2007.
68. **Kristjan Piirimäe**. Long-Term Changes of Nutrient Fluxes in the Drainage Basin of the Gulf of Finland – Application of the PolFlow Model. 2007.
69. **Tatjana Dedova**. Chemical Spray Pyrolysis Deposition of Zinc Sulfide Thin Films and Zinc Oxide Nanostructured Layers. 2007.
70. **Katrin Tomson**. Production of Labelled Recombinant Proteins in Fed-Batch Systems in *Escherichia coli*. 2007.
71. **Cecilia Sarmiento**. Suppressors of RNA Silencing in Plants. 2008.
72. **Vilja Mardla**. Inhibition of Platelet Aggregation with Combination of Antiplatelet Agents. 2008.
73. **Maie Bachmann**. Effect of Modulated Microwave Radiation on Human Resting Electroencephalographic Signal. 2008.
74. **Dan Hüvonen**. Terahertz Spectroscopy of Low-Dimensional Spin Systems. 2008.

75. **Ly Villo**. Stereoselective Chemoenzymatic Synthesis of Deoxy Sugar Esters Involving *Candida antarctica* Lipase B. 2008.
76. **Johan Anton**. Technology of Integrated Photoelasticity for Residual Stress Measurement in Glass Articles of Axisymmetric Shape. 2008.
77. **Olga Volobujeva**. SEM Study of Selenization of Different Thin Metallic Films. 2008.
78. **Artur Jõgi**. Synthesis of 4'-Substituted 2,3'-dideoxynucleoside Analogues. 2008.
79. **Mario Kadastik**. Doubly Charged Higgs Boson Decays and Implications on Neutrino Physics. 2008.
80. **Fernando Pérez-Caballero**. Carbon Aerogels from 5-Methylresorcinol-Formaldehyde Gels. 2008.
81. **Sirje Vaask**. The Comparability, Reproducibility and Validity of Estonian Food Consumption Surveys. 2008.
82. **Anna Menaker**. Electrosynthesized Conducting Polymers, Polypyrrole and Poly(3,4-ethylenedioxythiophene), for Molecular Imprinting. 2009.
83. **Lauri Ilison**. Solitons and Solitary Waves in Hierarchical Korteweg-de Vries Type Systems. 2009.
84. **Kaia Ernits**. Study of In_2S_3 and ZnS Thin Films Deposited by Ultrasonic Spray Pyrolysis and Chemical Deposition. 2009.
85. **Veljo Sinivee**. Portable Spectrometer for Ionizing Radiation "Gammamapper". 2009.
86. **Jüri Virkepu**. On Lagrange Formalism for Lie Theory and Operadic Harmonic Oscillator in Low Dimensions. 2009.
87. **Marko Piirsoo**. Deciphering Molecular Basis of Schwann Cell Development. 2009.
88. **Kati Helmja**. Determination of Phenolic Compounds and Their Antioxidative Capability in Plant Extracts. 2010.
89. **Merike Sõmera**. Sobemoviruses: Genomic Organization, Potential for Recombination and Necessity of P1 in Systemic Infection. 2010.
90. **Kristjan Laes**. Preparation and Impedance Spectroscopy of Hybrid Structures Based on $CuIn_3Se_5$ Photoabsorber. 2010.
91. **Kristin Lippur**. Asymmetric Synthesis of 2,2'-Bimorpholine and its 5,5'-Substituted Derivatives. 2010.
92. **Merike Luman**. Dialysis Dose and Nutrition Assessment by an Optical Method. 2010.
93. **Mihhail Berezovski**. Numerical Simulation of Wave Propagation in Heterogeneous and Microstructured Materials. 2010.
94. **Tamara Aid-Pavlidis**. Structure and Regulation of BDNF Gene. 2010.
95. **Olga Bragina**. The Role of Sonic Hedgehog Pathway in Neuro- and Tumorigenesis. 2010.
96. **Merle Randrüüt**. Wave Propagation in Microstructured Solids: Solitary and Periodic Waves. 2010.
97. **Marju Laars**. Asymmetric Organocatalytic Michael and Aldol Reactions Mediated by Cyclic Amines. 2010.
98. **Maarja Grossberg**. Optical Properties of Multinary Semiconductor Compounds for Photovoltaic Applications. 2010.

99. **Alla Maloverjan**. Vertebrate Homologues of Drosophila Fused Kinase and Their Role in Sonic Hedgehog Signalling Pathway. 2010.
100. **Priit Pruunsild**. Neuronal Activity-Dependent Transcription Factors and Regulation of Human *BDNF* Gene. 2010.
101. **Tatjana Knjazeva**. New Approaches in Capillary Electrophoresis for Separation and Study of Proteins. 2011.
102. **Atanas Katerski**. Chemical Composition of Sprayed Copper Indium Disulfide Films for Nanostructured Solar Cells. 2011.
103. **Kristi Timmo.** Formation of Properties of $CuInSe_2$ and $Cu_2ZnSn(S,Se)_4$ Monograin Powders Synthesized in Molten KI. 2011.
104. **Kert Tamm**. Wave Propagation and Interaction in Mindlin-Type Microstructured Solids: Numerical Simulation. 2011.
105. **Adrian Popp**. Ordovician Proetid Trilobites in Baltoscandia and Germany. 2011.
106. **Ove Pärn**. Sea Ice Deformation Events in the Gulf of Finland and This Impact on Shipping. 2011.
107. **Germo Väli**. Numerical Experiments on Matter Transport in the Baltic Sea. 2011.
108. **Andrus Seiman**. Point-of-Care Analyser Based on Capillary Electrophoresis. 2011.
109. **Olga Katargina**. Tick-Borne Pathogens Circulating in Estonia (Tick-Borne Encephalitis Virus, *Anaplasma phagocytophilum*, *Babesia* Species): Their Prevalence and Genetic Characterization. 2011.
110. **Ingrid Sumeri**. The Study of Probiotic Bacteria in Human Gastrointestinal Tract Simulator. 2011.
111. **Kairit Zovo**. Functional Characterization of Cellular Copper Proteome. 2011.
112. **Natalja Makarytsheva**. Analysis of Organic Species in Sediments and Soil by High Performance Separation Methods. 2011.
113. **Monika Mortimer**. Evaluation of the Biological Effects of Engineered Nanoparticles on Unicellular Pro- and Eukaryotic Organisms. 2011.
114. **Kersti Tepp**. Molecular System Bioenergetics of Cardiac Cells: Quantitative Analysis of Structure-Function Relationship. 2011.
115. **Anna-Liisa Peikolainen**. Organic Aerogels Based on 5-Methylresorcinol. 2011.
116. **Leeli Amon**. Palaeoecological Reconstruction of Late-Glacial Vegetation Dynamics in Eastern Baltic Area: A View Based on Plant Macrofossil Analysis. 2011.
117. **Tanel Peets**. Dispersion Analysis of Wave Motion in Microstructured Solids. 2011.
118. **Liina Kaupmees**. Selenization of Molybdenum as Contact Material in Solar Cells. 2011.
119. **Allan Olspert**. Properties of VPg and Coat Protein of Sobemoviruses. 2011.
120. **Kadri Koppel**. Food Category Appraisal Using Sensory Methods. 2011.
121. **Jelena Gorbatšova**. Development of Methods for CE Analysis of Plant Phenolics and Vitamins. 2011.
122. **Karin Viipsi**. Impact of EDTA and Humic Substances on the Removal of Cd and Zn from Aqueous Solutions by Apatite. 2012.

123. **David Schryer**. Metabolic Flux Analysis of Compartmentalized Systems Using Dynamic Isotopologue Modeling. 2012.
124. **Ardo Illaste**. Analysis of Molecular Movements in Cardiac Myocytes. 2012.
125. **Indrek Reile**. 3-Alkylcyclopentane-1,2-Diones in Asymmetric Oxidation and Alkylation Reactions. 2012.
126. **Tatjana Tamberg**. Some Classes of Finite 2-Groups and Their Endomorphism Semigroups. 2012.
127. **Taavi Liblik**. Variability of Thermohaline Structure in the Gulf of Finland in Summer. 2012.
128. **Priidik Lagemaa**. Operational Forecasting in Estonian Marine Waters. 2012.
129. **Andrei Errapart**. Photoelastic Tomography in Linear and Non-linear Approximation. 2012.
130. **Külliki Krabbi**. Biochemical Diagnosis of Classical Galactosemia and Mucopolysaccharidoses in Estonia. 2012.
131. **Kristel Kaseleht**. Identification of Aroma Compounds in Food using SPME-GC/MS and GC-Olfactometry. 2012.
132. **Kristel Kodar**. Immunoglobulin G Glycosylation Profiling in Patients with Gastric Cancer. 2012.
133. **Kai Rosin**. Solar Radiation and Wind as Agents of the Formation of the Radiation Regime in Water Bodies. 2012.
134. **Ann Tiiman**. Interactions of Alzheimer's Amyloid-Beta Peptides with Zn(II) and Cu(II) Ions. 2012.
135. **Olga Gavrilova**. Application and Elaboration of Accounting Approaches for Sustainable Development. 2012.
136. **Olesja Bondarenko**. Development of Bacterial Biosensors and Human Stem Cell-Based *In Vitro* Assays for the Toxicological Profiling of Synthetic Nanoparticles. 2012.
137. **Katri Muska**. Study of Composition and Thermal Treatments of Quaternary Compounds for Monograin Layer Solar Cells. 2012.
138. **Ranno Nahku**. Validation of Critical Factors for the Quantitative Characterization of Bacterial Physiology in Accelerostat Cultures. 2012.
139. **Petri-Jaan Lahtvee**. Quantitative Omics-level Analysis of Growth Rate Dependent Energy Metabolism in *Lactococcus lactis*. 2012.
140. **Kerti Orumets**. Molecular Mechanisms Controlling Intracellular Glutathione Levels in Baker's Yeast *Saccharomyces cerevisiae* and its Random Mutagenized Gluthatione Over-Accumulating Isolate. 2012.
141. **Loreida Timberg**. Spice-Cured Sprats Ripening, Sensory Parameters Development, and Quality Indicators. 2012.
142. **Anna Mihhalevski**. Rye Sourdough Fermentation and Bread Stability. 2012.
143. **Liisa Arike**. Quantitative Proteomics of *Escherichia coli*: From Relative to Absolute Scale. 2012.
144. **Kairi Otto**. Deposition of In_2S_3 Thin Films by Chemical Spray Pyrolysis. 2012.
145. **Mari Sepp**. Functions of the Basic Helix-Loop-Helix Transcription Factor TCF4 in Health and Disease. 2012.
146. **Anna Suhhova**. Detection of the Effect of Weak Stressors on Human Resting Electroencephalographic Signal. 2012.

147. **Aram Kazarjan**. Development and Production of Extruded Food and Feed Products Containing Probiotic Microorganisms. 2012.
148. **Rivo Uiboupin**. Application of Remote Sensing Methods for the Investigation of Spatio-Temporal Variability of Sea Surface Temperature and Chlorophyll Fields in the Gulf of Finland. 2013.
149. **Tiina Kriščiunaite**. A Study of Milk Coagulability. 2013.
150. **Tuuli Levandi**. Comparative Study of Cereal Varieties by Analytical Separation Methods and Chemometrics. 2013.
151. **Natalja Kabanova**. Development of a Microcalorimetric Method for the Study of Fermentation Processes. 2013.
152. **Himani Khanduri**. Magnetic Properties of Functional Oxides. 2013.
153. **Julia Smirnova**. Investigation of Properties and Reaction Mechanisms of Redox-Active Proteins by ESI MS. 2013.
154. **Mervi Sepp**. Estimation of Diffusion Restrictions in Cardiomyocytes Using Kinetic Measurements. 2013.
155. **Kersti Jääger**. Differentiation and Heterogeneity of Mesenchymal Stem Cells. 2013.
156. **Victor Alari**. Multi-Scale Wind Wave Modeling in the Baltic Sea. 2013.
157. **Taavi Päll**. Studies of CD44 Hyaluronan Binding Domain as Novel Angiogenesis Inhibitor. 2013.
158. **Allan Niidu**. Synthesis of Cyclopentane and Tetrahydrofuran Derivatives. 2013.
159. **Julia Geller**. Detection and Genetic Characterization of *Borrelia* Species Circulating in Tick Population in Estonia. 2013.
160. **Irina Stulova**. The Effects of Milk Composition and Treatment on the Growth of Lactic Acid Bacteria. 2013.
161. **Jana Holmar**. Optical Method for Uric Acid Removal Assessment During Dialysis. 2013.
162. **Kerti Ausmees**. Synthesis of Heterobicyclo[3.2.0]heptane Derivatives *via* Multicomponent Cascade Reaction. 2013.
163. **Minna Varikmaa**. Structural and Functional Studies of Mitochondrial Respiration Regulation in Muscle Cells. 2013.
164. **Indrek Koppel**. Transcriptional Mechanisms of BDNF Gene Regulation. 2014.
165. **Kristjan Pilt**. Optical Pulse Wave Signal Analysis for Determination of Early Arterial Ageing in Diabetic Patients. 2014.
166. **Andres Anier**. Estimation of the Complexity of the Electroencephalogram for Brain Monitoring in Intensive Care. 2014.
167. **Toivo Kallaste**. Pyroclastic Sanidine in the Lower Palaeozoic Bentonites – A Tool for Regional Geological Correlations. 2014.
168. **Erki Kärber**. Properties of ZnO-nanorod/In_2S_3/$CuInS_2$ Solar Cell and the Constituent Layers Deposited by Chemical Spray Method. 2014.